Norwegian University
of Life Sciences

Master's Thesis 2019 30 ECTS
Faculty of Science and Technology

A pilot study of insulated CLT

Torstein Reiten
Structural Engineering and Architecture

ABSTRACT

In order to face the rising challenges of increased global warming, coming up with new and sustainable solutions for the building industry is important. This has led to an increased interest for timber as a building material, with Cross Laminated Timber (CLT) emerging as a popular concept in recent years. Due to regulations regarding the energy efficiency of buildings, exterior CLT walls and roof structures have to be covered with insulation to achieve sufficient thermal resistance in cold climates. In this study, a new concept of insulated CLT is proposed, investigating possibility of using wood fibre boards as a structural layer within laminated timber structures.

The first part of the thesis contains an introduction to timber based hybrid structures, explaining some of the benefits that can be achieved by combining the properties of timber with that of other materials. The theoretical background for composite structures then follows in a separate chapter, laying the mathematical groundwork for an analytical evaluation of the proposed concept.

The second part of the thesis contains experimental investigations, designed to answer some of the most relevant questions regarding the mechanical properties of the material. The experiments include testing of shear strength and shear modulus of the fibre boards, and their sensitivity to moisture content. Composite action between timber and fibre boards is also studied through an out-of-plane bending test on a composite beam, and in-plane shear tests on composite panels.

In the final part of the thesis, the feasibility of creating insulated CLT is investigated based on results from the experiments. The flexural performance of conceptual composite panels are modelled through the use of conventional calculation methods and finite element analysis.

The study has shown that the investigated fibre boards can be used as a structural layer within laminated timber structures, achieving sufficient bonding quality to prevent failure at the glue interface. The material has a shear modulus of approximately 50N/mm^2, which is high enough to achieve considerable composite action. The shear strength may pose limitations for possible applications, with characteristic values ranging from 0.219N/mm^2 to 0.282N/mm^2 depending on the density and the configuration of the test pieces. The main limiting factor for the concept seems to be the material's sensitivity to moisture.

AKNOWLEDGEMENTS

I wish to express my gratitude to professor Roberto Tomasi, who introduced me to the concept of this thesis and served as my supervisor. I would also like to thank my co-supervisor, PhD candidate Dag Pasquale Pasca, for giving me input and guidance throughout the project, and for his help with experiments at the laboratory. I am also very grateful to Engineer Roar Økseter, who spent numerous hours with me at the lab, preparing materials and assisting me with experiments.

Important contributions to this work were also made by Development Manager Dag Molteberg at Norske Skog Saugbrugs, who provided the fibre boards, and by Research and Innovation manager at Splitkon, Kristine Nore, who provided timber boards and adhesives for the testing material. I also have to thank Erik Larnøy, Head of department for the Division of Forest and Forest Resources at Norwegian Institute of Bioeconomy Research (NIBIO), who helped me assemble the composite panels used for the study.

Lastly I would like to thank my wife for her support during my work with this thesis.

CONTENTS

LIST OF TABLES AND FIGURES

1 INTRODUCTION

Sustainability is a word that often comes up when discussing the future of our society. Whether it be with regard to developing our means of transportation, production of our goods and services, or when designing buildings for the future, we strive to find cost effective solutions that can also ensure a healthy planet and environment for coming generations. The goal of this study has been to make a contribution to the modern development within the field of civil engineering, by investigating the possibility of using a new type of insulating wood fibre boards as a structural layer within CLT panels. The hope has been to provide groundwork for further development within sustainable building industry.

The work with the thesis has involved experimental investigations aimed to answer some of the most relevant questions regarding the suitability for structural use of the wood fibre boards:

- Can the material be glued with sufficient bonding quality to achieve composite action?
- What values can be achieved for the shear strength and shear modulus of the material, and how does the density affect these material properties?
- How sensitive are the mechanical properties of the material to moisture variations?
- Will the actual behavior of the material within a composite load bearing structure match the theoretical predictions from conventional calculation methods?
- How will insulated CLT panels behave with regard to delamination?
- How will insulated CLT panels behave under out-of-plane and in-plane loading?

Since this has been a pilot study, the collection of data has been aimed at gathering basic information about the material, rather than obtaining exact values with high reliability. Although some of the findings might be of limited value from a statistical standpoint, they should give an indication of how suitable the material is for the proposed use.

By combining calculation methods from well established literature with findings from the experiments, the mechanical and thermal performance of conceptual insulated CLT panels has been modelled. These models laid the basis for the evaluation of the proposed concept.

2 HYBRID STRUCTURES

A modern building must not only provide barriers against varying outdoor climate, but also be strong enough to provide sufficient safety for anyone who depends on the functionality of the building. Roof structures must be able to keep the interior of the building warm and dry, while also supporting their own weight on a snowy day. Floors must be able to support the weight of people, furniture and other objects, while also serving as barriers against temperature, noise and fire. They must also be able to take up horizontal forces during a storm or an earthquake, and transfer these to the stabilizing vertical frames of the building. These frames are typically walls, which might have to provide the same kinds of barriers as roofs or floor structures, while also providing sufficient stability for the building as a whole. In this thesis, what is meant by a hybrid structural element is an element designed from dissimilar materials, to have different properties of the materials complimenting each other so that the functionality of the structural element is improved.

Since the industrial revolution took place, steel and concrete have been the predominant building materials used by architects and engineers to design buildings due to their beneficial mechanical properties. However, the use of these materials are responsible for contributing to the global increase of atmospheric CO_2. In addition to having problematic thermal properties on their own, the production processes of these materials are quite energy intensive. This has forced environmentally aware building designers to look for other options, which in turn has sparked an increased interest for timber as a building material for the future. In addition to being renewable, the energy required to modify and prepare timber for structural use is relatively moderate.

A lot of work and research is being done around the world, aimed at optimizing the use of timber as a building material. Many proposed concepts revolve around hybrid structures, combining certain properties of timber with that of other materials. One group of researchers have for instance proposed the use of timber-steel-hybrid elements in multi-storey buildings, listing increased fire resistance and earthquake resistance as some of the achieved benefits (Tavoussi et al., 2015) [1]. Others have investigated how the serviceability performance of timber floors can be improved by adding a concrete topping, reducing the perception of vibration responses to dynamic excitations (Martins et al., 2013) [2]. Other researchers and designers focus on developing timber based hybrid structures that are designed to reduce heat transfer through exterior walls and roof structures, as this thesis is an example of.

State of the art

2.1.1 Hybrid CLT-concrete slabs

Although CLT is gaining increased popularity as a structural material, there are certain challenges remaining regarding the design of CLT buildings. While design criteria for the ultimate limit state often can be met without too much effort, vibrations and sound transmission are known to be more problematic issues. In order to improve the serviceability performance, extra mass can be added to the slabs. While helping to solve problems regarding vibrations and sound transmission, this extra mass will typically increase the required thickness of the CLT panels in order to support it. It is however possible to add mass while also enhancing the flexural properties of the floors by designing timber-concrete composite slabs. Designing these kinds of structures can be very complicated, since the deflections and distribution of internal forces change over time. Important aspects and possible benefits are well described in a state-of-the-art report by Dias et al. (2018) [3].

CLT-concrete composite slabs rely heavily on adequate detailing of the shear connection at the interface between the materials. The most common ways of designing shear connections involve grooves, notches, dowels or screws, often in combination with each other. It is also important to design the connection in a manner that prevents perpendicular separation of timber and concrete. Although timber-concrete composite structures are not given much attention in EN 1995-1-1 [4], it is stated in EN 1995-2 [5] (regarding design of timber bridges) that the shear connection should be designed to resist a perpendicular tensile force equal to 10% of the horizontal shear force.

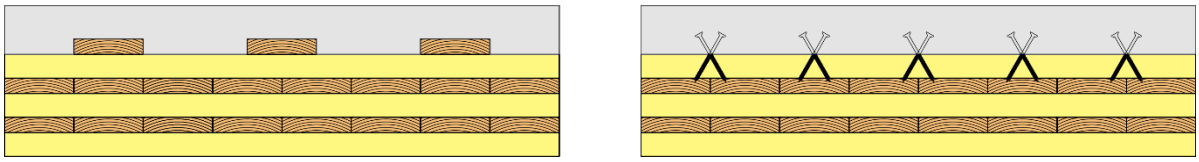

Figure 1: Shear connections in CLT-concrete composite slabs

2.1.2 Heterogeneous CLT

Heterogeneous CLT is a mixed concept of framework and CLT, where cross laminated timber panels are created with spaced voids, reducing the use of materials. The heterogeneous structure of the panels makes modeling of their mechanical behavior quite complicated. An equivalent-layer model has been proposed for the evaluation of the panels' bending properties, a method which has been investigated and compared to experimental results by Lebée et al. (2015) [6].

Panobloc is a commercially available product designed by the French company Techniwood, based on the concept of heterogeneous CLT. The spaced voids between the boards can be filled with insulation material, while the thermal bridges are reduced due to the large three-dimensional effective thickness of the timber layers. The product is being marketed as flexible with regard to configurations and layout, with thickness varying from 6 to 60cm, and element sizes measuring up to 8,50 x 3,50 meters.

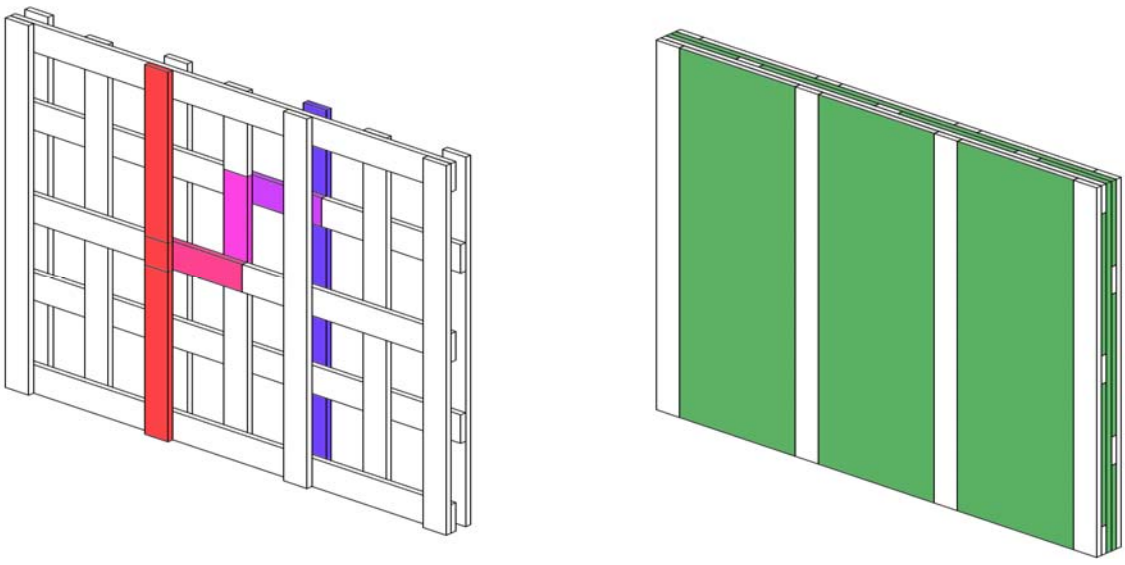

Figure 2: Heterogeneous CLT

2.1.3 SIP panels

Structural insulated panels (SIPs) have been commercially available for decades, and are most widely used in North America. The panels are mainly designed for residential and light commercial constructions. The concept is a typical sandwich structured composite, where foam typically made out of polystyrene, polyisocyanurate or polyisocyanurate makes up the internal insulation core. The outer structural layers are often made out of plywood or oriented strand boards, but a large variety of materials can be used for sheeting. SIPs are commonly marketed as cost, time and energy saving.

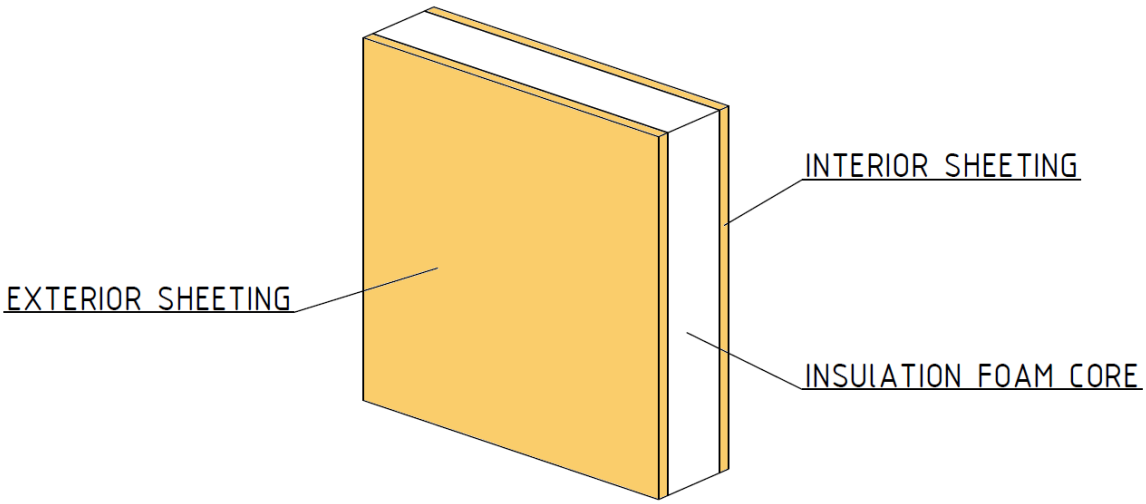

Figure 3: Typical SIP panel

A draft version of an American engineering design guide for SIPs is currently available at the homepage of the Structural Insulated Panel Association [7], with a new version expected to be published in 2019. Producers of SIPs can obtain CE marking of their products through European Technical Assessments (ETAs), in order to make them available for the internal European market.

While a large variety of SIP panels have been available for a long time, a mixed concept of SIP and CLT was more recently investigated by Leoskool and Descamps (2014) [8], using CLT as structural sheeting and preserving mechanical behavior through inclined screws.

2.1.4 Iso3

Iso3 is a commercially available hybrid product that can be used as studs or sills. The concept is based on a custom designed cross-section, where two timber segments are separated by an insulating core of polyurethane foam. In addition to increasing the thermal resistance of the cross-section, the foam acts as a shear connection between the timber segments so that composite action is achieved. A technical approval for the product was issued in 2010 by SINTEF, listing thermal performances as well as structural capacities. The vertical capacities given in the technical approval also account for simultaneous bending produced by horizontal wind pressure.

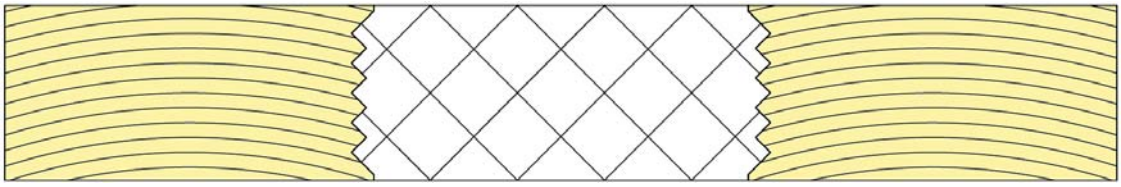

Figure 4: Typical cross-section of Iso3

3 COMPOSITE ACTION IN TIMBER STRUCTURES

A composite structure can generally be described a structural element (e.g. a load-carrying beam, column or slab), that consists of other separate components or materials. These components or materials must be strongly bound together, so that neither can be deformed without also deforming the other. The effect caused by this bond is commonly referred to as composite action.

In timber structures composite action is generally achieved by stacking timber elements on top of each other and binding them together in a manner that prohibits slipping in the contact area. If no attempt to prevent slipping is made, no composite action is achieved. In this case, the combined stiffness of the stacked elements is equal to the sum of their individual stiffness. However, if the connection between the individual elements is made completely rigid, the combined stiffness and strength of the stacked cross-section is vastly increased. The figure below illustrates how composite action will affect the deflection of a beam subject to a vertical load.

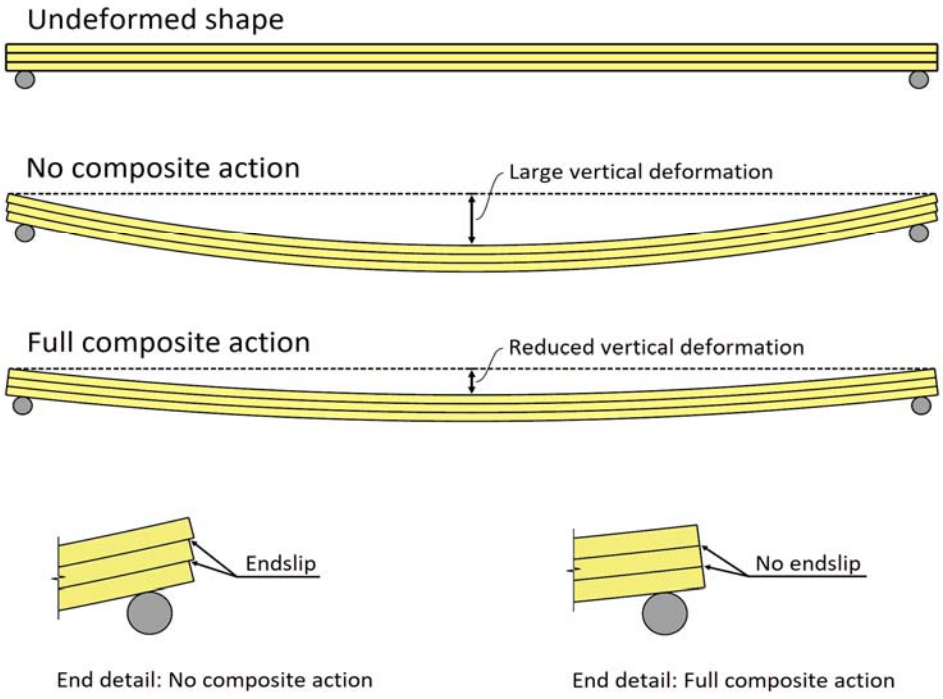

Figure 5: Effect of composite action on deflection

Timber is an orthotropic material, which means that its mechanical properties are dependent on the direction of loading. When loads are applied parallel to the direction of the grain, much higher strength values are achieved, than if the loads are being applied normal to the grain. As will be shown in chapter 3, the orthotropic material properties of timber become apparent when comparing traditional glulam to CLT.

Glued laminated timber

Traditional glulam is the simplest and most basic example of a composite timber structure, where all boards are aligned in the same direction. If the layers also have the same material quality, the material properties are homogeneous for the whole cross-section. Since full composite action is achieved in glulam, the effective stiffness of a combined cross-section, consisting of a set of smaller cross-sections can be calculated using the parallel axis theorem, also known as Steiner's theorem:

$$I_{ef} = \sum_{i=1}^{n} \left(I_i + A_i \cdot z_i^{\,2} \right) \tag{1}$$

Where:

I_i *represents the area moment of inertia for each individual component.*

A_i *represents the cross-section area for each individual component.*

z_i *represents the distance between local centers of gravity and the global neutral axis.*

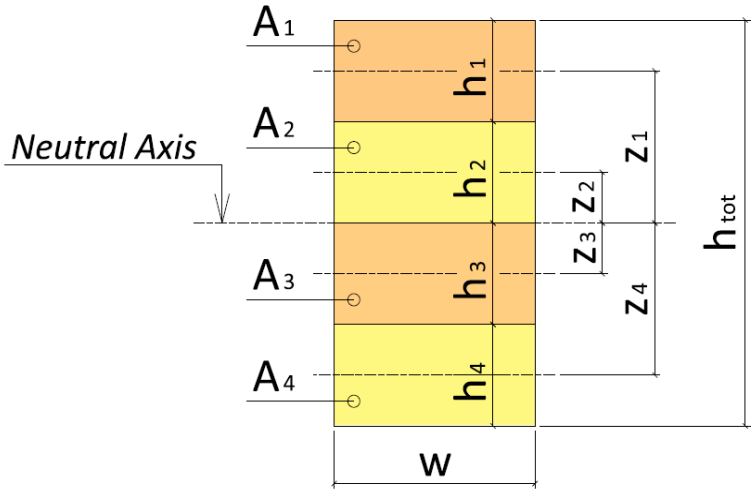

If the cross-section is of a regular rectangle shape, as is usually the case, the effective stiffness is also equal to the area moment of inertia for the combined cross-section, as expressed below:

$$I_{ef} = \frac{w \cdot h_{ef}^{\,3}}{12} \tag{2}$$

Where:

w *represents the width of the cross-section (equal to width of individual boards)*

h_{ef} *represents the total height of the combined cross-section.*

Cross laminated timber

While the design of traditional glulam is quite simple, determining the flexural properties of CLT is a more complicated task. Since the layers are oriented in alternating directions, the orthotropic mechanical properties of timber become apparent through increased shear deformations of the transversal layers. These deformations are analogous to slipping between layers, and therefore affect the composite action within CLT panels.

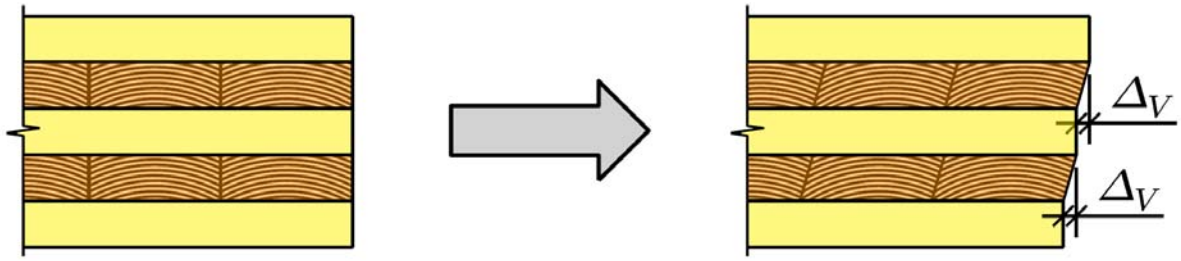

Figure 7: Shear deformations in CLT

Several analytical approaches have been proposed to describe the flexural behavior of CLT, the most common of which are well described by Gagnon and Pirvu (2011) [9] in the CLT Handbook, Canadian edition. In this thesis, two of the methods in the book will be explained, namely the Mechanically Jointed Beams Theory (also known as the gamma method), and the Shear Analogy Method. In addition to the CLT handbook, "*Timber Engineering - Principles for Design* by" Blass and Sandhaas (2017) [10], and a master thesis by Colbacchini (2010) [11] served as valuable inspiration when writing this chapter.

3.2.1 The gamma method

The gamma method was originally developed to describe composite structures where the components are connected using mechanical fasteners (e.g. nails, screws, dowels). The method was developed in 1955 by professor Karl Möhler (1955) [12], and is implemented EN 1995-1-1 [4]. The approach is based on determining a connection efficiency factor (gamma), which depends on the stiffness of the mechanical fasteners, which are assumed to be equally distributed along the beam length. Along with the stiffness properties of the mechanically jointed beams, the value of gamma is used to define the effective bending stiffness of the composite beam. The value of gamma varies from 0.0 in the case of no composite action to 1.0 in the case of full composite action.

The mechanically jointed beams method is based on Bernoulli-Euler bending theory, which means that shear deformations are neglected (apart from the deformation of mechanical fasteners). The method provides a closed solution for the differential equation governing simply supported beams with a sinusoidal load distribution. The difference between the exact solution and those for uniformly distributed loads and point loads are minimal, and acceptable for engineering practice.

With some adaptations the approach can also be used to describe CLT panels, by treating the perpendicular layers as mechanical fasteners between the parallel layers. The stiffness and distribution parameters of mechanical fasteners in the original equations are substituted with mechanical and geometrical parameters of the perpendicular layers, so that:

$$\frac{s}{K_i} = \frac{t_i}{G_p \cdot w_p} \tag{3}$$

Where:

- s *represents spacing between fasteners in the original problem.*
- K_i *represents the slip modulus of the mechanical fasteners in the original problem.*
- t_i *represents the thickness of perpendicular layers*
- G_p *represents the shear modulus of board layers perpendicular to the action*
- w_p *represents the widh of the panel (usually 1 meter)*

When the original parameters have been substituted in accordance with equation (3), the value of γ_i for a layer of boards parallel to the action is calculated using the following equation:

$$\gamma_i = \frac{1}{1+\left(\pi^2 \cdot \frac{E_i \cdot A_i}{L^2} \cdot \frac{t_i}{G_p \cdot w_p}\right)} \tag{4}$$

Where:

- E_i *represents the modulus of elasticity of the longitudinal layers*
- A_i *represents the area of the longitudinal layers*
- L *represents the span width of the beam/panel*

Note that it follows from the expression that the value of γ increases for long span widths. As a result, the degree of composite action is dependent on the span width of the structure.

Once the value of γ has been determined, the effective bending stiffness of the cross-section can be calculated as follows:

$$EI_{eff} = \sum_{i=1}^{n} \left(E_i \cdot I_i + \gamma_i \cdot E_i \cdot A_i \cdot {z_i}^2\right) \tag{5}$$

Where:

- I_i *represents the area moment of inertia for an individual component's cross-section*
- A_i *represents the cross-section area of an individual component's cross-section*
- z_i *represents the distance between local centers of gravity for individual components and the global center of gravity for the cross-section*

Since the shear deformation in longitudinal layers is ignored, the accuracy of the effective bending stiffness derived from this method depends on the span width of the beam/panel. The best results are acquired for span-to-width ratios of 30 and higher. Furthermore, the mechanically jointed beams theory assumes a simply supported beam of span width L. For cantilever CLT slabs it is common design practice to use an effective length of two times the cantilever length L_c. For continuous multi-supported slabs, the value of γ depends on the distance between inflection points. This distance can be found by iteration, typically starting from 0,8 x L_c.

According to the mechanically jointed beams theory, the total stress within a longitudinal layer is equal to the sum of axial stress (developed due to bending of the panel) and local bending stress (developed due to bending of the individual layer):

$$\sigma_{total} = \sigma_{global} + \sigma_{local} \tag{6}$$

The local and global stress contributions are as follows:

$$\sigma_{global} = \frac{\gamma_i \cdot E_i \cdot z_i \cdot M}{EI_{eff}} \tag{7}$$

$$\sigma_{local} = \frac{0.5 \cdot E_i \cdot t_i \cdot M}{EI_{eff}} \tag{8}$$

Where:

M	*represents the bending moment that the panel is subject to*
E_i	*represents the modulus of elasticity of the longitudinal layer*
z_i	*represents the distance from the center of a layer to the center of gravity for the cross-section*
t_i	*represents the thickness of the layer*

The expression can be rewritten so that:

$$\sigma_{total} = \frac{M \cdot E_i}{EI_{eff}} \cdot \left(\gamma_i \cdot z_i + 0.5 \cdot t_i\right) \tag{9}$$

Or, if the modulus of elasticity is the same for all longitudinal layers:

$$\sigma_{total} = \frac{M}{I_{eff}} \cdot \left(\gamma_i \cdot z_i + 0.5 \cdot t_i\right) \tag{10}$$

3.2.2 Shear analaogy method

The shear analogy method is another, more recently developed method to describe composite action in layered structural elements. The method was developed by Heinrich Kreuzinger (1999) [13], and differs from the gamma method by taking shear deformations into account for all layers. The method can be implemented for any configuration and number of layers. The shear analogy method is commonly viewed as the most accurate and adequate method to predict the stiffness properties of CLT.

In the shear analogy method, the characteristics of a multi-layer cross-section is separated into two virtual beams (A and B), coupled together by virtual web members.

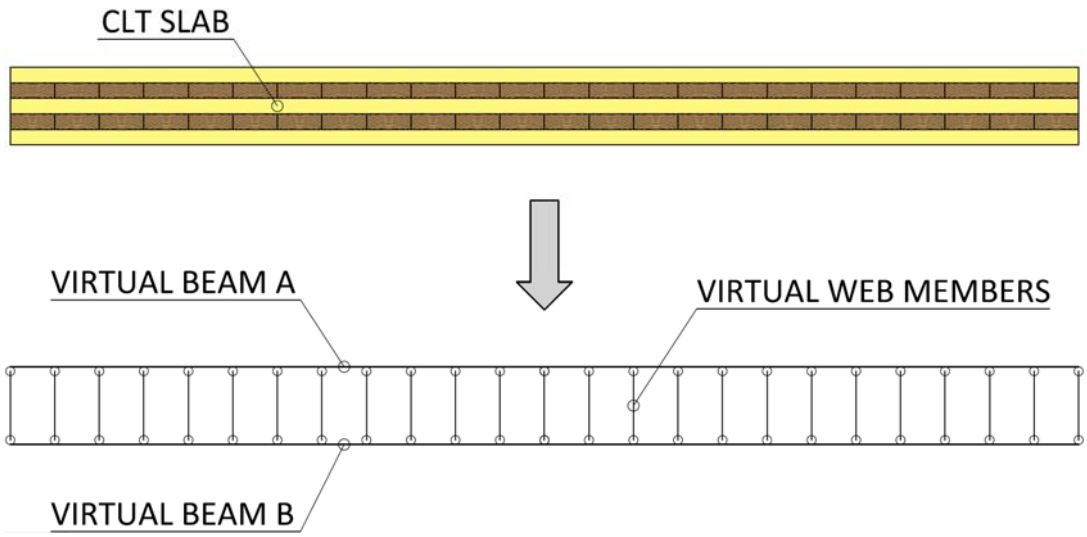

Figure 8: Visualisation of the shear analogy method

The method is based on the following assumptions with regard to the beams:

- The bending stiffness of beam A (EI_A) is equal to the sum of inherent flexural stiffness of individual longitudinal layers.
- The bending stiffness of beam B (EI_B) is equal to the sum of stiffness provided by the interaction of individual longitudinal layers through Steiner's parts.
- The shear stiffness of beam A (GA_A) is assumed to be infinite.
- The shear stiffness of beam B (GA_B) is equal to the sum of shear stiffness provided by each layer, and (if present) the stiffness of mechanical fasteners connecting the layers.
- The virtual web members connecting beams A and B have infinite axial rigidity, so that the virtual beams always undergo the exact same vertical displacement at any given point.

The deformation of the system is found by superimposing deflection caused by bending and shear:

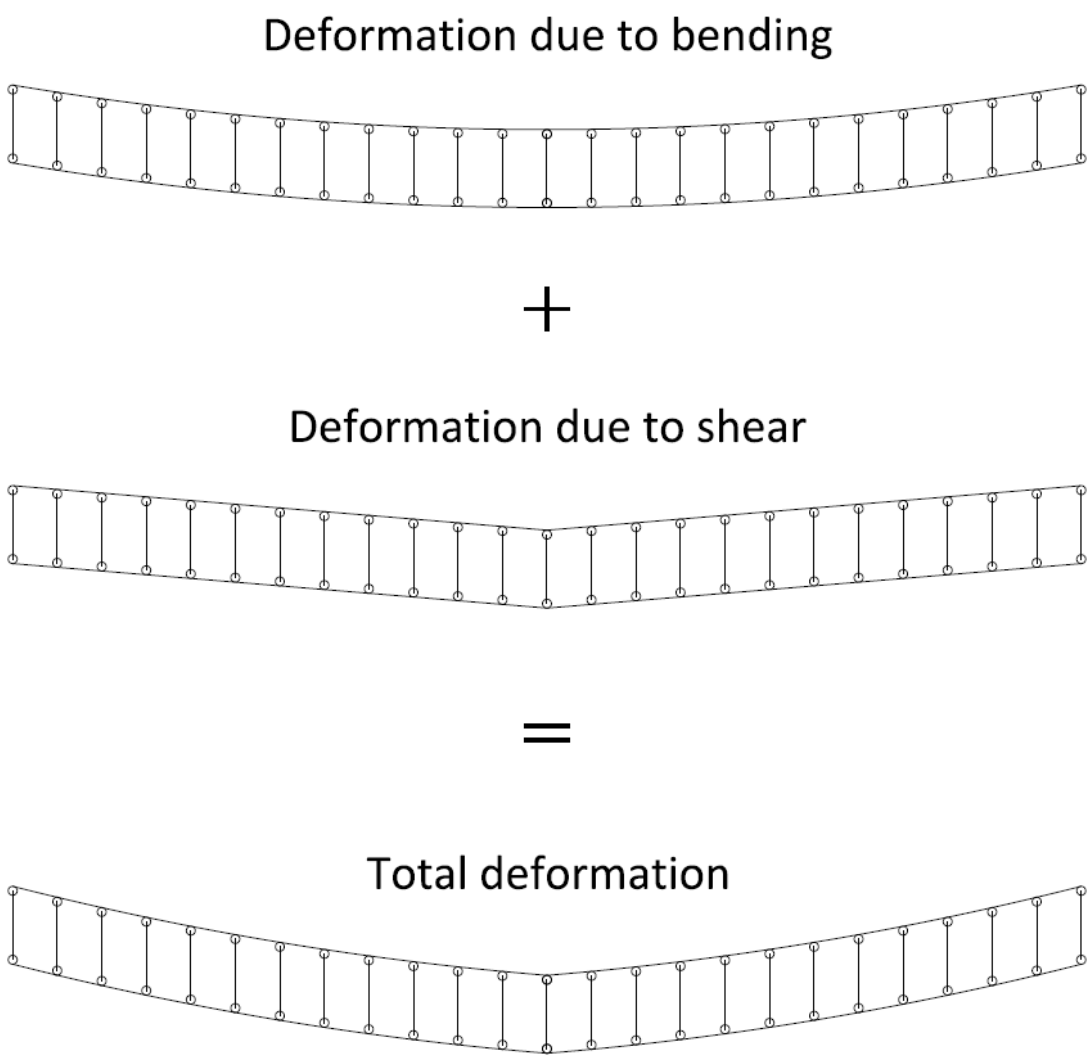

Figure 9: Deformation of virtual member system

Due to the vertical connection between the virtual beam members, the bending stiffness of the system EI_{eff} is equal to the sum provided by each member:

$$EI_{eff} = EI_A + EI_B \tag{11}$$

While the effective shear stiffness GA_{eff} is equal to that of beam B:

$$GA_{eff} = GA_B \tag{12}$$

In the case of CLT, the stiffness parameters EI_A, EI_B and GA_B of the virtual members can be expressed as follows:

$$EI_A = \sum_{i=1}^{n} E_i \cdot \frac{w \cdot h_i^3}{12} \tag{13}$$

Where:

E_i *represents the modulus of elasticity of each longitudinal layer*

w *represents the width of the panel (typically 1 meter)*

h_i *represents the thickness of each layer*

$$EI_B = \sum_{i=1}^{n} E_i \cdot A_i \cdot z_i^2 \tag{14}$$

Where:

A_i *represents the cross-section area of each longitudinal layer*

z_i *represents the distance between local and global centers of gravity*

$$GA_B = \frac{2 \cdot a^2}{\frac{h_1}{2 \cdot G_1 \cdot w} + \sum_{i=2}^{n-1} \frac{h_i}{G_i \cdot w} + \frac{h_n}{2 \cdot G_n \cdot w}} \tag{15}$$

Where:

a *represents the distance between the centers of the first and last layer*

G_1 *represents the shear modulus of the first layer*

h_1 *represents the thickness of the first layer*

G_n *represents the shear modulus of the last layer*

h_n *represents the thickness of the last layer*

G_i *represents the shear modulus of other layers*

h_i *represents the thickness of other layers*

w *represents the width of the whole panel – typically 1 meter*

In the case of a simply supported beam under a uniformly distributed load, the total deflection due to bending and shear can be expressed by the following formula:

$$u_{max} = \frac{5}{384} \cdot \frac{q \cdot L^4}{EI_{eff}} + \frac{1}{8} \cdot \frac{q \cdot L^2 \cdot k}{GA_{eff}} \quad (16)$$

While the deflection under a concentrated load in the middle of the span can be expressed as follows:

$$u_{max} = \frac{1}{48} \cdot \frac{P \cdot L^3}{EI_{eff}} + \frac{1}{4} \cdot \frac{P \cdot L \cdot k}{GA_{eff}} \quad (17)$$

In both cases, the first part of the expression represents deformation due to bending, while the second part represents deformation due to shear, where:

q *represents the evenly distributed load in equation (16)*

P *represents the concentrated load in equation (17)*

L *represents the span width of the beam in both cases*

k *represents the Timoshenko shear coefficient (6/5)*

Note that the Timoshenko shear coefficient is dependant on the Poisson's ratio of the material and the geometry of the cross-section. For materials with Poisson's ratio close to 0.3, the shear coefficient for a rectangular cross-section is approximately 6/5. This value is also used in the shear analogy method.

When the system undergoes deformation, the virtual members are subject to internal forces. The force distribution among each member can be found through finite element analysis, where certain calculation input must be assigned to each member. The cross-section data of both members must be equal to that of the real cross-section, while the material properties must be calculated based on cross-section data and numerical values for EI_A and EI_B, as expressed by equations (13) to (15):

$$A_A = A_B = w \cdot h_{tot} \tag{18}$$

$$I_A = I_B = \frac{w \cdot h_{tot}^{\,3}}{12} \tag{19}$$

Where:

A_A *represents the cross-section area of virtual member A*

A_B *represents the cross-section area of virtual member B*

I_A *represents the area moment of inertia for virtual member A*

I_B *represents the area moment of inertia for virtual member B*

w *represents the width of the actual cross-section (usually 1 meter)*

h_{tot} *represents the total height of the actual cross-section*

$$E_A = \frac{EI_A}{I_A} \tag{20}$$

$$E_B = \frac{EI_B}{I_B} \tag{21}$$

$$G_B = \frac{GA_B}{A_B} \tag{22}$$

Where:

E_A *represents the modulus of elasticity for virtual member A*

E_B *represents the modulus of elasticity for virtual member B*

G_B *represents the shear modulus for virtual member B*

Note that the shear modulus for virtual member A is assumed to be infinite.

Once the correct material parameters have been calculated and assigned to each virtual member, the finite element software can determine the force distribution among the members, as illustrated in the figure below. M_A and M_B represent bending moments acting on virtual member A and B, while V_A, and V_B represent the shear forces.

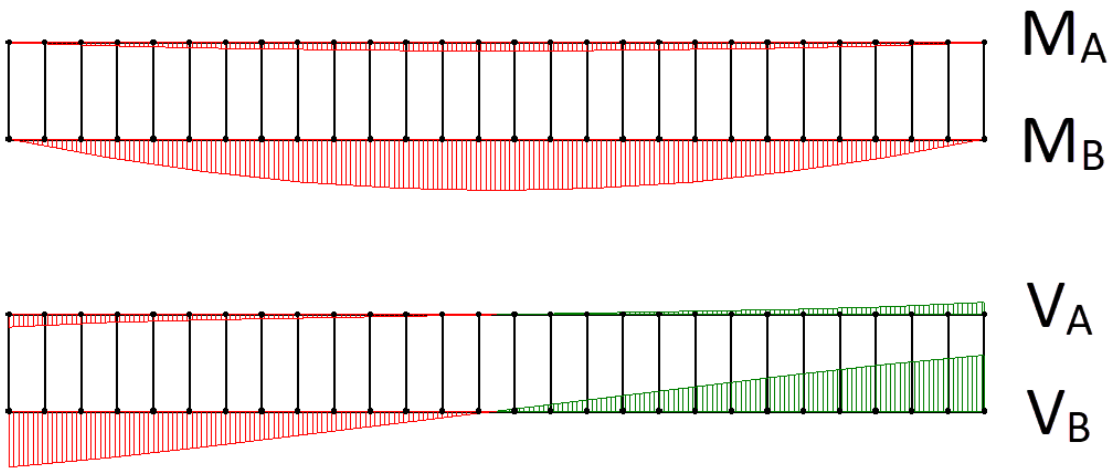

Figure 10: Force distribution among virtual members

The internal forces M_A, M_B, V_A, and V_B acting on the virtual beams can be broken down into real internal forces acting on each layer within the composite beam. M_A produces bending stress within each layer, while M_B produces normal forces. V_A produces local shear stress of parabolic distribution within each layer, while V_B produces a global shear stress that accumulates over the whole cross section. The total stress at any given point within the cross section can be found by superimposing all individual stress contributions, as illustrated below:

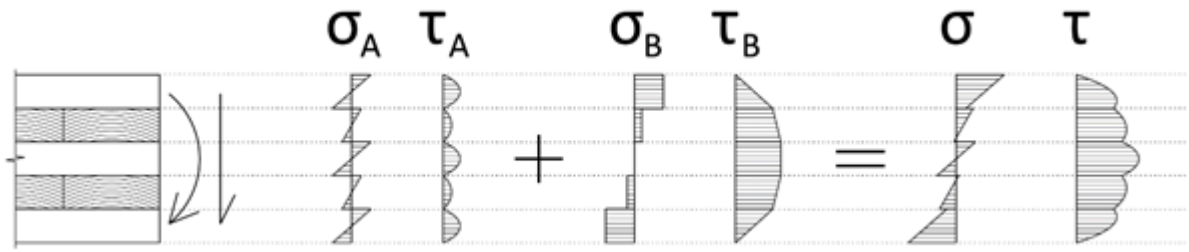

Figure 11: Total stress distribution within the actual cross-section

The magnitudes of the internal forces caused by bending moments acting on the virtual members can be expressed as follows:

$$M_{A.i} = M_A \cdot \frac{E_i \cdot I_i}{EI_A} \tag{23}$$

$$N_{B.i} = M_B \cdot \frac{E_i \cdot A_i \cdot z_i}{EI_B} \tag{24}$$

Where:

$M_{A.i}$ represents the local bending moment within the i'th layer, produced by $M_{A.}$

$N_{B.i}$ represents the local normal force within the i'th layer, produced by $M_{B.}$

Note that the actual modulus of elasticity for each layer now applies. The material parameters expressed by equations (20) to (22) are only used in the finite element analysis, in order to determine the force distribution among the virtual members.

Based on these local internal forces, the corresponding stress contributions can be calculated:

$$\sigma_{A.i} = \pm \frac{M_{A.i}}{I_i} \cdot \frac{h_i}{2} \tag{25}$$

$$\sigma_{B.i} = \frac{N_{B.i}}{A_i} \tag{26}$$

Where:

$\sigma_{A.i}$ *represents the maximum bending stress within the i'th layer, produced by* $M_{A.i}$

I_i *represents the local moment of inertia for the i'th layer*

h_i *represents the thickness of the i'th layer*

$\sigma_{B.i}$ *represents the normal stress within the i'th layer, produced by* $N_{B.i}$

A_i *represents the local cross-section area of each layer*

Note that equation (25) in the shear analogy method is analogous to equation (7) in the gamma method, while (26) is analogous to equation (8).

The parabolic shear stress within each layer, caused by the shear force acting on virtual member A can be expressed by the following formula:

$$\tau_{A.i} = -\frac{V_A \cdot E_i}{EI_A} \cdot \left(\frac{z_{0.i}^{\,2}}{2} - \frac{h_i^{\,2}}{8} \right) \tag{27}$$

Where:

$\tau_{A.i}$ *represents the local shear stress within the i'th layer.*

$Z_{0.i}$ *represents the local coordinate within the i'th layer, at which* $\tau_{A.i}$ *occurs.*

h_i *represents the thickness of the layer in question.*

Note that the maximum value $\tau_{A.i\_max}$ *is located at the center of the board, where* $z_{0.i} = 0$.

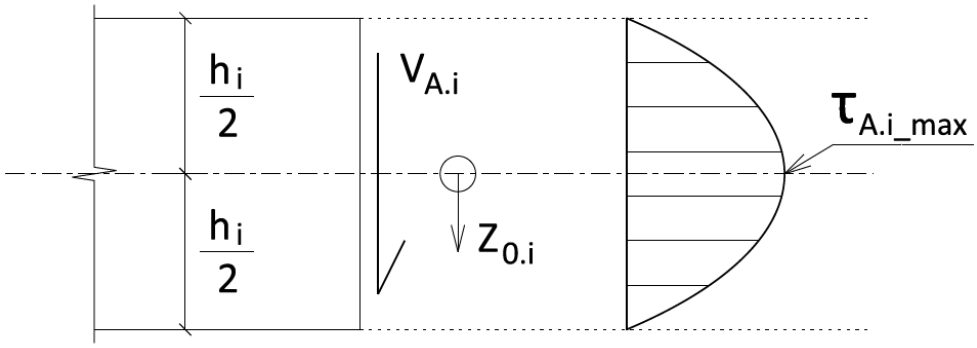

Figure 12: Parabolic shear stress within each layer

The global shear stress that accumulates through the whole cross-section, caused by the shear force acting on virtual member B can be expressed shown below , with the following values at the interface between layers:

$$\tau_{B.i\_0} = \frac{V_B}{EI_B} \cdot \sum_{i=1}^{n-1} E_i \cdot z_i \cdot h_i \tag{28}$$

$$\tau_{B.i\_1} = \frac{V_B}{EI_B} \cdot \sum_{i=1}^{n} E_i \cdot z_i \cdot h_i \tag{29}$$

Where:

$\tau_{B.i\_0}$ *represents the shear stress at the interface between the i'th and the previous layer.*

$\tau_{B.i\_1}$ *represents the shear stress at the interface between the i'th and the next layer.*

z_i *represents the distance from the global center of gravity to the local center of gravity for the i'th layer.*

h_i *represents the thickness of the i'th layer.*

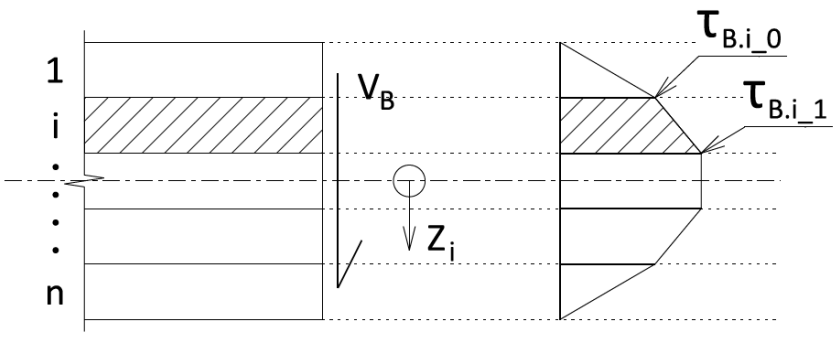

Figure 13: Accumulation of shear stress within the cross-section

4 EXPERIMENTAL INVESTIGATION

The experimental tests conducted in the study are described in detail in this chapter. The first part of the chapter contains material descriptions and preparations, while the experimental methodology is explained in the second part. The results are presented in chapter 5.

All experiments and were carried out at the laboratory for timber materials at the Norwegian University of Life Sciences (NMBU). The experiments were performed using hydraulic UTM testing machines from Instron, capable of recording applied loads and deformations.

For some of the experiments deformations were more accurately recorded using a state-of-the-art optical analysis system from LaVision. Length gauges from Heidenhain were also used to record deformations in some cases.

Material preparations were carried out at the NMBU laboratory, while the composite panels were assembled at the Norwegian Institute of Bioeconomy Research (NIBIO). The specimens were finally cut and prepared at the NMBU timber laboratory. All of the production stages are explained in the following chapter sections.

Materials

4.1.1 Fibre boards

The investigated material is a new type of fiber board product, produced from thermomechanical pulp by Norske Skog Saugbrugs. The mechanical properties of the material can be altered in a variety of ways, such as adjusting the refinement energy used to produce the pulp, adjusting density of the boards, or through the use of additives such as clay. An earlier study by Amthor (2018) [14] has shown how these kinds of modifications influence various material properties, such as thermal conductivity, fire properties, mechanical strength and modulus of elasticity. The table below was provided by the producer, and lists some material properties for various density grades:

Table 1: Density grades and material properties for fibre boards

Property	Unit	Grade 1	Grade 2	Grade 3	Grade 4	Grade 5	Grade 6	Grade 7	Grade 8	Grade 9	Grade 10
Density, kg/m3		125	125	200	200	250	250	300	300	400	400
Thickness after drying and sanding, mm		15	30	10	30	10	30	10	25	7	15
Grammage, g/m2		1875	3750	2000	6000	2500	7500	3000	7500	2800	6000
Production share, %		5	20	5	30	10	10	5	5	5	5
Refining energy		Low	Low	Low	Low	High	High	High	High	High	High
Thermal conductivity	W/(mK)	0,045	0,045	0,051	0,051	0,055	0,055	0,059	0,059	0,067	0,067
Fire, Figra		836	836	884	884	916	916	948	948	1012	1012
Hardness	N/mm2	0,045	0,045	0,087	0,087	0,160	0,160	0,188	0,188	0,244	0,244
Bending strength	MPa	0,423	0,423	0,731	0,731	1,414	1,414	1,620	1,620	2,031	2,031
Bending stiffness MOE	MPa	56,4	56,4	135,1	135,1	187,5	187,5	240,0	240,0	344,9	344,9
Compressive strength	MPa	0,122	0,122	0,260	0,260	0,431	0,431	0,523	0,523	0,707	0,707
Shear strength	MPa	0,142	0,142	0,297	0,297	0,474	0,474	0,577	0,577	0,783	0,783

All experiments conducted in this study were performed on samples with densities of 216kg/m^3 and 171kg/m^3, including an estimated 10% moisture content (according to the producer). The fibre boards were produced from pulp refined at 1600kWh per metric ton of material.

As described in chapter 3, the degree of composite action in CLT elements depends on the shear deformation within the transversal layers. This deformation is determined by the shear modulus of the material, a material property that had not been investigated before.

4.1.2 Timber boards

The timber boards used for the experiments were provided by Splitkon, a Norwegian producer of CLT elements. The boards belonged to a strength class of T22, according to NS-EN 338:2016 [15].

4.1.3 Glue

All composite panels that were produced for experiments were assembled using Prefere 4546, a liquid melamine urea adhesive produced by Dynea. The adhesive was used together with the liquid hardener Prefere 5022.

4.1.4 Material preparations

Due to the early stage manufacturing process of the fibre boards, the materials provided for the experiments had a rough surface texture that had to be improved before glue could be applied. Since the thickness varied a bit for each panel, it was decided to plan all panels down to 35mm.

Figure 14: Preparation of fibre boards

Allthough the planing did improve the texture of the material, there were still visible pits on the surface of the fibre boards after the procedure had been carried out. The panels were finally cut into samples measuring 600mm x 600mm, in order to fit into the manufacturing press that was available for the experiment.

The timber boards were also planed down to 35mm in order to improve and prepare the surface for glue application.

Figure 15: Preparation of timber boards

Most of the timber boards were cut into 600mm segments, in order to produce composite panels that would be used for shear tests and in-plane tests. Some boards were kept at full length, in order to produce a bending test specimen.

Figure 16: Pile of prepared materials

In order to achieve an approximate moisture content of 12% during the tests, all of the specimens were contained in a controlled environment at the NMBU timber laboratory for minimum one week, following the completion of the test samples.

Test configurations

In order to investigate the shear strength and shear modulus of the material, it was decided to set up an experiment closely resembling the procedure described in chapter 18 of EN 408 [16]. Although this method is designed to investigate the shear strength of timber parallel to the grain, the configuration was deemed suitable for the purpose, since deformations could be measured through the position of the loading cell. A similar method was recently used in a paper on hybrid CLT (Wang et al., 2017) [17], although deformations were measured locally on the samples in that study.

The impact of moisture content was evaluated by performing shear tests on samples that had been subject to extreme climatic conditions. Some of these tests also laid the basis for evaluation of delamination, combined with visual inspection of the test pieces.

The results from the shear tests were used to predict the stiffness of a composite beam. The beam was then produced and the actual stiffness investigated through a three point bending test.

In-plane loading tests were conducted on three different configurations of composite panels, replicating a setup suggested for regular CLT by Andreolli et al. (2012) [18].

4.2.1 Shear tests

As explained earlier, the shear deformation of the material separating the longitudinal layers is critical for the flexural behavior of CLT. The ratio of shear deformation to material thickness is commonly referred to as shear strain. The figure below displays a cube of height *h*, subject to a shear force *F*, and its corresponding shear deformation δ_v:

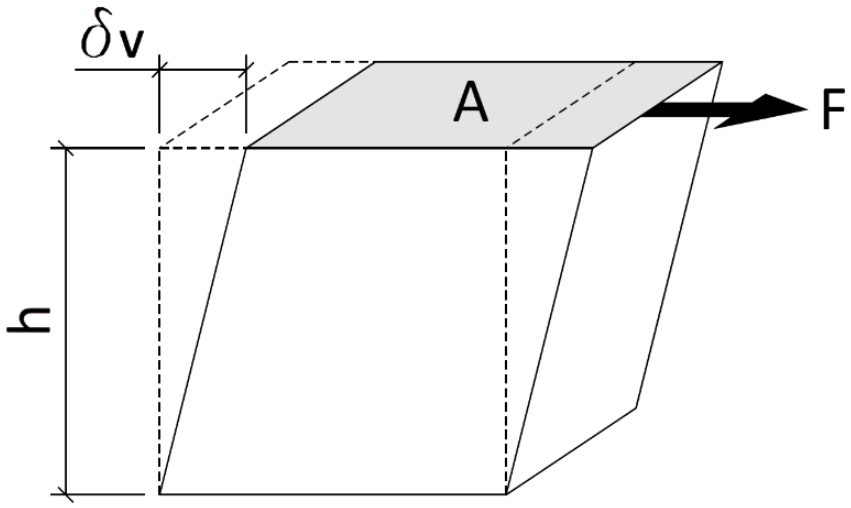

Figure 17: Shear deformations

For the cube in the picture, the shear stress τ, shear strain γ, and the relationship between them, also known as the shear modulus (G), can be calculated using the following expressions:

$$\tau = \frac{F}{A} \tag{30}$$

$$\gamma = \frac{\delta_v}{h} \tag{31}$$

$$G = \frac{\tau}{\gamma} \tag{32}$$

A similar deformation to what was illustrated on the previous page can be produced in experiments with the right kind of setup. In this study, shear deformations were produced by imposing a longitudinal force at one end of a composite beam segment. This force then had to be transferred through the central insulating layer in order to be taken up by a counteracting force at the opposite end of the specimen, as illustrated in the figure below.

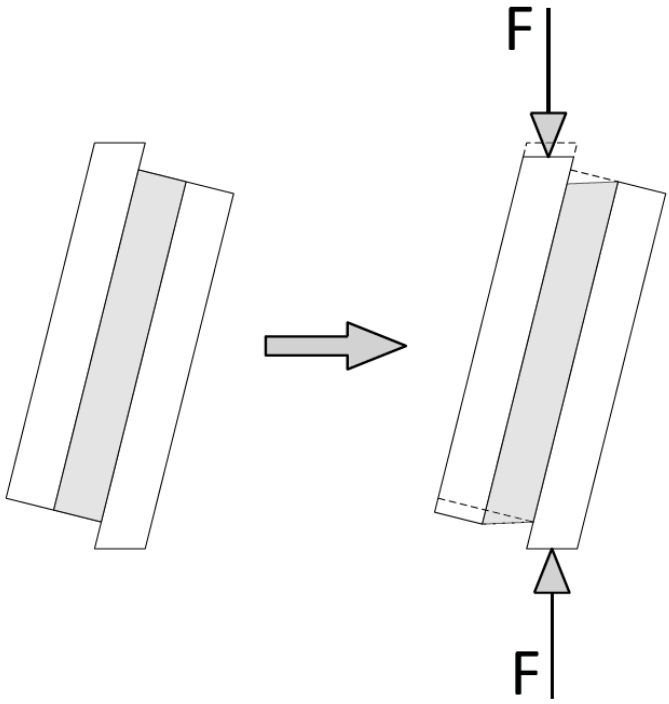

Figure 18: Deformation during shear test

The Instron machine that was used for the experiment recorded both deformations and forces in the vertical direction. The vertical force was then decomposed into a shear component parallel to the longitudinal direction of the specimen, and a perpendicular compressional component. The shear stress within the central layer could then be calculated using the following formula:

$$\tau = \frac{F \cdot cos(\alpha)}{A} \tag{33}$$

Where:

F *represents the measured vertical force.*

α *represents the angle between the sample neutral axis and the applied force (14˚).*

A *represents the effective shear area (width x length) of the central layer.*

Since the shear stiffness of the central layer was assumed to be lower than the modulus of elasticity, and because the shear component of the force was much larger than its perpendicular counterpart, the compressional deformation of the specimen was assumed to be negligible. The figure below illustrates how the samples were assumed to be deformed during the experiment.

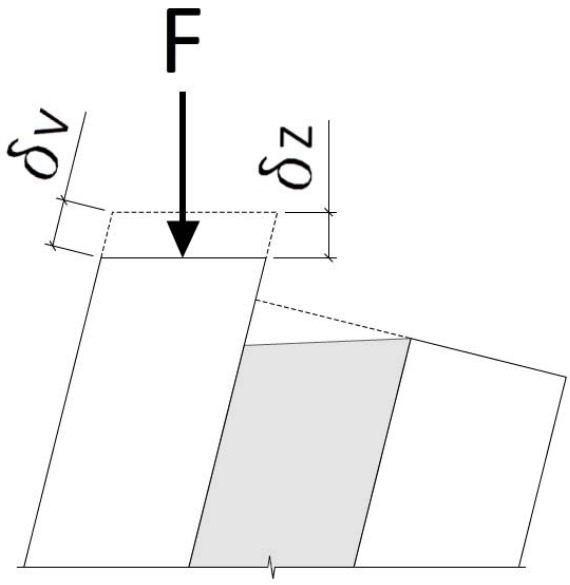

Figure 19: Shear deformation VS vertical deformation

From this assumption, it followed that the shear deformation in the longitudinal direction of the specimen could be expressed by the following formula:

$$\delta_v = \frac{\delta_z}{cos(\alpha)} \tag{34}$$

Expression (32) can then be restructured so that the shear modulus could be calculated directly from the data recorded by the Instron machine, taking the inclination of the specimen into account:

$$G = \frac{F_z}{\delta_z} \cdot \frac{h}{A} \cdot cos(\alpha)^2 \tag{35}$$

Due to the experimental nature of the study, no standardized procedure of manufacturing was available for the production of the composite panels. Glue application and pressure intensity had to be based on the information about the material available at the time.

One set of test samples was produced using the heaviest density grade (216kg/m^3), and a glue to hardener ratio of 100:50. Another set of test samples was produced from the lightest density (171kg/m^3), with a glue to hardener ratio of 100:25. In order to improve gap filling at the glue interface, it was decided to apply a relatively high amount of glue. For the first set of samples (heaviest density grade) 500g/cm^2 was applied. The amount was increased to 600g/cm^2 for the second set of samples (lightest density grade).

Technical datasheets from the glue supplier described a recommended pressure intensity of 0.6-1.0N/mm² for softwoods, and 0.8-1.2N/mm² for hardwoods. Due to the low compressive strength of the fibre boards, it was however decided to restrict the pressure intensity to 0.1N/mm^2 during the curing process. The pressing time was set to 120 minutes for the first set of samples, and 210 minutes for the second set.

Figure 20: Manufacturing of composite CLT panel at NIBIO

The composite panels were sliced into board width samples after the curing process was done. The smaller samples were then trimmed along the edges, so that all samples measured 90mm in width. The shear test specimens were then cut from the 90mm panel segments.

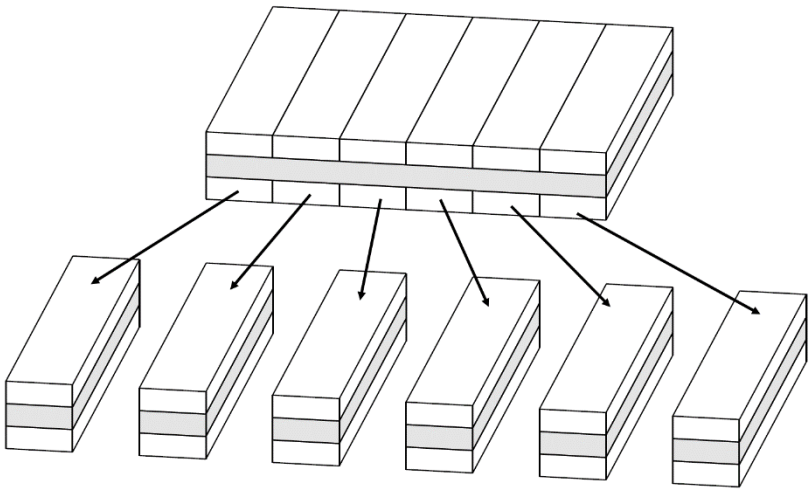

The test pieces were prepared so that the angle between the load direction and the longitudinal axis of the test pieces was 14°. The sample lengths were then adjusted to ensure that the points of loading would be located directly above each other. The figure below displays the cut configuration of test pieces using single and double insulation layers in the middle of the specimens.

In order to prevent compression in the longitudinal direction of the central layers, it was decided to remove some of the material near the ends of the test pieces. This removal of material was exactly equal for all samples belonging to the same setup configuration. The effective contact length between timber and fibre boards was adjusted to 250mm for all specimens containing single fibre board layers, and to 350mm for all specimens containing double layers.

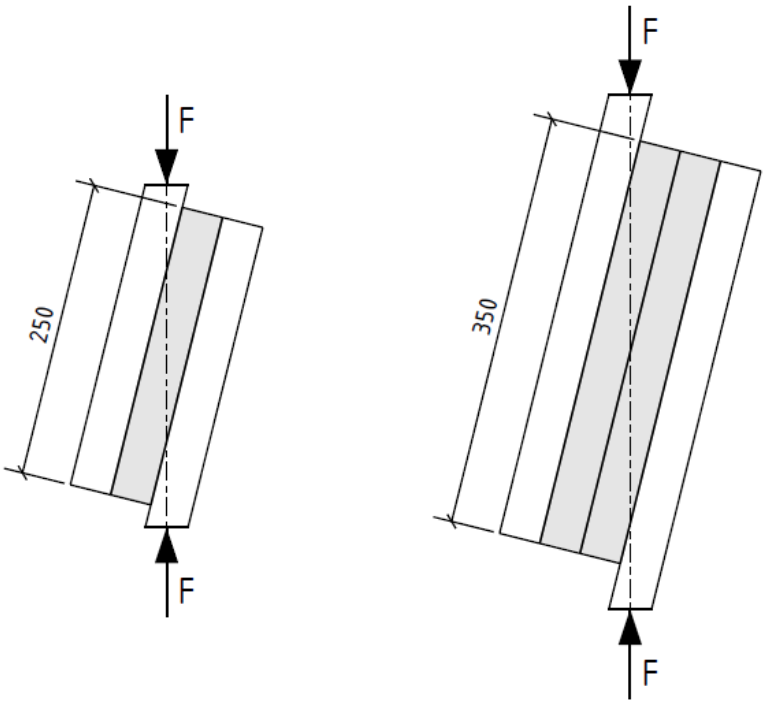

Figure 23: Geometry of shear test specimens

Single layer test samples were produced from both density grades. All of the samples were completed with the following geometric parameters:

- Effective shear area (A_{ef}) of the central insulation layer : 22500mm^2 (90mm x 250mm)
- Effective thickness of central layer: 35mm

Double layer test samples were only produced from the highest density grade. All of the samples were completed with the following geometric parameters:

- Effective shear area (A_{ef}) of the central insulation layer: 31500mm^2 (90mm x 350mm)
- Effective thickness of central layer: 70mm

The majority of the tests were performed on test pieces that had been contained at standard climatic conditions at the laboratory, having an approximate moisture content of 12%. Average performance values were determined from these tests. In order to evaluate the sensitivity to moisture variations, a smaller set of samples were subject to extreme climatic conditioning, so that results from these samples could be compared to the averages from tests at standard conditioning:

- One sample (heaviest density grade) was contained at 87% relative humidity for one week.
- One sample (heaviest density grade) was submerged in water for one week.
- One sample (heaviest density grade) was contained in a drying closet (103°C) for one day.
- Five samples (lightest density grade) were submerged in water for three weeks and then contained in a drying closet (103°C) for 20 hours.

The vertical load was applied at a constant speed, varying from 0.3mm to 0.5mm per minute, in order to produce a failure within 300 seconds +/- 120 seconds. The picture below shows a finished sample ready to be tested.

Figure 24: Experimental setup for shear tests

One shear test of the lowest density grade was analyzed using an optical analysis system from LaVision. This system works by analyzing deformations within a grid on the surface of the material, using cameras and digital image correlation algorithms. The grid used for the analysis was painted onto the material using white and black paint. The paint was applied using spray cans. The figure below shows a section of the painted specimen.

Figure 25: Grid painted onto a test sample

The system was used to measure local vertical deformations within the specimen, and compare those to the vertical movement of the loading cell. In addition, the actual shear deformation of the test piece was measured, in order to verify the hypothesis that compressional deformations were negligible. The figure below shows a screenshot from the LaVision software.

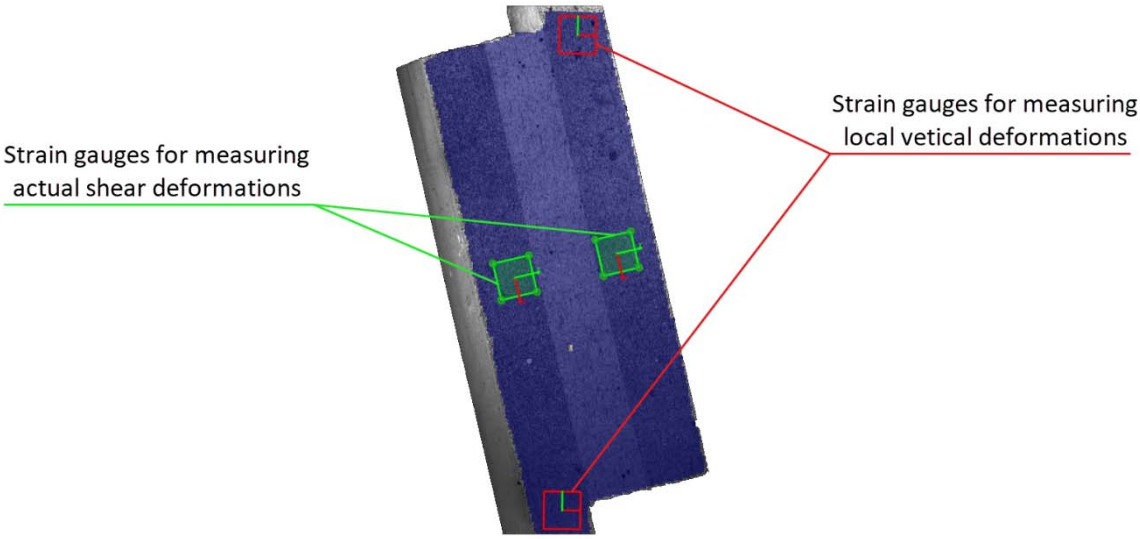

Figure 26: Optical analysis of local deformations

The difference in registered vertical deformations within the red squares was used to determine the vertical deformation of the specimen, while the difference registered in longitudinal deformation within the green squares was used to determine the actual shear deformation.

4.2.2 Delamination tests

When CLT is subject to fluctuating moisture levels, internal stress will build up, due to the prohibition of swelling and shrinking of individual boards. This will in turn produce tensile stress perpendicular to the glue lines, so that delamination might occur if the bonding quality is not sufficient. Since this phenomenon deteriorates the quality of CLT, EN 16351 [19] sets specific requirements to the bonding quality of the gluelines.

A standardized testing procedure is described in annex C of the standard, describing a test cycle where a pressure vessel is used to control the moisture content of the material. Such equipment was not available for this experiment, so an alternative method had to be improvised. In order to maximize deformations caused by swelling and shrinkage, the materials were soaked in water for about 3 weeks and then dried in a drying closet at 103°C for 20 hours.

According to the standard, if the delamination length cannot be determined sufficiently through visual inspection, the specimen is to be split using a wedge and hammer. Due to the flexible structure of the insulation material, this would be impossible. An alternative method of splitting the materials therefore had to be found. It was decided to split the specimens by following the shear test procedure, to investigate if the climatic cycle had impaired the bonding quality.

Four cubical test pieces were produced for visual inspection of the glueline, while five shear test pieces were produced in order to inspect the glueline after mechanical separation of the materials. The rectangular test pieces measured 100mm in length, while the shear test pieces were produced with the same geometry as previously investigated single layer samples.

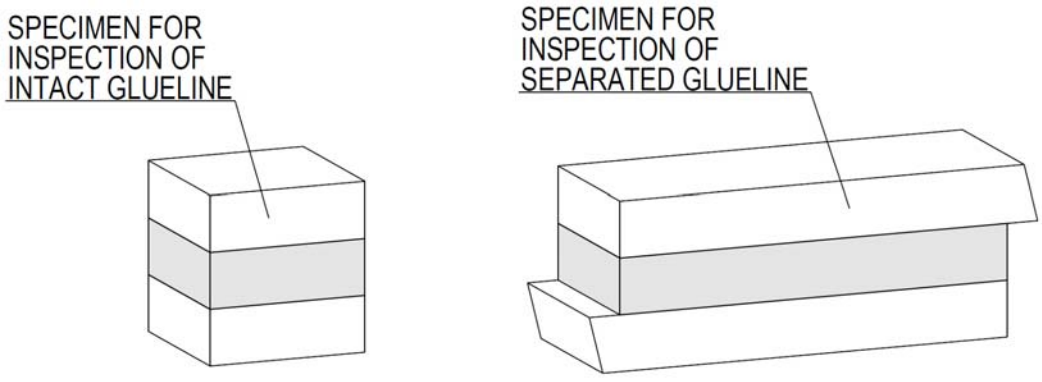

Figure 27: Delamination test pieces

4.2.3 Bending test

Based on results from the shear tests and conventional calculation methods for CLT, it was possible to make theoretical predictions regarding the flexural behavior of conceptual composite structures where the fiber boards are used as a structural layer. However, such theories can only be verified through experimental tests. A composite beam was therefore produced in order to study the composite behavior more directly.

As explained in chapter 3.2 the flexural stiffness of a composite beam is made up of two parts. The first part, described by equation (13), comes from the local bending stiffness of individual layers, and is not dependent on the composite action between them. The second part, described by equation (14) is on the other hand dependent on the composite action within the beam. By designing a beam where the composite part makes up the majority of the total stiffness, the shear modulus of the central layer will have a large influence on the deformation during a bending test.

When a beam is subject to an increasing load, there is a linear relationship between the applied load and the following vertical deflection, given that the load is of moderate magnitude compared to the capacity of the beam. This means that the static system of a simply supported beam can be represented by a spring, with an equivalent stiffness K_{eq}:

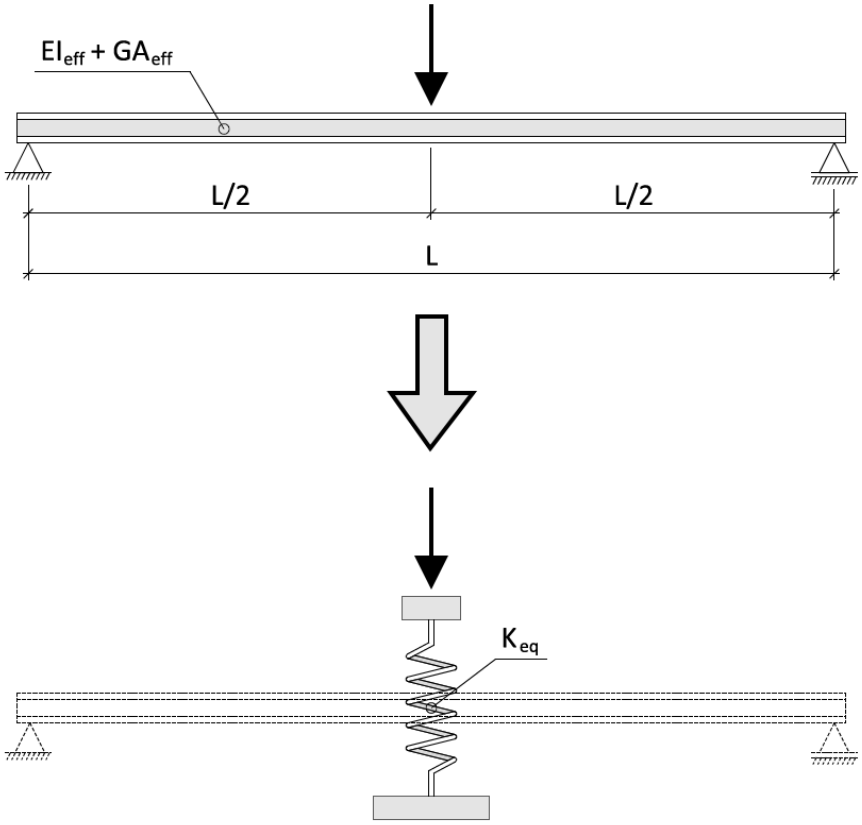

Figure 28: Simply supported beam represented by an equivalent spring

The stiffness of the equivalent spring can be expressed mathematically, by modifying the equation governing the deflection of a beam under a concentrated load in the middle of the span. Using the stiffness parameters calculated with the shear analogy method, equation (17) gives the following formula for the stiffness of the spring, taking the effect of composite action into account:

$$K_{eq} = K_{eff} = \frac{1}{\frac{L^3}{48 \cdot EI_{eff}} + \frac{L \cdot \kappa}{4 \cdot GA_{eff}}} \tag{36}$$

Where:

EI_{eff} is the effective bending stiffness according to the Shear Analogy Method

GA_{eff} is the effective shear stiffness according to the Shear Analogy Method.

By substituting the stiffness parameters EI_{eff} and GA_{eff}, the stiffness of the spring can be expressed so that the formula satisfies the condition of no composite action. In this case, EI_0 and GA_0 represent the local bending stiffness and shear stiffness of the two outer layers:

$$K_{eq} = K_0 = \frac{1}{\frac{L^3}{48 \cdot EI_0} + \frac{L \cdot \kappa}{4 \cdot GA_0}} \tag{37}$$

By recording the actual applied force and the corresponding vertical deflection of the beam, the real stiffness K_{real} of the system can be measured directly, and compared to the stiffness expressed by equations (36) and (37), in order to evaluate if composite action has been achieved. If all other geometric and material related parameters are known, an approximate value for the shear modulus of the central layer can also be found by iteration.

The beam was assembled from two timber boards, and three strips of insulation material. Since the fibre boards only acted as shear connectors between the outer layers, the discontinuity of the central layer did not matter. The beam was assembled using clamps, since the pressing machine available for the experiment was restricted to a maximum size of 600mm x 600mm. Because of the uncontrolled pressure intensity, the glue spread was increased to 925g/m^2, using a total of 200 grams of glue. The glue was mixed with a pbw ratio of 100:50 and applied with a ribbon spreader.

Figure 29: Assembly of the bending test specimen

In order to highlight the performance of the insulation material, the outer layers of the beam were adjusted before the experiment was conducted. It was calculated that a thickness reduction of these layers would have a much larger impact on their local bending stiffness than on the stiffness produced by composite action. The geometrical data for the beam during the test were as follows:

- Span width of the static system: 1750mm
- Beam width: 80mm
- Thickness of outer layers: 20mm
- Thickness of central insulation layer: 35mm

In order to record data within the elastic range of the beam, the capacity was estimated using FEM-Design 18. The load during the test was applied in three cycles, ranging from approximately 10% to 40% of the estimated capacity. The load was applied at constant speed of 10mm per minute. The stiffness of the beam was calculated from a force/deformation linear regression, based on data from the third loading cycle.

4.2.4 In-plane tests

In order to fulfill all desired mechanical functions of a structural panel, floor and roof elements must have sufficient in-plane integrity to work as diaphragms, transferring horizontal load effects to the stabilizing bracing system or shear walls of a building. Similarly, if insulated CLT is to be used as walls, shear wall functionality is obviously desired. Since the main goal of this study is to evaluate practical aspects of the insulation material, an experiment was set up to investigate the in-plane shear stiffness of insulated CLT panels.

Three different panel configurations were manufactured and tested through diagonal compression, a method proposed by Andreolli et al. (2012) [18]. Deformations were recorded for the central part of the panels, using cameras and the image correlation system from LaVision.

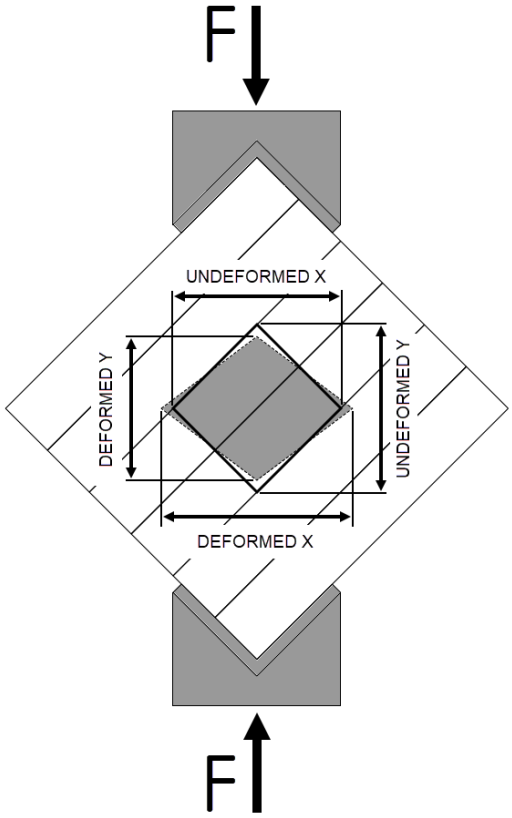

Figure 30: Deformation of in-plane tests

The recorded data was used to derive the shear modulus of an equivalent panel made from a linear elastic homogeneous and isotropic material. This mathematical operation was done according to a method described in a master thesis written at the university of Trento (D'Amato, 2012) [20], taking the stress distribution within the area of measurement into account (Frocht, 1931) [21]. The equivalent shear modulus was calculated from a stress/strain linear regression for each panel.

For CLT panels subject to in-plane shear there are three main the three main modes of failure (Brandner et al., 2013) [22]. These three modes are net-shear (shearing perpendicular to the grain), gross-shear (shearing parallel to the grain) and torsion. Because the panels investigated in this study were produced without edge bonding, only two of the mentioned modes of failure were relevant, namely net-shear and torsion.

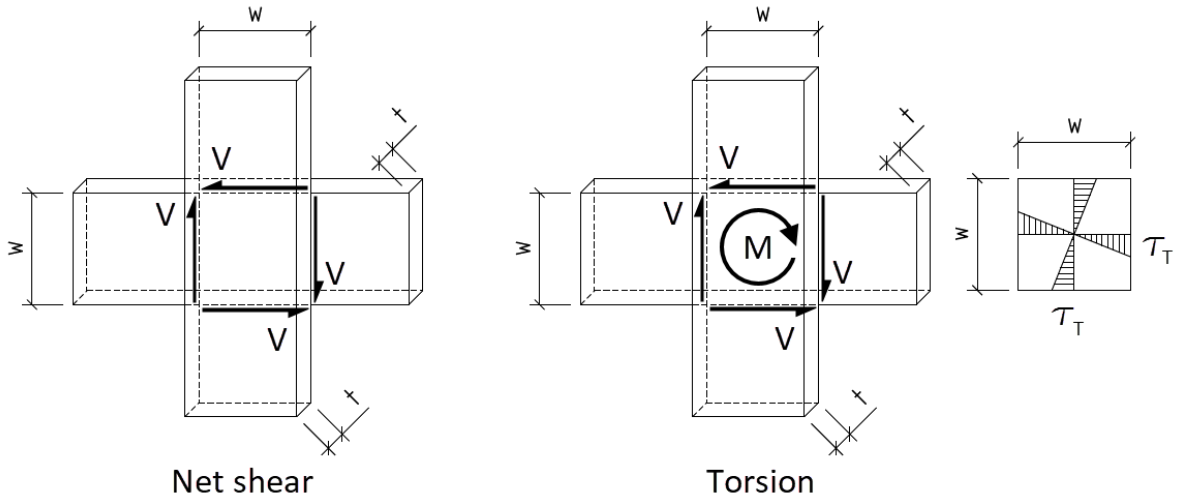

Figure 31: Net shear and Torsion in CLT panels

The stress from net shear is caused by forces being transfered via the cross-sections of the boards, while the stress from torsion is due to prohibition of rotation in the glue interface between board layers. The stress values for each mechanism are described by these formulas respectively:

$$\tau_V = \frac{V}{w \cdot t} \tag{38}$$

$$\tau_T = \frac{M}{I_p} \cdot \frac{w}{2} = \frac{3 \cdot V}{w^2} \tag{39}$$

Where:

V	*represents the shear force that is transferred via the cross-section of a board*
M	*is the torsional moment acting on the glue interface between two boards*
Ip	*is the polar moment of inertia for the glue interface*
w	*represents the width of the board (100mm for the investigated panels)*
t	*represents the thickness of the board (35mm for the investigated panels)*

Since the mechanical properties of the insulation material are weak compared to regular timber, they are likely to cause limitations with respect to in-plane behavior. It was however hypothesized that this problem could overcome, by encapsulating the insulation layer with cross laminated timber on both sides. The experiment was designed to verify this hypothesis. Out of the three panels that were made for the tests, two panels were designed so that shear forces had to be taken up by the fibre boards, while the third panel was designed to mainly take up shear forces in the outer cross laminated layers. The lay-up of each panel configuration is shown in the figure below.

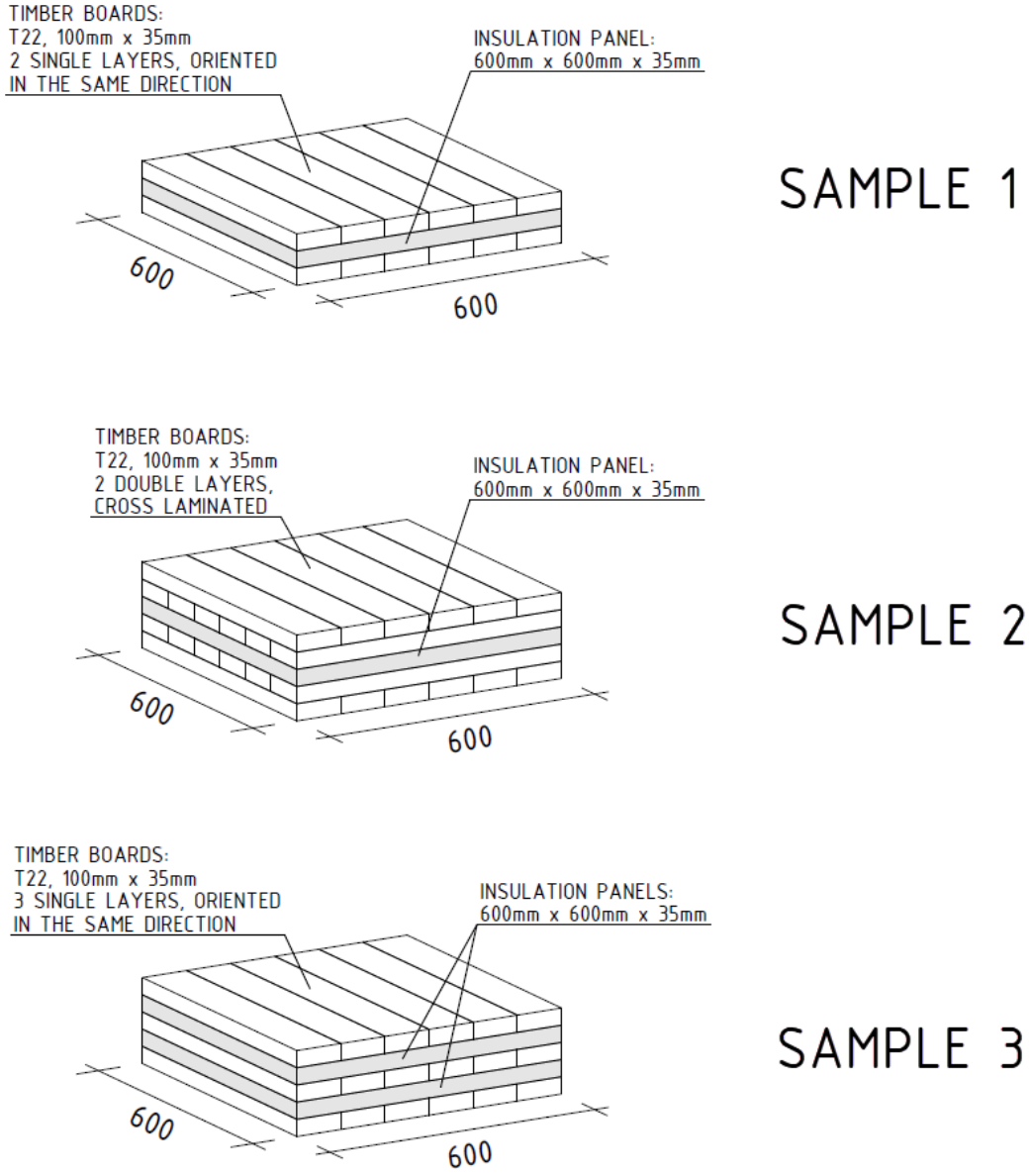

Figure 32: Lay-up of panels produced for in-plane tests

All insulation panels that were used for the in-plane tests belonged were taken from the lowest density grade (171kg/m^3). The glue to hardener ratio was 100:25, and the glue spread was 500g/m^2 for all interfaces. The two cross laminated timber panels used for sample 3 were cured separately for 135 minutes under a pressure intensity of 1,0 N/mm^2, while the rest of the materials were cured for 210 minutes, at a pressure intensity of 0,1N/mm^2.

To ensure an even distribution of pressure during the loading cycles, the panels had to be trimmed along the edges. Upon completion each panel measured approximately 575mm along each side. The figure below shows the three panels.

Figure 33: In-plane test samples upon completion

The grids for the optical analysis were painted onto the panels using white and black paint, applied with roller brushes. The figure below shows a painted section from the central part of one sample.

Figure 34: Analytical grid as painted onto samples

The panels were placed in a welded steel plate fitting, placed on the base of the Instron machine. A similar fitting was connected to the loading cell pushing down on the panels. The fittings were designed to make sure loads would be applied to all four 45° contact areas. The picture below shows how the panels were placed during the tests.

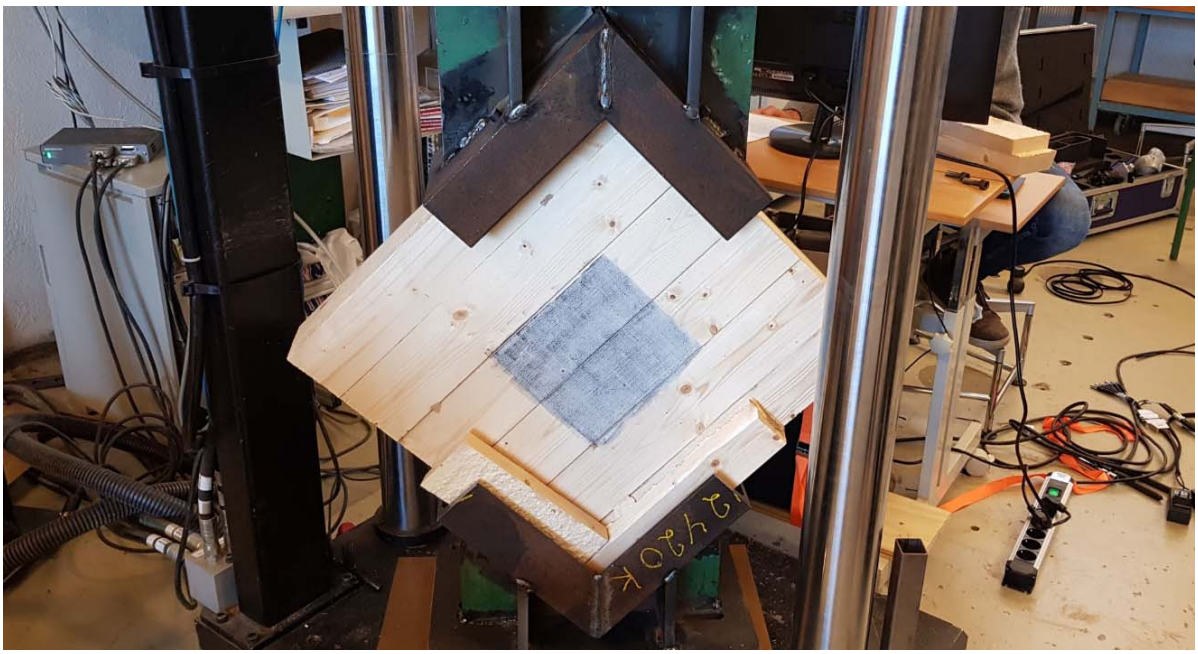

Figure 35: Experimental setup for in-plane tests

In order to record data within the elastic range of the panels (ranging from 10% to 40% of the theoretical maximum load), the capacity of each panel had to be estimated. This was done with help from Francesco Boggian at the Univresity of Trento. His contribution can be found in appendix A of this thesis. The following theoretical capacities were estimated for the panels:

- Sample 1: 4.6kN
- Sample 2: 9.1kN
- Sample 3: 208kN

The load during the tests was applied in three cycles, ranging from approximately 10% to 40% of the estimated capacities. The load was applied at constant speed (0.5mm per minute for sample 1 and 2, and 1.0mm per minute for sample 3). The equivalent shear modulus for each panel was calculated based on recorded data from one of the two final loading cycles.

Local vertical and horizontal deformations were measured through virtual extensometers available through the LaVision software. The virtual extensometers were 200mm long in all cases.

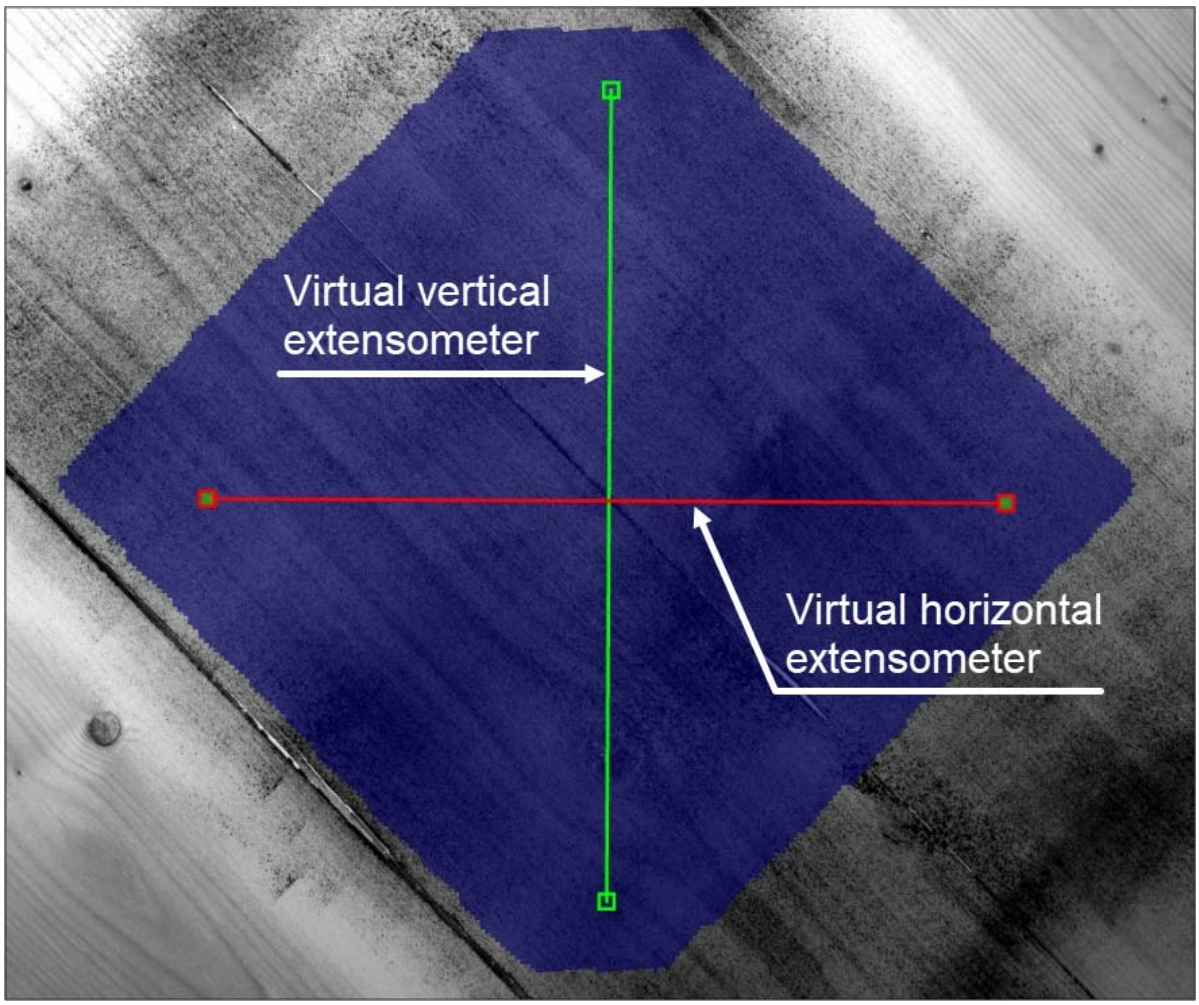

Figure 36: In-plane deformations, virtual extensometers

5 RESULTS

The results from the experimental tests are presented in this chapter, along with a short discussion of each experiment. Future research and the prospects of the material are discussed in chapter 6.

The results from the shear tests are presented in a table, as well as through graphical plots, displaying force-displacement diagrams where the maximum load is marked for each sample. The findings from the optical analysis are supplemented with an illustration and a stress-strain diagram.

The results from the delamination tests are presented through written descriptions, along with pictures that were taken as a part of the investigation.

The result from the bending test is presented graphically, along with theoretical predictions regarding the stiffness of the beam, calculated using the shear analogy method.

The results from the in-plane tests are presented graphically, showing plots of active and passive deformations as well as stress-strain diagrams for each panel.

Shear tests

The tests revealed that the insulation material can be glued to timber with sufficient bonding quality. None of the tests showed failure in the glue interface, apart from in very restricted local areas. The picture below shows the typical mode of failure, which was equal for all samples.

Figure 37: Typical mode of failure for shear tests

There was no visible difference between samples glued with different amounts of glue. It seems reasonable to assume that sufficient bonding quality could also have been achieved with a lower glue spread than what was used.

The characteristic shear strengths (5-percentile) was calculated for each configuration with respect to layers, density grade and moisture content. This was done in accordance with EN 14358 [23]. Mean values were also calculated, both for the recorded shear strength and for the shear modulus.

The optical analysis showed that the assumption that was made in chapter 4.4, regarding the deformation of the test pieces was wrong. This is further explained in chapter 5.1.1. As a result, the values that were calculated for the shear modulus were underestimated by a large margin. The values are still listed in the table below, to give an idea of the relative stiffness variance for each configuration, and to highlight the importance of measuring technique when investigating the shear modulus in this kind of test.

Table 2: Shear test performances

Type of configuration	Number of tests	Avg. shear strength [MPa]	Char. shear strength [MPa]	Avg. Shear modulus [MPa]
Single layer, heavy (Standard moisture)	7	0.317	0.282	8.838*
Single layer, light (Standard moisture)	5	0.249	0.219	8.187*
Double layer, heavy (Standard moisture)	6	0.265	0.234	9.891*
Single layer, heavy (Low humidity)	1	0.160	-	8.883*
Single layer, heavy (High humidity)	1	0.178	-	5.339*
Single layer, heavy (Soaked in water)	1	0.011	-	0.656*
Single layer, light (Delamination tests)	5	0.059	0.033	1.542*

* The listed values for average shear modulus are incorrect, due to the incorrect assumption regarding the deformation of the specimens. See chapter 5.1.1.

5.1.1 Optical control analysis

The optical analysis revealed important information about the deformation of the test pieces, rejecting the assumptions that were made in chapter 4.4. The findings from the optical analysis can explain why the shear modulus of the insulation material was underestimated by the original tests.

There was a large difference between the recorded position of the loading cell and the vertical deformation of the test pieces. When the vertical deformations were recorded for two small segments at each end of the test piece, the actual vertical deformation was found to be much smaller than the vertical movement of the loading cell. In addition, the analysis revealed horizontal deformations at the top end of the specimen. This horizontal movement indicates rotation of the specimen, which might have allowed some vertical deformations to take place without producing shear deformations in the insulation material.

The analysis also showed that perpendicular deformations of the insulation material were in fact not negligible. When longitudinal and perpendicular deformations were recorded for two segments at the central part of the specimen, the perpendicular deformations were found to be considerably larger than the longitudinal shear deformations.

The described findings are illustrated in the figure below, marking the areas where the deformations were recorded and listing the measured displacement values. The values were calculated based on data from the elastic range of the force-displacement curve, ranging from 10% to 40% of the maximum force.

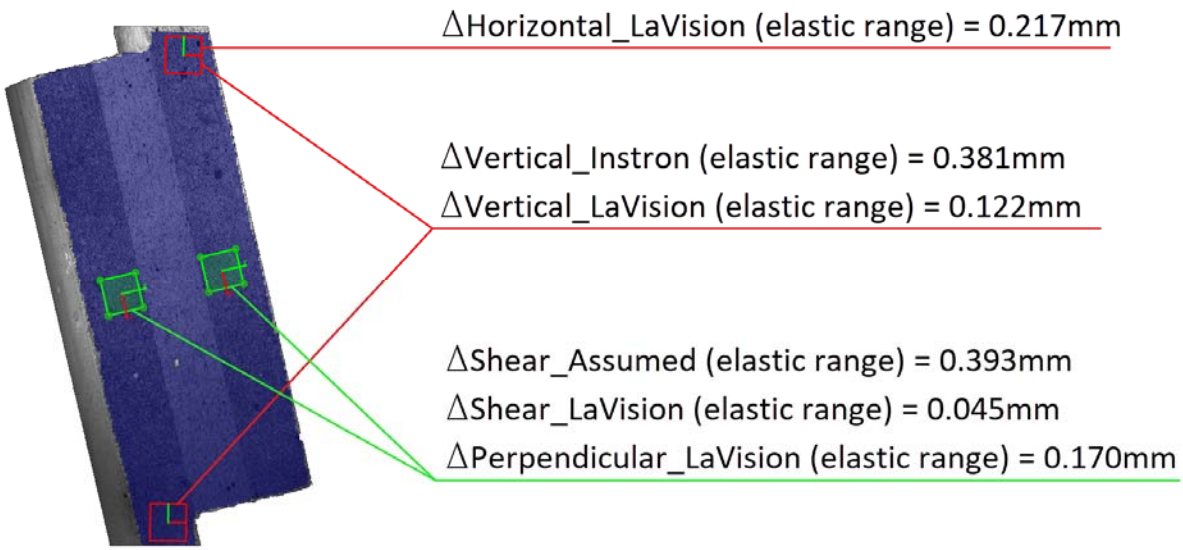

Figure 38: Measured horizontal, vertical and shear deformations - Instron VS LaVision

The figure below illustrates the difference between the vertical deformation of the test piece and the movement of the loading cell. Note that the red curve representing the vertical deformations from the LaVision software is considerably steeper than the black curve representing the movement of the loading cell.

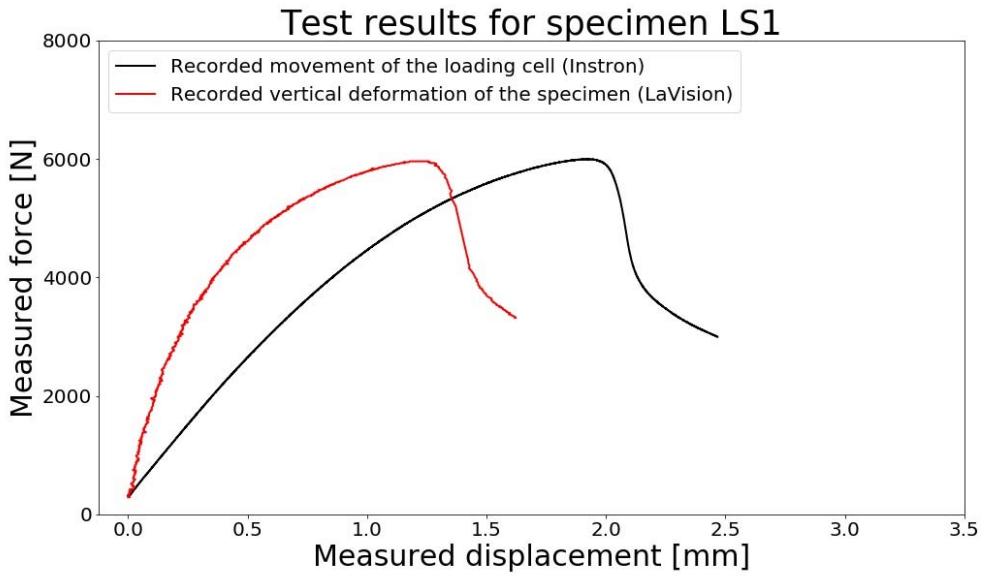

Figure 39: Force/displacement diagram - Instron VS LaVision

When the measured shear deformations were implemented in the calculations, the value for the shear modulus of the insulation material was increased to 52.57N/mm^2 (from 7.39N/mm^2). The new value agrees much better with the results from the bending test than the original, as will be shown in chapter 5.3.

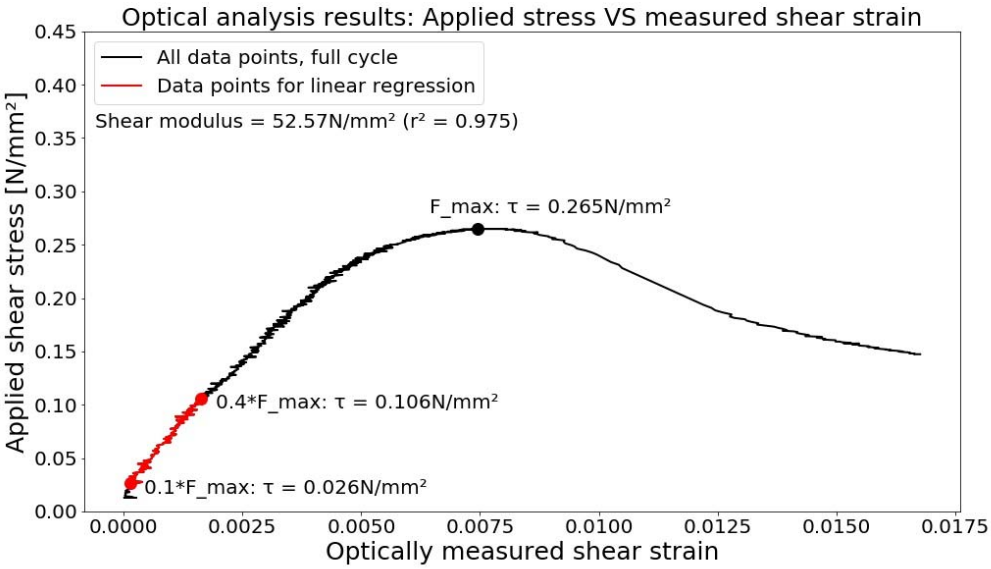

Figure 40: Stress/strain diagram - Instron VS LaVision

5.1.2 Graphical results: Single layer, higher density grade, standard moisture content

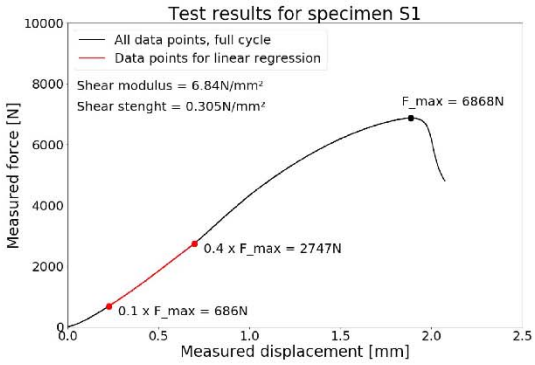

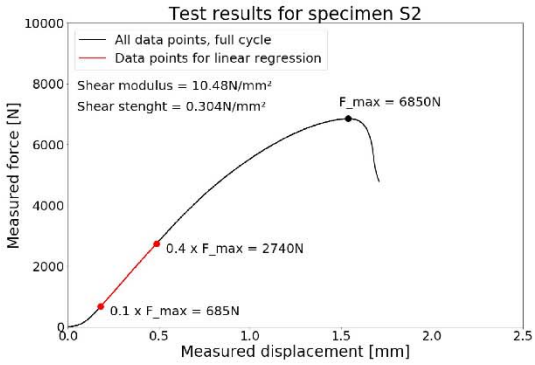

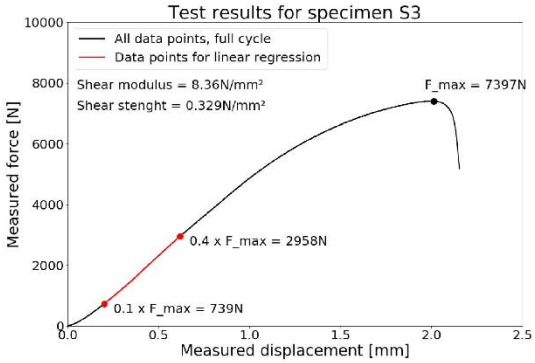

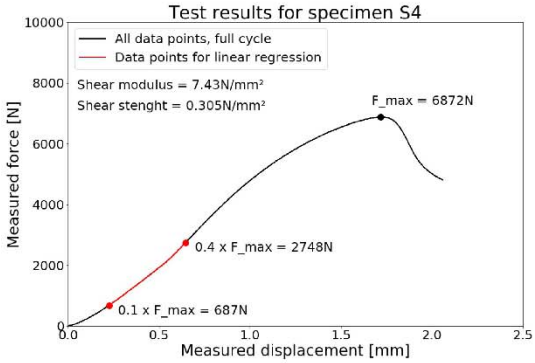

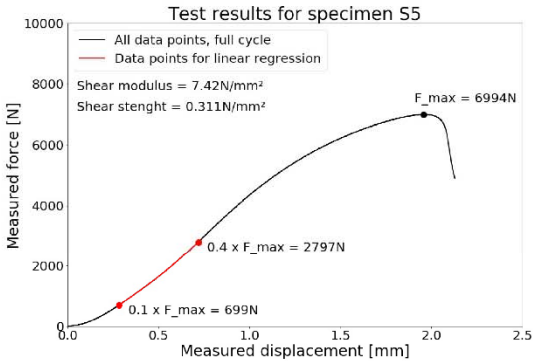

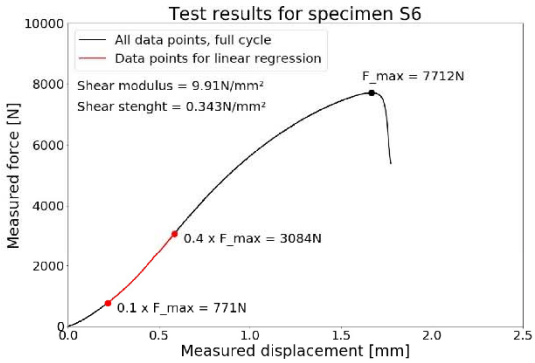

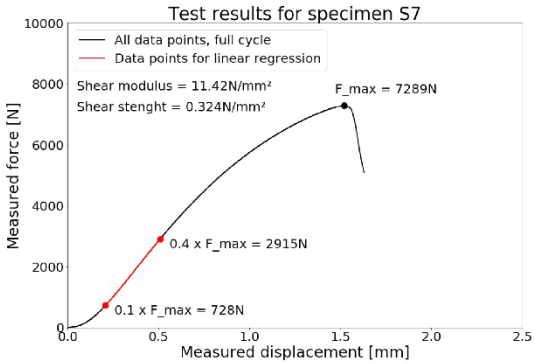

5.1.3 Graphical results: Single layer, lower density grade, standard moisture content

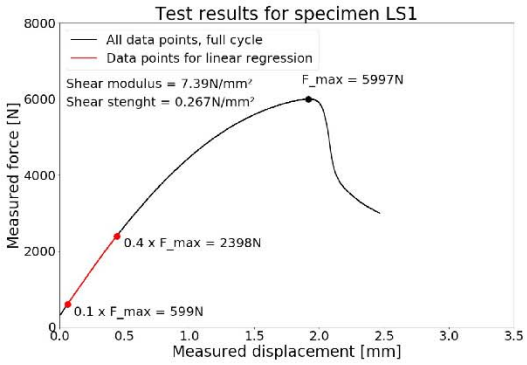

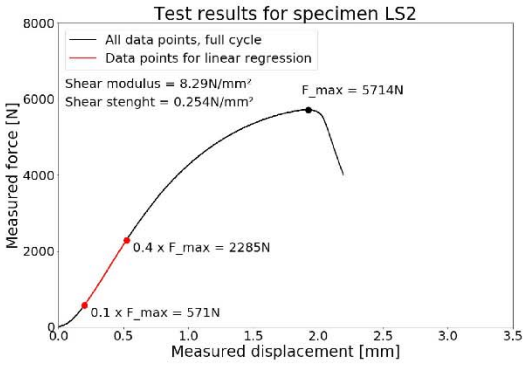

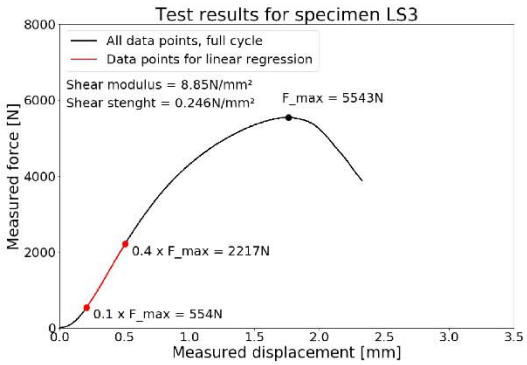

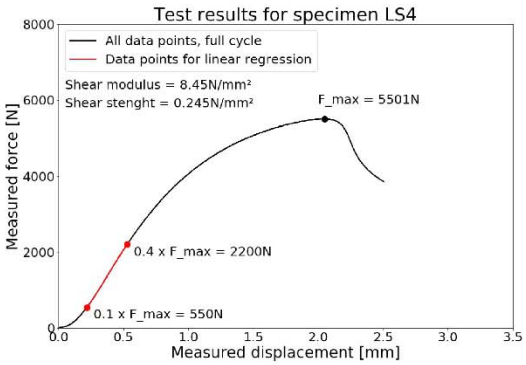

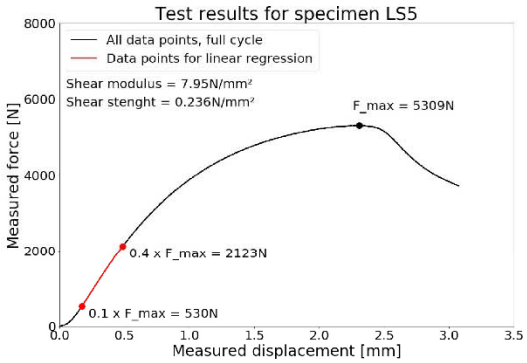

5.1.4 Graphical results: Double layer, higher density grade, standard moisture content

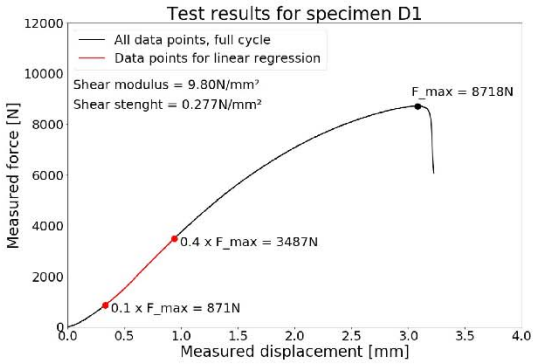

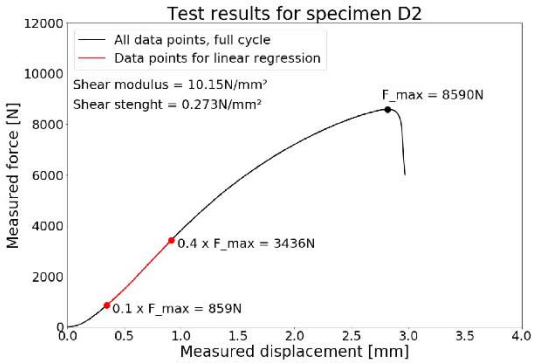

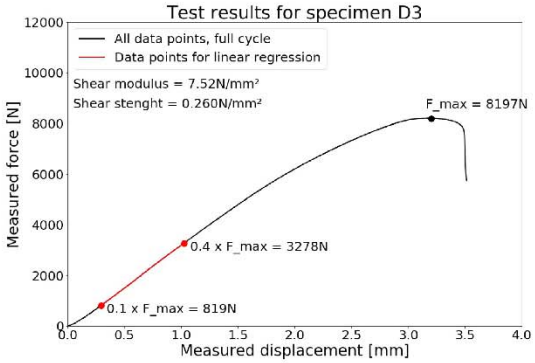

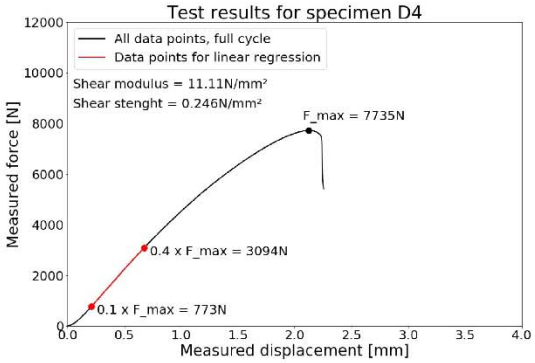

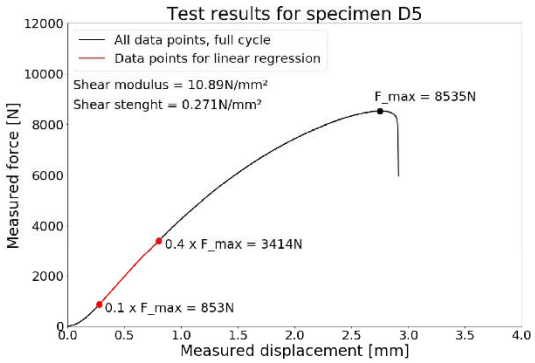

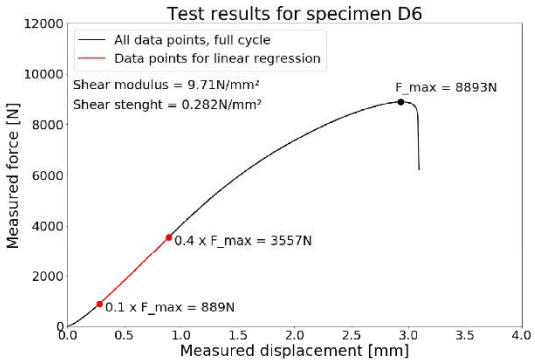

5.1.5 Graphical results: Single layer, higher density grade, extreme moisture conditions

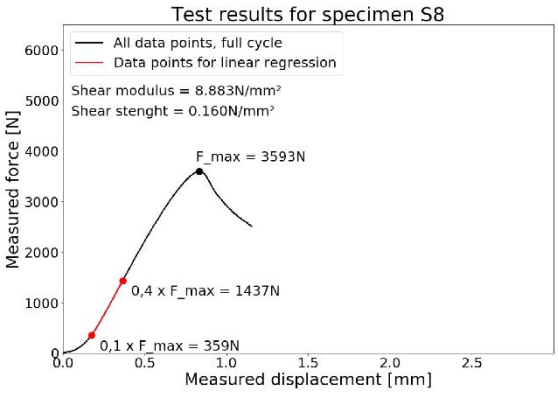

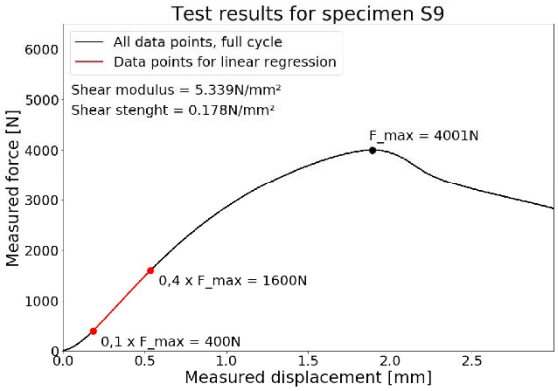

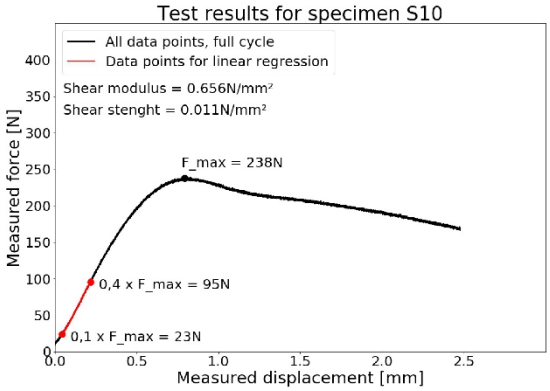

5.1.6 Graphical results: delamination tests, lower density grade

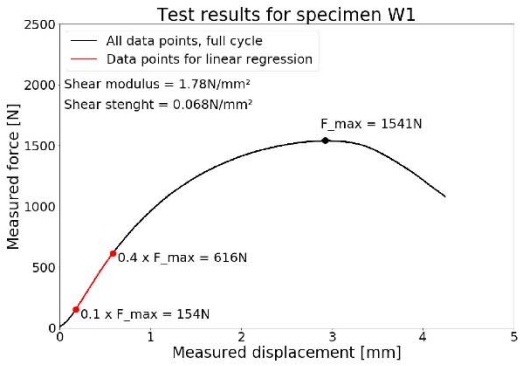

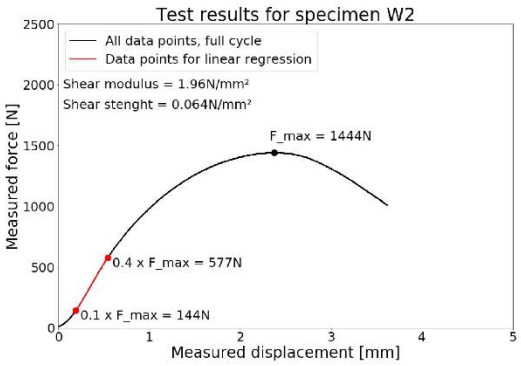

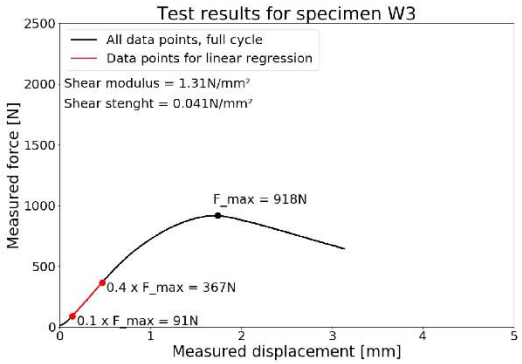

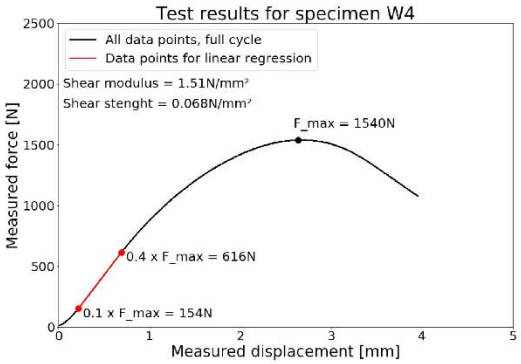

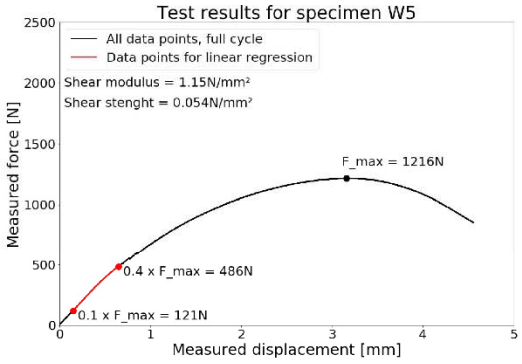

5.1.7 Discussion: Shear test results

The experiment did not reveal a clear link between the shear strength of a sample and its stiffness properties. For instance, the measured strength of sample S1 and S2 were almost identical, while the measured stiffness within the elastic range was about 50% higher for S2 than for S1. Since the deformations were recorded through the position of the loading cell, it is possible that much of the difference can be explained by other factors than the stiffness properties of the material. All of the test pieces were hand cut, which means that the geometry might have differed somewhat from one sample to another. This could in turn affect the deformation at the endpoints, or cause larger rotational deformations for some samples.

The samples made from the highest density grade performed slightly better than those made from the lowest, regarding both strength (27% higher on average) and stiffness (8% higher on average). This makes sense, since more material should be able to resist higher loads.

When comparing the double layer samples to the single layer samples of the same density grade, the stiffness was higher for the double layer samples (12% higher on average), while the strength was higher for the single layer samples (20% higher on average). This observed strength difference might be due to geometry dependent stress concentrations near the ends, as can be demonstrated using finite element software. The figure below shows three different test configurations that were analyzed using FEM-Design 18.

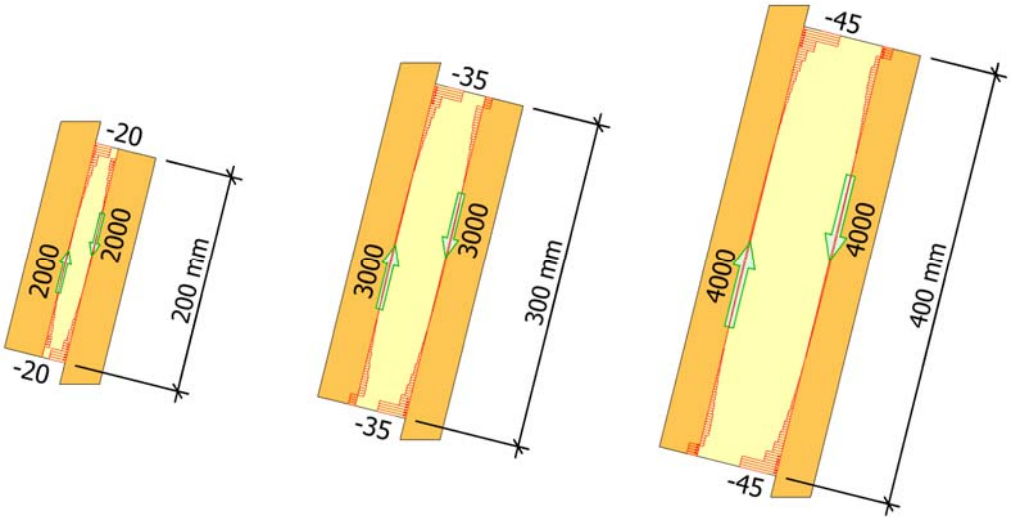

Figure 41: Geometry dependent stress concentrations

The green arrows in the figure represent total shear forces [N] acting between timber and insulation, while the red arrows show how the perpendicular forces [N/mm] vary along the glueline. Note that the shear force to length ratio is equal for all configurations, while the perpendicular stress concentrations vary among the samples.

A substantial decrease in shear strength was seen in all samples that had been subject to altered climatic conditions. Compared to the average, an approximate strength reduction of 50% was registered for the sample contained at 87% relative humidity. The stiffness of the sample was also roughly 40% lower than the average for the same density grade. A similar strength reduction was registered for the sample contained in a drying closet, although the stiffness of the sample did not seem to be affected. It seems likely that the dehydration of the timber boards caused them to curve, producing perpendicular stress in the fibre boards and thus affecting their resistance to shear stress. The samples that had been soaked in water performed dramatically worse than all other test samples. These were in practice completely dissolved, nearly eliminating all strength and stiffness properties.

Density measurements were taken from some of the samples after the tests had been carried out, to check if performance variations could be related to varying density. Two single layer samples were selected based on recorded stiffness, comparing the density of sample S1 (lowest measured stiffness) to that of sample S7 (highest measured stiffness). A density difference of 5% was registered, while the difference with respect to measured stiffness was 67%. It seems likely that most of the difference was due to the measuring technique. Note that the highest stiffness was measured for the sample with the lowest density. Two double layer specimens were selected based on measured shear strength, comparing the density of sample D4 (lowest measured strength) to that of sample D6 (highest measured strength). The measurements showed a density difference of 2%, while the difference in measured strength was 19%. The lowest density sample produced the highest strength, showing that small density variations were insignificant compared to natural variations in strength properties.

The average density for the selection of samples was measured to be 248kg/m^3 at standard moisture, and 221kg/m^3 when completely dried. The average moisture content was measured to be 12,1% (ranging from 11,7% to 12,3%). The measured density was notably higher than what had been reported (217kg/m^3 at approximately 10% moisture content). Due to the difference between reported and measured density, it was decided to also check two samples of the lowest density grade. These measurements showed an average density of 166kg/m^3 at 11.5% moisture content, compared to the reported 171kg/m^3 at approximately 10% moisture.

Delamination tests

When the material had been contained in water for 3 weeks, it was clear that the fibre boards had been damaged, even before samples had been dried. Visible cracks could be seen in all samples, close to the glue interface. Once the samples had been dried, the cracks seemed to close, darkening the material localy. The visible cracks did not seem to be related to delamination of the glue, but rather a failure occurring within the insulation material.

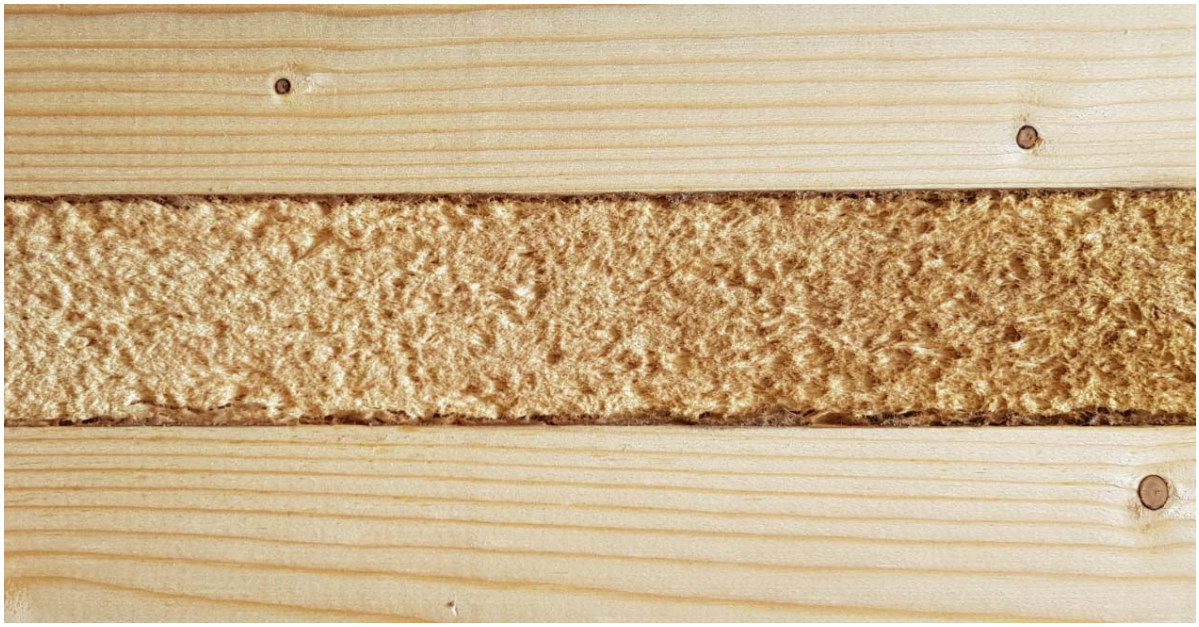

Figure 43: Material structure after 20 hours in a drying closet

Following the drying process, the cubical test pieces could be split open by hitting them on the side. The glue interface was still intact, with the failure occurring within the insulation material. The same observation was made for all four test pieces.

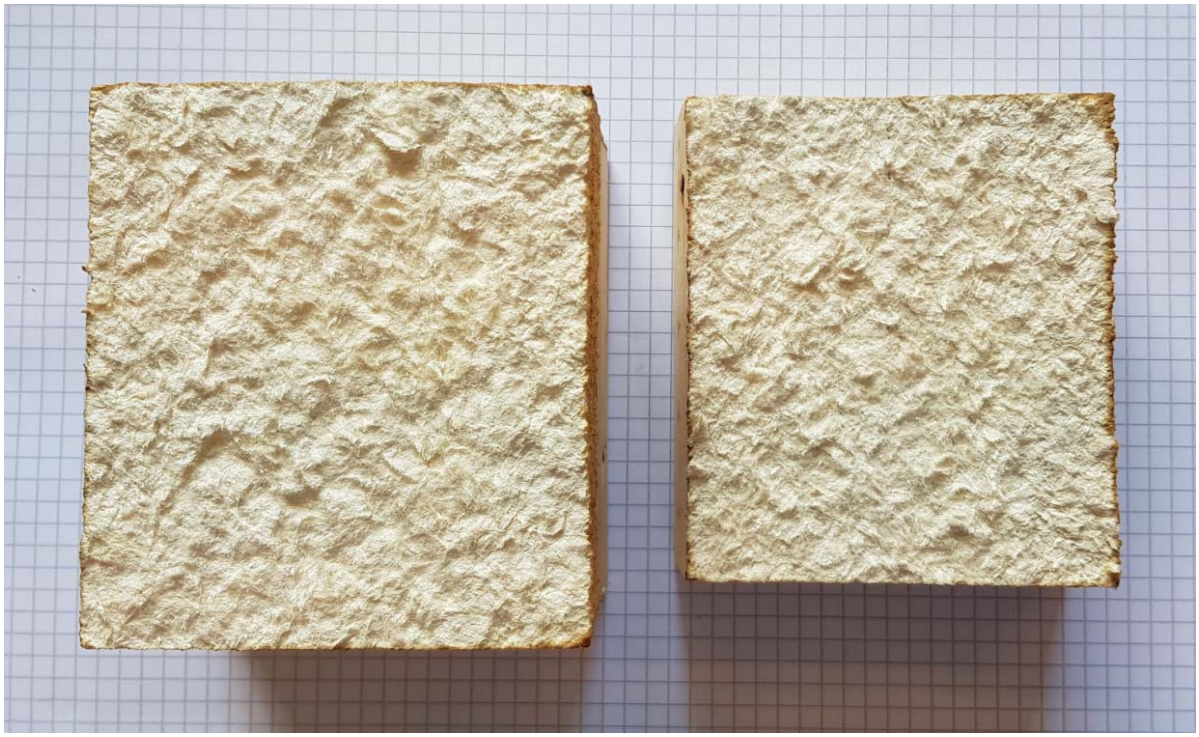

Figure 44: Typical mode of failure for delamination tests

The same observation was also made for the samples that were split through shear tests. All of the samples showed failure within the insulation material, while the glue interface was still intact. The tests showed tendencies of having regained some of their initial stiffness and strength, with an average shear strength of about 0.06N/mm^2. This performance was somewhat higher than that of the test piece that had been soaked in water, but not dried (0.011N/mm^2)

Four density samples were taken from the fibre boards after the visual inspection. Two samples were taken from the cubical test pieces, while the other two were taken from the pieces that had been split through shear tests. The material was weighed, dried for another 20 hours and then weighed again, revealing an approximate moisture content of 9% for the cubical test pieces, and 41% for the shear tests. The relatively high moisture content of the shear tests was likely due to slower diffusion caused by larger material thickness.

Bending test

The stiffness of the beam was calculated from a load/deformation linear regression. The magnitude of loading roughly spanned from 200N to 800N. The estimated stiffness of the beam was calculated as described in chapter 4.6, using Mathcad Prime. The full calculation is shown in appendix B of the thesis. The following predictions were made regarding the performance of the composite beam:

- Without any composite action, the theoretical stiffness of the beam should be 12.4N/mm.
- Given a shear modulus of 8.838N/mm^2 (based on recorded vertical deformations for shear tests of the highest density grade), the stiffness of the beam should be 83.0N/mm.
- Given a shear modulus of 52.57/mm^2 (based on optical analysis of the lower density grade), the theoretical stiffness of the system should be 204.2N/mm.

The results from the test showed a near perfect linear relationship between applied force and the corresponding deformation of the beam. The bonding quality was sufficient to achieve composite action, as predicted by the shear tests. The stiffness of the beam was measured to be 220.8N/mm.

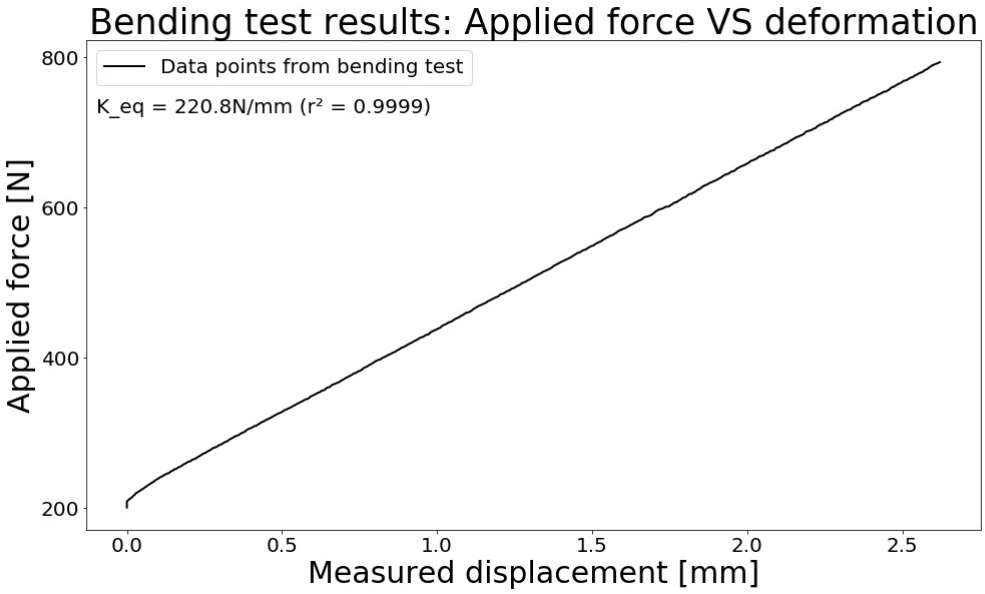

Figure 45: Force/displacement diagram for the bending test

The data from the bending test indicates that the shear modulus of the insulation material must have been close to the value derived from the optical analysis, and much higher than calculated from the original shear tests. Uncertainties regarding geometry and the modulus of elasticity of the outer timber layers cannot account for the large stiffness that was measured.

In-plane tests

The equivalent shear modulus for each panel was calculated from a stress/strain linear regression.

The data from the tests showed considerable fluctuations, regarding both loading intensity and deformations. The fluctuations were most prominent in the data from sample 1 and 2, resulting in unsatisfying correlation coefficients for the stress/strain relationship for these samples.

As expected, the equivalent shear modulus for sample 3 was quite high, and comparable to values found by D'Amato (2012) [20]. This indicates that the weaker properties of the fibre boards can be overcome by designing CLT panels in a matter which causes the insulation material to remain inactive. The equivalent shear modulus for sample 1 and 2 were roughly 50% lower, although there are considerable uncertainties regarding these results.

Table 3: In-plane test performances

Sample	Layer configuration	Measuring range [N]	Equivalent shear modulus [MPa]	r^2
1	3-layer (straight)	397 - 1867	208	0.485
2	5-layer (straight)	883 - 3555	185	0.669
3	5-layer (crossed)	22047 - 82878	412	0.990

It I worth noting that the measuring range for sample 1 and 2 was very low compared to the capacity and ideal measuring range of the loading cell. This is likely to have had implications for the quality of the results. If the actual capacities of the panels were underestimated, the measuring ranges could have been increased, possibly producing better data.

5.4.1 Graphical results: Sample 1 (3-layer straight)

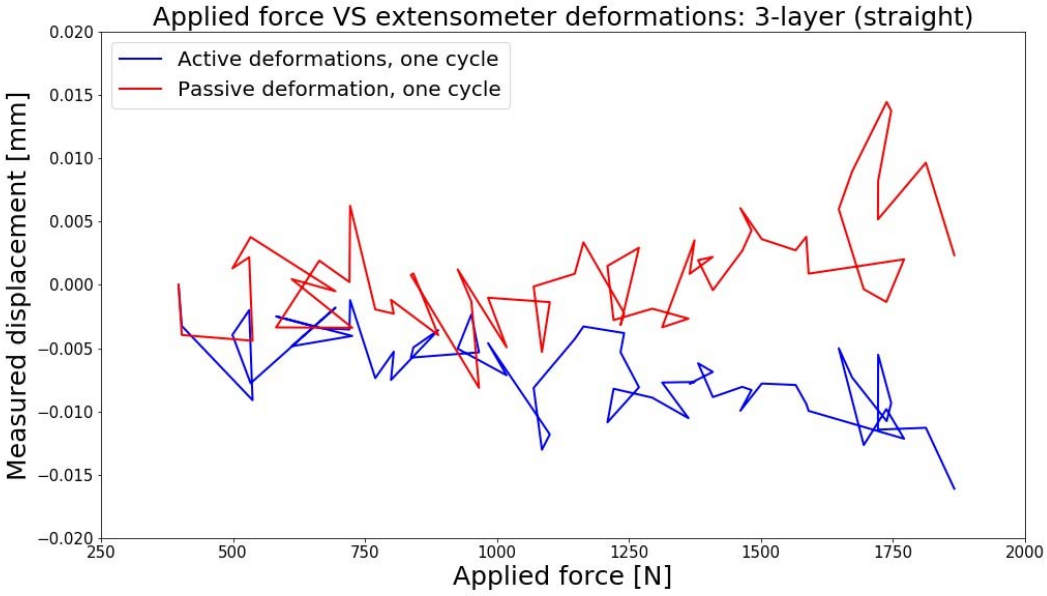

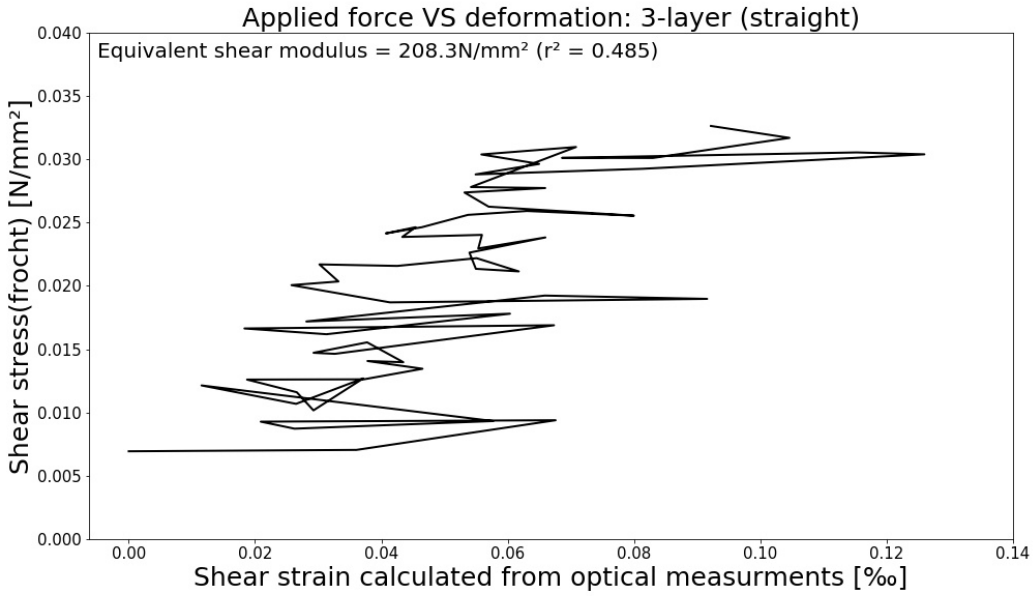

5.4.2 Graphical results: Sample 2 (5-layer straight)

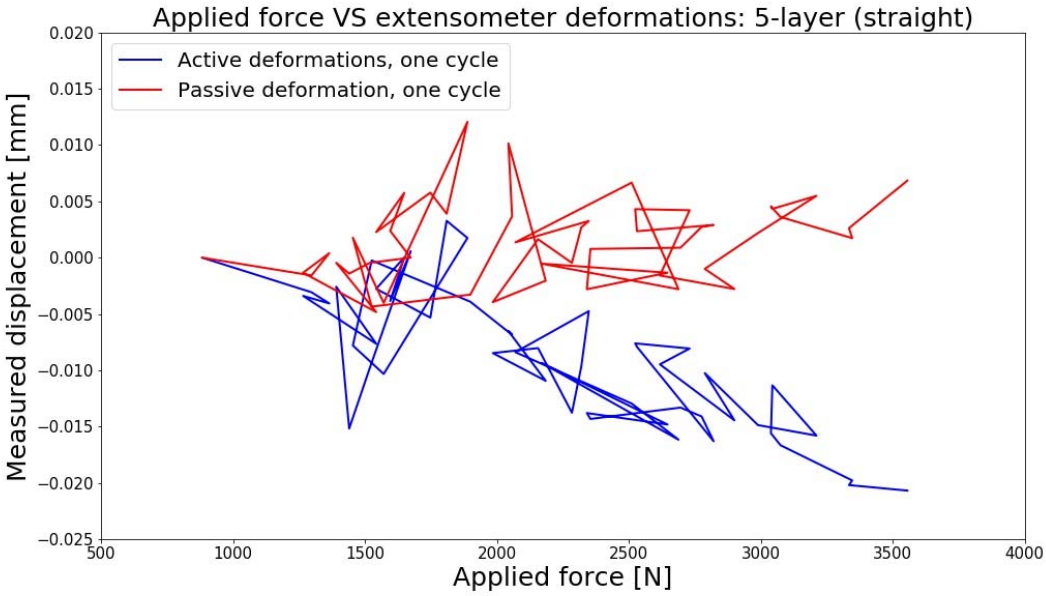

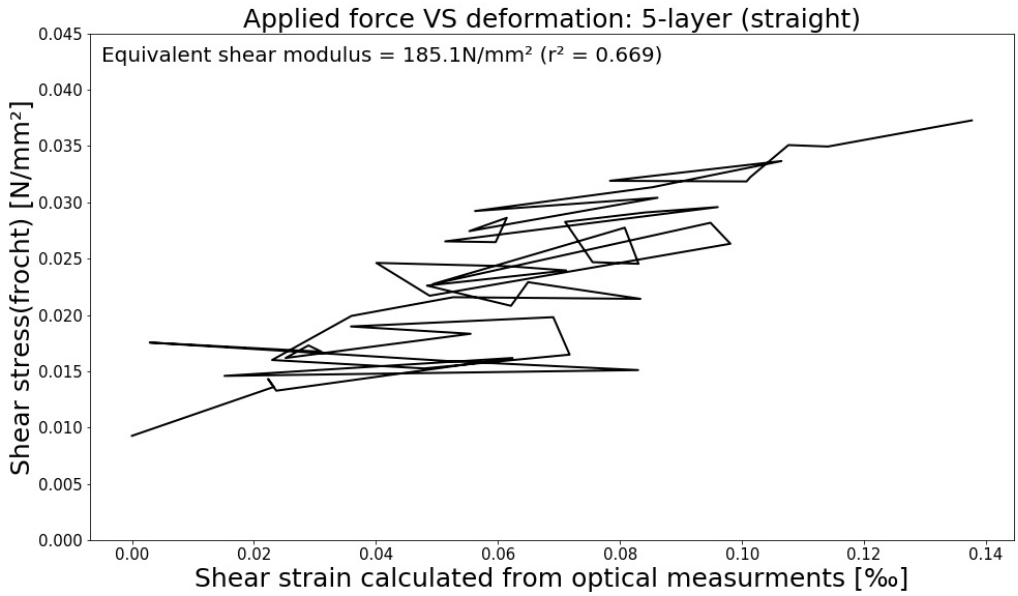

5.4.3 Graphical results: Sample 3 (5-layer crossed)

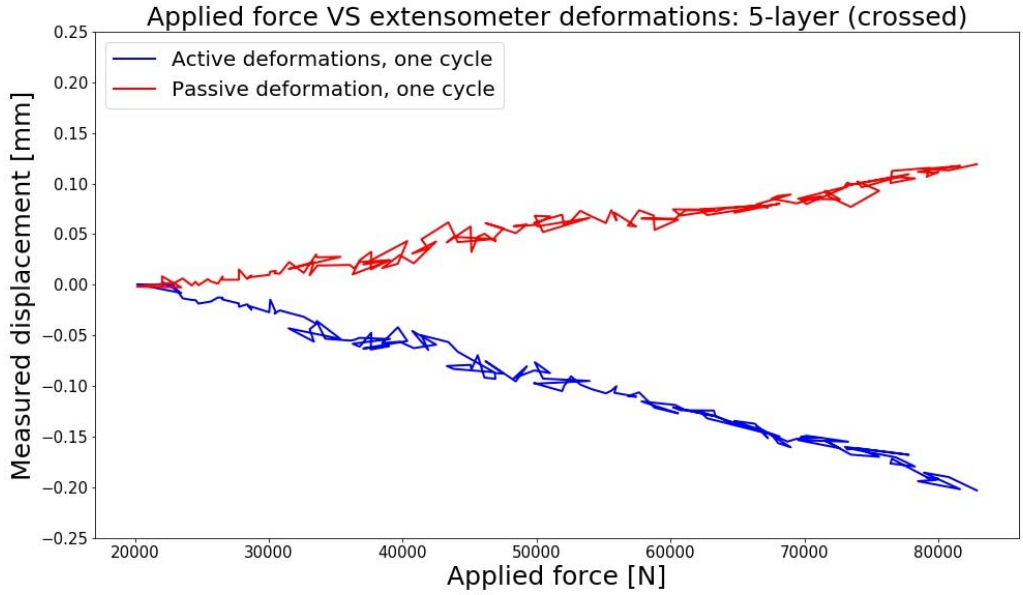

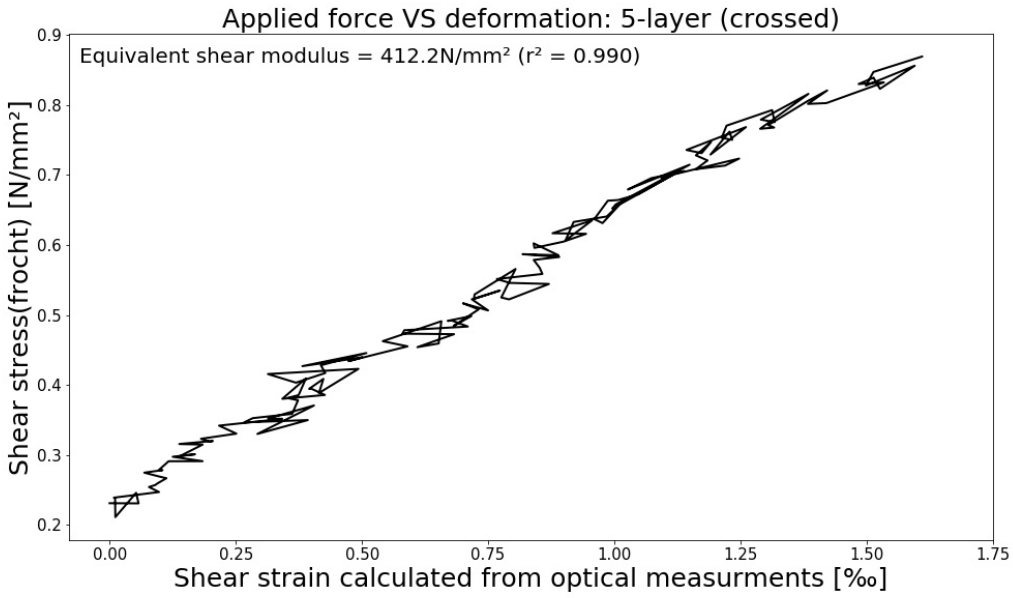

6 DISCUSSION

This chapter is dedicated to discussing the proposed concept of insulated CLT, in light of the results from the experimental investigation. The chapter also contains a summary of the investigation and suggestions for future research.

Prospects and limiting factors of the material

From a building design standpoint, it is now clear that the investigated wood fibre boards have some very interesting features. The measured shear modulus was much higher than anticipated, and the shear strength quite decent relative to the thermal properties of the material. Although much work remains before definite conclusions can be drawn, the idea of creating insulated CLT with the use of fibre boards does not seem unrealistic so far. Based on current findings, the strength properties seem to be the limiting factor of the material, rather than its stiffness.

Since the shear strength of the material is much lower than that of ordinary timber, and because regular CLT panels already are prone to shear failure modes, it is clear that cross-section sizes have to be increased considerably if sufficient load bearing capacities are to be achieved. It is however worth noting that large cross-sections are encouraged in the first place, since the concept revolves around reduced heat transfer through the structure.

Apart from the shear strength of the fibre boards, there are at least three other major issues that have to be addressed if such conceptual CLT panels are to become a reality, namely moisture conditions, fire security and long-term behavior. All of these issues are quite complicated, and are only briefly mentioned in this study.

6.1.1 Moisture and material properties

The shear tests conducted in this study have demonstrated that the fibre boards are sensitive to changing humidity. The mechanical properties of the material were negatively influenced when the air humidity deviated from the standard climatic conditions at the laboratory. The problem seems to be most critical for rising levels of moisture, since this also alters the stiffness properties of the fibre boards. As was shown in chapter 3, the stress distribution within a composite structure depends on the local deformations of individual layers. It then follows that uncontrolled levels of moisture not only affects the shear strength of the material, but also the stress distribution within the whole structure. As the shear stiffness of the insulation decreases, the internal stress due to bending of individual layers will increase. In places with large seasonal temperature variations, indoor air humidity will typically change over the year, from low levels during the winter to relatively high levels during the summer. This could pose a challenge for designers, if the stress distribution within the composite structure changes over time.

Apart from what has been mentioned, it is possible that fluctuating air humidity could lead to internal stress building up inside the insulation material, as shrinkage and swelling of the outer timber layers might cause unintentional deformations of the fibre boards. Fluctuating moisture levels might also have an influence on the thermal properties of the material (Amthor, 2018) [14].

Although changing air humidity might be a limiting factor on its own, potential water leaks could be much more dramatic. As has been demonstrated, liquid water will completely deteriorate all mechanical properties of the fibre boards. This means that composite structures made from the material must be designed so that they are protected from water.

6.1.2 Fire and structural safety

The European standards describe requirements that apply to structures in the event of a fire. Referring to the Council Directive 89/106/ECC [24], the standards state that in such an event, the load-bearing capacity of a building has to be maintained for a certain duration of time. Specific requirements for timber structures are described in detail in EN1995-1-2 [25].

Since timber is a combustible material, the effective cross-section of a timber structure will decrease over time as the fire progresses. This phenomenon is accounted for by considering the effective charring depth at the end of a required duration of time. For a regular CLT panel, a decrease in thickness of the outer layers may take place while still preserving some of the structural integrity of the panel. Since regular panels contain several layers in the load-bearing direction, it might take a long time before charring leads to collapse. However, if the panels are to be designed with a large portion of the cross-section made up of fibre boards, all of the structural strength has to be provided by layers near the surface of the panel. If these are lost during a fire, the panels will collapse. This could be a deciding factor for the thickness of the outer layers, or possibly require an increased number of load-bearing layers. Another option could be to cover the elements with gypsum or other incombustible materials.

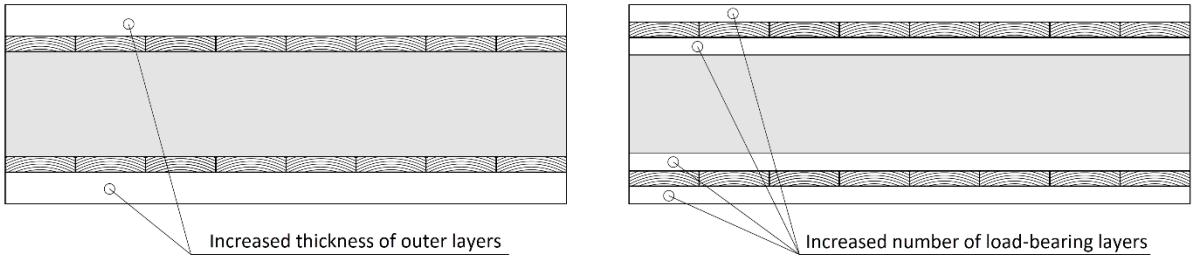

Figure 46: Methods to inrease structural performance of insulated CLT in the event of a fire

6.1.3 Creep deformations and long-term effects

The experiments conducted in this study were limited to loads of short durations. Although it has been shown that composite action can be achieved using fibre boards, it remains an open question how the material will behave with respect to long term load effects. It is a well known fact that load durations are important factor when designing timber structures, regarding both deformations and load bearing capacities. This is also clear from EN 1995-1-1:2004 [4], which states that the design value X_d for any given material property in the ultimate limit state can be defined as follows:

$$X_d = k_{mod} \cdot \frac{X_k}{\gamma_M} \tag{40}$$

Where:

X_k *represents the characteristic design value for a given material property*

γ_M *represents the partial safety factor for the given type of material*

k_{mod} *is a strength factor taking moisture content and load duration into account*

The values for k_{mod} depend on the duration of the load, and the climatic conditions where the structure is located. The value also depends on the type of material. The value may range from a minimum of 0.2 for various types of fibre boards, to a maximum of 1.10 for some other timber products. Low values indicate large strength reductions.

The standard further states that for structural elements consisting of several components with different time dependent properties (e.g. creep properties), that are relevant for serviceability limt state calculations, the final mean values for the modulus of elasticity $E_{mean.fin}$, the shear modulus $G_{mean.fin}$ and the slip modulus $K_{ser.fin}$ can be defined as follows:

$$E_{mean.fin} = \frac{E_{mean}}{(1+k_{def})} \tag{41}$$

$$G_{mean.fin} = \frac{G_{mean}}{(1+k_{def})} \tag{42}$$

$$K_{ser.fin} = \frac{K_{ser}}{(1+k_{def})} \tag{43}$$

Where:

E_{mean} *is the mean value for the modulus of elasticity*

G_{mean} *is the mean value for the shear modulus*

K_{ser} *is the slip modulus*

k_{def} *is a deformation factor*

Unlike the values for $k_{mod,}$ the values for k_{def} only depend on the climatic conditions and the type of material. The values may range from a maximum of 3.0 for various types of fibre boards to a minimum of 0.6 for some other timber products. High values indicate large creep deformations.

Regarding the ultimate limit state, if the distribution of internal forces and moments are affected by the distribution of stiffness within the construction (e.g. composite stuctures), the standard lists an separate set of equations for the same stiffness properties:

$$E_{mean.fin} = \frac{E_{mean}}{\left(1+\psi_2 \cdot k_{def}\right)} \tag{44}$$

$$G_{mean.fin} = \frac{G_{mean}}{\left(1+\psi_2 \cdot k_{def}\right)} \tag{45}$$

$$K_{ser.fin} = \frac{K_{ser}}{\left(1+\psi_2 \cdot k_{def}\right)} \tag{46}$$

Where:

ψ_2 *is a factor representing the quasi-permanent part of the load causing the greatest tension relative to strength properties (EN 1990)* [26].

This study makes no attempt to evaluate what values would be sensible to apply for k_{mod} and k_{def} for the investigated fibre boards, but if tables 3.1 and 3.2 in EN 1995-1-1:2004 are to serve as a guideline, it seems that loads of long term durations should be kept at a moderate level.

Conceptual applications of the material

Since the strength properties of the investigated material are limited compared to regular timber, ideal applications have to involve concepts where the properties of large cross-sections are taken advantage of. In this section of the thesis, two possible applications will be taken a closer look at, namely a conceptual roof slab, and a conceptual exterior wall element.

According to the physical principles of heat transfer, the thermal resistance *R* of a material can be calculated based on its thickness *t* and its thermal conductivity λ, using to the following formula:

$$R = \frac{t}{\lambda} \tag{47}$$

The total thermal resistance of a structure made up of several layers with varying thickness and thermal conductivity is then equal to the sum of thermal resistance provided by each layer:

$$R_{tot} = \sum_{i=1}^{n} R_i \tag{48}$$

The thermal transmittance of the layered structure, generally referred to as U-value is then equal to the reciprocal of the total R-value:

$$U = \frac{1}{R_{tot}} \tag{49}$$

According to current Norwegian regulations, the minimum allowed U-value for roof structures is 0.18W/m^{2}K (SINTEF, guide 473.101) [27], while the minimum allowed value for exterior walls is 0.22W/m^{2}K. If a thermal conductivity of 0.13W/mK is implemented for timber (SINTEF, guide 471.010) [28], and the reported thermal conductivity of 0.055W/mK is implemented for the fibre boards (table 1), equations (43) to (45) show that the minimum criteria for roofs and exterior walls can be satisfied with approximate total thicknesses of 380mm and 325mm respectively.

6.2.1 Conceptual roof element

The conceptual roof element is shown in the figure below, along with calculations showing that the minimum criteria regarding U-values for roof structures is satisfied.

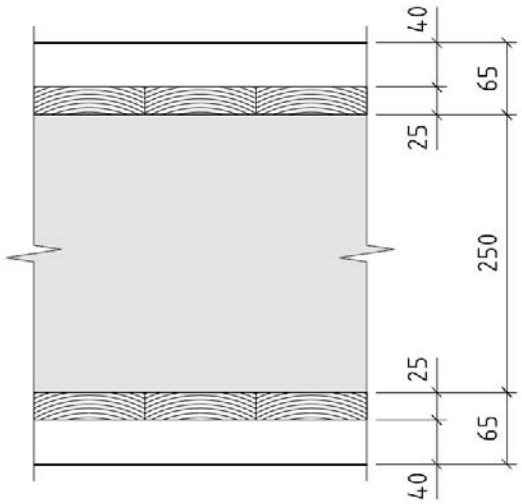

$$R_{roof} := \frac{130\ mm}{0.13\ \frac{W}{m \cdot K}} + \frac{250\ mm}{0.055\ \frac{W}{m \cdot K}}$$

$$U_{roof} := \frac{1}{R_{roof}} = 0.180\ \frac{W}{m^2 \cdot K}$$

The natural question is how the proposed insulated CLT panel would preform with respect to out-of-plane loading, when loads are applied according to current standards. As explained in chapter 6.1.3, a proper evaluation of this kind would require taking the long-term behavior of the panel into account. Without considering these effects, it can however be shown that conceptual slab will perform quite well for short-term loads, both with respect to deflections and to internal stress.

Manual calculations for short-term loads were performed for a 7 meter roof slab. The calculations were done in Mathcad Prime 4.0, using the shear analogy method. The full calculation is shown in appendix C of the thesis. The calculations include instantaneous deflection, maximum shear stress in the central layer and maximum longitudinal stress in the outer layers. A summary of the calculation is shown on the next page.

In addition to the manual calculations, the deflection of the slab was controlled using ANSYS APDL 19.2. The shear stress in the central layer was controlled using FEM-Design 18. The results from finite element models agreed with the manual calculations in both cases.

The table below shows the input data for the manual calculations, as well as the resulting instantaneous deflection and internal stress.

Table 4: Calculation summary, conceptual roof slab

Span width of the slab	7000mm
density of timber (T22)	470kg/m3
density of fibre boards	250kg/m3
Additional dead load (technical installations etc)	0.5kN/m2
Snow load	3.0kN/m2
Longitudinal modulus of elasticity for timber (T22)	13000N/mm^2
Transversal modulus of elasticity for timber	0N/mm^2
Longitudinal shear modulus for timber (T22)	810
Assumed rolling shear modulus for timber (T22)	69
Assumed modulus of elasticity for fibre boards	150
Assumed shear modulus for fibre boards	50
Resulting instantaneous deflection	6.6mm (L/1050)*
Resulting shear stress in central layer	0.068N/mm^2
Resulting longitudinal stress in outer layers	3.071N/mm^2

* The total defelction will be considerably larger when long term effects are considered.

The figure below shows that the calculated deflection is very close to the results from the finite element analysis.

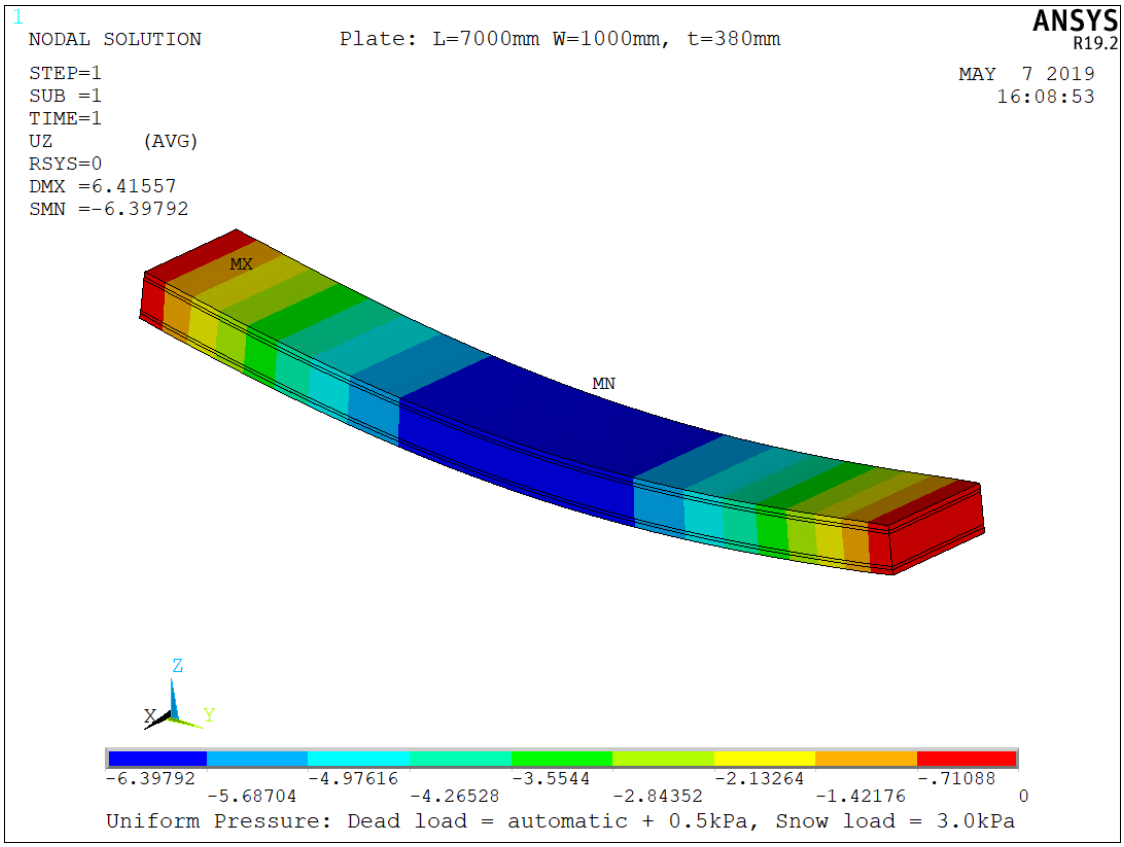

Figure 47: Conceptual roof slab – instantaneous deflection, calculated with ANSYS

The figure below shows that the calculated shear stress in the central layer is very close to the results from the finite element analysis.

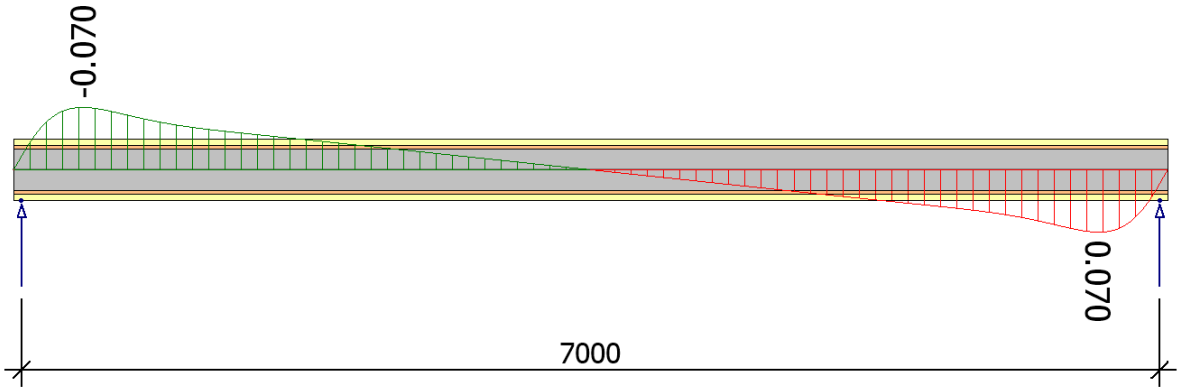

Figure 48: Conceptual roof slab - shear stress in the central layer, calculated with FEM-design.

6.2.2 Conceptual wall element

The conceptual element is shown in the figure below, along with calculations showing that the minimum criteria regarding U-values for exterior walls is satisfied.

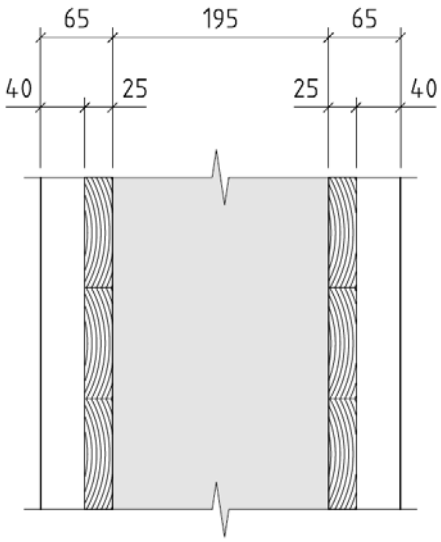

$$R_{wall} := \frac{130\ mm}{0.13\ \frac{W}{m \cdot K}} + \frac{195\ mm}{0.055\ \frac{W}{m \cdot K}}$$

$$U_{wall} := \frac{1}{R_{wall}} = 0.220\ \frac{W}{m^2 \cdot K}$$

Since walls are primarily subject to in-plane loading, this kind of application of the material is perhaps the most realistic. In the proposed wall element, the main structural purpose of the central layer to provide resistance against out-of-plane buckling. The strength required to prevent buckling is very moderate compared to what will be required for load-bearing horizontal slabs.

Investigation summary and future research

It has been demonstrated that the investigated fibre boards can be used to produce insulated laminated timber panels, achieving sufficient bonding quality to prevent failure at the glue interface. The fibre boards also have sufficient stiffness to provide considerable composite action in composite panels. The study has shown that decent shear stiffnes for in-plane loading can be achieved, by producing composite panels with outer layers made up of regular cross laminated timber.

The main findings regarding the mechanical properties of the fibre boards are presented in the table bleow. The shear strength was dependent on the test configuration, as explained in chapter 5.1.7. The shear modulus of the lower density grade was directly measured for one shear test sample, using cameras and digital image correlation algorithms. The shear modulus of the higher density grade was indirectly measured, through an out-of-plane bending test. The bending test indicated that the shear modulus of the higher density grade must have been equal to or higher than that of the lower density grade.

Table 5: Fibre board performance summary

Density grade	Reported density	Measured density	Characteristic shear strength [MPa]	Shear modulus [MPa]
Higher grade	216kg/m^3 (10% moisture)	248kg/m^3 (12% moisture)	0.234 / 0.282 (double layer / single layer)	52.57+
Lower grade	171kg/m^3 (10% moisture)	166kg/m^3 (11.5% moisture)	0.219 (single layer)	52.57

The shear strength of the material seems to be the limiting factor for its use in composite load-bearing structures. Due to the structure of the material, design values for the strength properties in the ultimate limit state must likely be reduced notably, which is typical for fibre board products.

In this study, loading up to the point of failure was only carried out for shear tests, with a setup similar to which is described in EN 408 [16]. The presence of simultaneous perpendicular stress is a weakness of this setup, which seems to have affected the results. Future research should therefore involve other setups, producing failure mechanisms that are more representative for practical applications of the material.

The study has shown that determination of shear modulus through experiments requires precise, local measurements of shear deformations. Decent data was only obtained for one test sample during this investigation. In order to obtain more reliable values, the tests should therefore be repeated using accurate measuring techniques.

Regarding the bending test and the in-plane tests, future research should involve loading the composite structures up to failure, in order to investigate failure mechanisms and to assess the strength properties of the material for these applications.

Other issues that require attention involve long term behavior of the material, and the influence of moisture content on its structural performance. Creep effects can be very notable for wood fibre products, which might pose limitations for the use of the material. It has already been shown that the structural properties of the investigated fibre boards will deteriorate if liquid water is allowed to be absorbed into the material. Future research might want to look at more common climatic variations in buildings, and how these influence the structural performance of the material.

Lastly, since the experiments conducted in this study were performed on small-scale test samples, it would be very interesting to see if the findings can be replicated in tests performed on large-scale insulated CLT-panels.

7 REFERENCES

1. Tavoussi K, Winter W, Pixner T, Kist M. (2015). Steel reinforced timber structures for multi storey buildings.

2. Martins C, Skinner J, Bregulla J, J H, Paine K, Walker P, et al. (2013). Concrete upgrade to improve the vibration response of timber floors.

3. Dias A, Schänzlin J, Dietsch P. (2018). Timber-concrete composite structures. A state-of-the-art report by COST Action FP1402 / WG 4.

4. EN 1995-1-1: Eurocode 5: Design of timber structures, Part 1-1: General Common rules and rules for buildings. (2004). CEN.

5. 1995-2 E. Eurocode 5: Design of timber structures, Part 2: Bridges. CEN.

6. Lorenzo Franzoni, Arthur Lebée, Gilles Forêt, Florent Lyon. (2015). Advanced modelling for design helping of heterogeneous CLT panels in bending. International Network on Timber Engineering Research - INTER - Meeting 48, Sibenik - Croatia, Aug 2015, Sibenik, Croatia. hal-01233249.

7. SIPA 100-2018 final draft. Structural Insulated Panel Association.

8. Leoskool L, Descamps T. (2014). Development of a structural insulated panel (SIP) with wood based material.

9. Gagnon S, Pirvu C. (2011). CLT Handbook - Canadian Edition

10. Blass HJ, Sandhaas C. (2017). Timber Engineering - Principles for Design, pp 256-262.

11. Colbacchini R. (2010). Metodi di analisi per elementi composti in legno.

12. Möhler K. (1955). Über das Tragverhalten von Biegeträger und Ruckstäben mit zusamengeszten Querschnitten und nachgiebigen Verbindungsmitteln. Habiliation (TH Karlsruhe).

13. Kreuzinger H. (1999). Flaechentragwerke – platten, scheiben und schalen – ein Berechnungsmodell fuer gaengige statikprogramme. Bauen mit Holz (1/1999), pp. 34-39.

14. Amthor. (2018). Factors affecting pressure resistant insulation wood fibre boards.

15. NS-EN 338. Konstruksjonstrevirke - Fasthetsklasser. (2016). CEN.

16. EN 408. Timber structures, Structural timber and glued laminated timber, Determination of some physical and mechanical properties. (2010). CEN.

17. Zhiqiang Wang, Hongmei Fu, Meng Gong, Jiayan Luo, Weiqun Dong, Ting Wang, Ying Hei Chui. (2017). Planar shear and bending properties of hybrid CLT fabricated with lumber and LVL. Construction and Building Materials, vol. 151, pp. 172-177.

18. Andreolli M, Tomasi R, Polastri A. (2012). Experimental investigation on in-plane behaviour of crosslaminated-timber elements. In: Proc. CIB-W18, CIB-W18/45-12-4, Växjö, Sweden.

19. EN 16351: Timber structures - Cross laminated timber - Requirements. (2015). CEN.

20. D'Amato G. (2012). Analisi teorico-sperimentale sul comportamento nel piano di pannelli.

21. Frocht M. M. (1931). Recent advances in photoelasticity and an investigation of the stress distribution in square blocks subjected to diagonal compression. Trans, ASME, vol. 55.

22. Brandner R, Bogensperger T, Schickhofer G. (2013). In plane Shear Strength of Cross Laminated Timber (CLT): Test Configuration, Quantification and influencing Parameters. CIB-W18/46-12-2, Vancouver, Canada.

23. EN 14358: Timber structures - Calculation and verification of characteristic values. (2016). CEN.

24. Construction Products Directive 89/106/EEC. (1988).

25. EN 1995-1-2: Eurocode 5: Design of timber structures, Part 1-2: General – Structural fire design. (2004). CEN.

26. EN 1990: Eurocode: Basis of structural design. (2002). CEN.

27. Building Research Design Guide 473.101: Energikrav til bygninger. Oversikt. (2016). SINTEF.

28. Building Research Design Guide 471.010: Varmekonduktivitet og varmemotstand for bygningsmaterialer. (2003). SINTEF.

8 APPENDIX

Appendix A: Capacity of in-plane tests

Chapter 1

Shear Stresses for CLT panel

In order to obtain a simple and significant exposition a common notation will be used: the one present in the COST document [7] and [8], see fig. 1.1 which will also be the base for the future Eurocode section regarding CLT products. The first index indicates the plane normal to the action, the second index indicates the axis the action is parallel to;

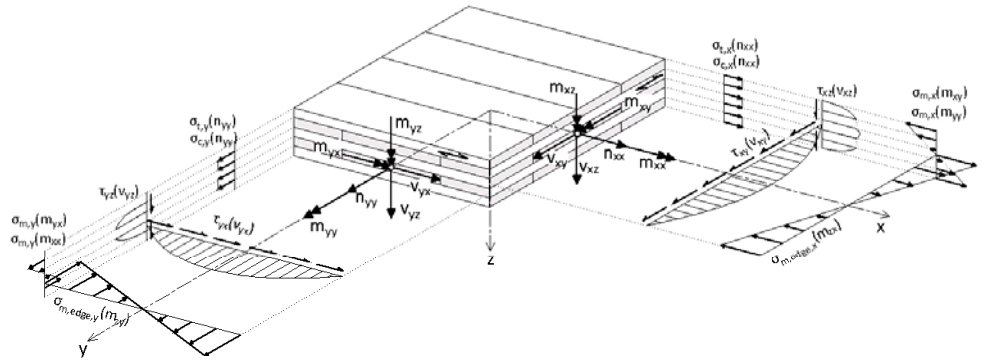

Figure 1.1: Shear stresses, modified from COST document [7]

for the following section then the direction x would be the one parallel to the grain of outer layers (the layers in major number usually), y is perpendicular to x, z is the direction through the thickness t_{CL} of the panel. The shear force is expressed as force per unit of length and for rotational equilibrium:

$$v_{xy} = v_{yx} = v \tag{1.1}$$

The layers oriented as the x axis (so the major number of layers for a usual panel with an odd total number of layers) will have thickness $t_1\, t_3\, t_5$, while the layers oriented as the y axis (so the minor number of layers) will have thickness $t_2\, t_4$. The width of the laminations b_l is assumed to be equal the for boards oriented in both directions, if cracks are present or it is not constant for each board then $b_{l,\mathrm{mean}}$ is to be used (unless otherwise specified).

1.0.1 Equilibrium method

This method is based on equilibrium equations for each layer and glued interfaces [2], see fig. 1.2, and assumes that shear stresses are only present in the cross section of the boards oriented perpendicular respect to the shear action. This means that no glue is present on the narrow face of boards so only net shear or torsional shear failure are possible.

12 **3 Layer panel**

Shear stresses τ_{xy} and τ_{yx} are calculated using the thicknesses of the layers oriented as the respective direction:

$$\tau_{xy} = \frac{v}{t_1 + t_3} \tag{1.2}$$

$$\tau_{yx} = \frac{v}{t_2} \tag{1.3}$$

For panels with symmetric layup $t_1 = t_3$ the stress τ_{yx} can be expressed as a function of τ_{xy}:

$$\tau_{yx} = \tau_{xy} \cdot \frac{2 \cdot t_1}{t_2} \tag{1.4}$$

The global equilibrium to rotation poses:

$$M_{T12} - M_{T21} - M_{T23} + M_{T32} = 0 \tag{1.5}$$

At each glued interface, for action reaction:

$$\begin{cases} M_{T12} = M_{T21} \\ M_{T23} = M_{T32} \end{cases} \tag{1.6}$$

Rotational equilibrium is calculated for each layer:

$$\begin{cases} M_{T12} - \tau_{xy1} \cdot b_l^2 \cdot t_1 = 0 \\ M_{T21} - \tau_{yx2} \cdot b_l^2 \cdot t_2 + M_{T23} = 0 \\ M_{T32} - \tau_{xy3} \cdot b_l^2 \cdot t_3 = 0 \end{cases} \tag{1.7}$$

So considering that $\tau_{xy1} = \tau_{xy3} = \tau_{xy}$ and $\tau_{yx2} = \tau_{yx}$ and using the relations previously found it can be obtained:

$$M_T = M_{T12} = M_{T21} = M_{T23} = M_{T32} = \tau_{xy} \cdot b_l^2 \cdot t_1 \tag{1.8}$$

It is then possible to evaluate torsional shear stresses as a function of τ_{xy} considering that $W = W_1 = W_2 = W_3 = \frac{b_l^3}{3}$:

$$\tau_T = \tau_{T12} = \tau_{T21} = \tau_{T23} = \tau_{T32} = \frac{M_T}{W} = 3 \cdot \frac{\tau_{xy} \cdot t_1}{b_l} \tag{1.9}$$

13 **5 layer panel**

Shear stresses τ_{xy} and τ_{yx} are calculated using the thicknesses of the layers oriented as the respective direction:

$$\tau_{xy} = \frac{v}{t_1 + t_3 + t_5} \tag{1.10}$$

$$\tau_{yx} = \frac{v}{t_2 + t_4} \tag{1.11}$$

For panels with symmetric layup $t_1 = t_3 = t_5$ and $t_2 = t_4$ the stress τ_{yx} can be expressed as a function of τ_{xy}:

$$\tau_{yx} = \tau_{xy} \cdot \frac{3t_1}{2t_2} \tag{1.12}$$

The global equilibrium to rotation poses:

$$M_{T12} - M_{T21} - M_{T23} + M_{T32} + M_{T34} - M_{T43} - M_{T45} + M_{T54} = 0 \tag{1.13}$$

At each glued interface, for action reaction:

$$\begin{cases} M_{T12} = M_{T21} \\ M_{T23} = M_{T32} \\ M_{T34} = M_{T43} \\ M_{T45} = M_{T54} \end{cases} \tag{1.14}$$

Rotational equilibrium is calculated for each layer:

$$\begin{cases} M_{T12} - \tau_{xy1} \cdot b_l^2 \cdot t_1 = 0 \\ M_{T21} - \tau_{yx2} \cdot b_l^2 \cdot t_2 + M_{T23} = 0 \\ -M_{T32} + \tau_{xy3} \cdot b_l^2 \cdot t_3 - M_{T34} = 0 \\ M_{T43} - \tau_{yx4} \cdot b_l^2 \cdot t_4 + M_{T45} = 0 \\ M_{T54} - \tau_{xy5} \cdot b_l^2 \cdot t_5 = 0 \end{cases} \tag{1.15}$$

So considering that $\tau_{xy1} = \tau_{xy3} = \tau_{xy5} = \tau_{xy}$ and $\tau_{yx2} = \tau_{yx4} = \tau_{yx}$ and using the relations previously found it can be obtained:

$$\begin{cases} M_{T,\text{ext}} - M_{T12} - M_{T21} - M_{T45} - M_{T54} - \tau_{xy} \cdot b_l^2 \cdot t_1 \\ M_{T,\text{int}} = M_{T23} = M_{T32} = M_{T34} = M_{T43} = \frac{\tau_{xy}}{2} \cdot b_l^2 \cdot t_1 \end{cases} \tag{1.16}$$

It is then possible to evaluate torsional shear stresses as a function of τ_{xy} considering that $W = W_1 = W_2 = W_3 = W_4 = W_5 = \frac{b_l^3}{3}$:

$$\begin{cases} \tau_{T,\text{ext}} = \tau_{T12} = \tau_{T21} = \tau_{T45} = \tau_{T54} = \frac{M_{T,\text{ext}}}{W} = 3 \cdot \frac{\tau_{xy} \cdot t_1}{b_l} \\ \tau_{T,\text{int}} = \tau_{T23} = \tau_{T32} = \tau_{T34} = \tau_{T43} = \frac{M_{T,\text{int}}}{W} = \frac{3}{2} \cdot \frac{\tau_{xy} \cdot t_1}{b_l} \end{cases} \tag{1.17}$$

So differently from the case of a 3 layer panel torsional shear stresses are not equal for all glued interfaces, but are major on external ones.

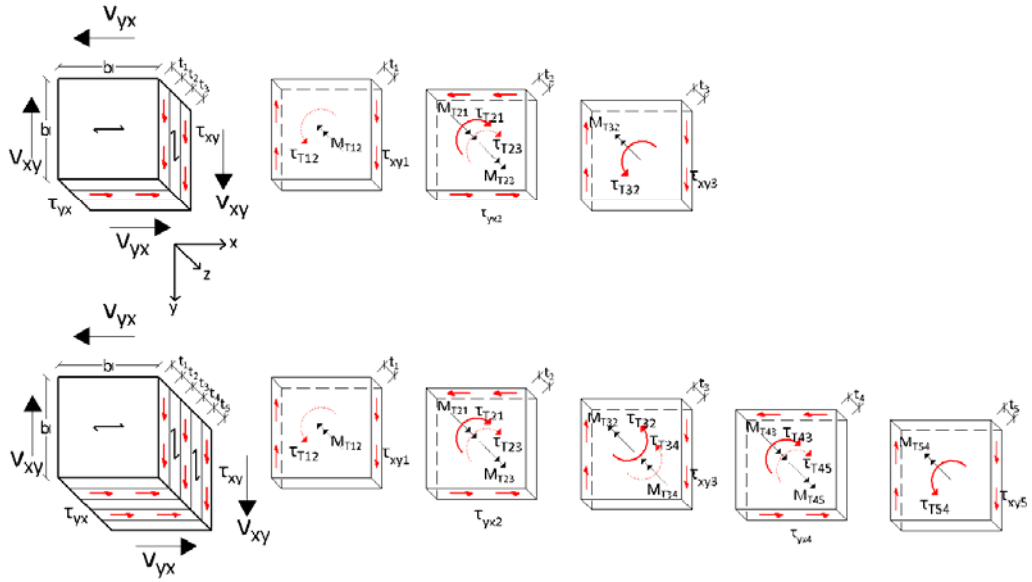

Figure 1.2: Shear stresses for the equilibrium method

Chapter 2

Type A

The product is assembled without using edge bonding, so the equilibrium method appears to be applicable to this case since the shear stresses are indeed transferred only via the cross section between one layer and another. Given the huge difference in strength and stiffness value between the two materials a simplification is considered to reconduce this case to the case of a 3 layer CLT panel: in the direction where the timber has grain oriented perpendicular to the shear force all stresses are in the timber layers (in theory instead probably also a component in the insulation is present, such as a τ_{xy2}). In timber layers the shear stress is:

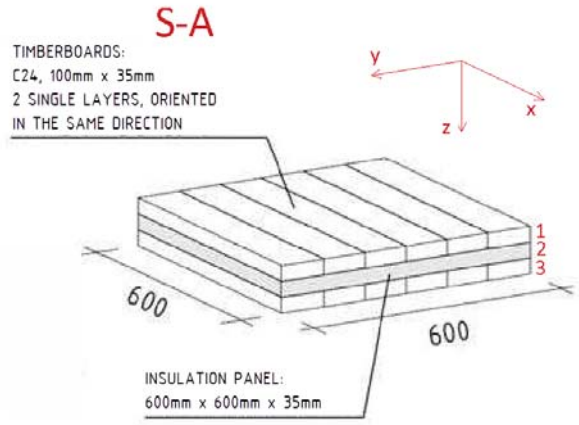

Figure 2.1: Shear stresses for the equilibrium method

$$\tau_{xy} = \tau_{xy1} = \tau_{xy3} = \frac{v}{t_1 + t_3} \tag{2.1}$$

In insulation layers the shear stress is:

$$\tau_{yx} = \tau_{yx2} = \frac{v}{t_2} \tag{2.2}$$

Obviously the limiting element is the insulation, so failure is obtained when $\tau_{yx} > f_{v,\text{ins}}$. Considering a diagonal compression test where the applied force is F and the core of the specimen is 40% of the overall dimensions we have:

$$v = \alpha_{\text{Frocht}} \cdot \frac{F/\sqrt{2}}{l} \tag{2.3}$$

- $\alpha_{\text{Frocht}} = 1,429$ is a correctional factor to consider the influence of compression forces

- F is the applied vertical force
- $l = 600\,\text{mm}$ is the side of the CLT specimen

Considering a mean value $f_{v,\text{ins}} = 0,22\,\text{MPa}$ the approximate maximum force would be $F_{\max} = 4,6\,\text{kN}$, so a very low value. Additional considerations are needed regarding torsional shear stresses at the glue interface, for which a strength value is not provided.

5

Chapter 3

Type B

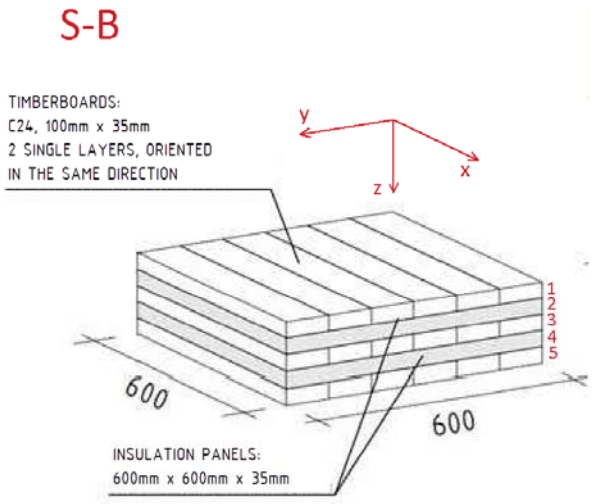

Figure 3.1: Shear stresses for the equilibrium method

This configuration is the same as the previous case, since the limiting elements are always the insulation panels, the only difference being that now 2 insulation layers are present. In timber layers the shear stress is:

$$\tau_{xy} = \tau_{xy1} = \tau_{xy3} = \tau_{xy5} = \frac{v}{t_1 + t_3 + t_5} \tag{3.1}$$

In insulation layers the shear stress is:

$$\tau_{yx} = \tau_{yx2} = \tau_{yx4} = \frac{v}{t_2 + t_4} \tag{3.2}$$

Considering that all layers have equal thickness so the maximum reachable force is $F_{\max} = 9,1\,\text{kN}$. Additional considerations are needed regarding torsional shear stresses at the glue interface, for which a strength value is not provided.

6

Chapter 4

Type C

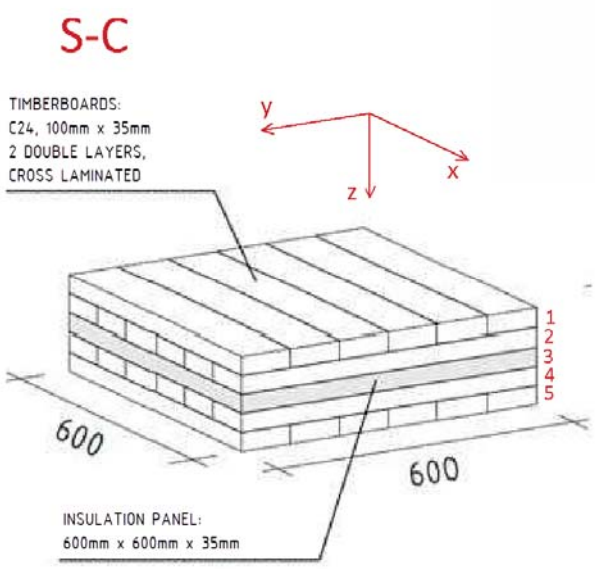

Figure 4.1: Shear stresses for the equilibrium method

This configuration is different from the previous two and presents two glued interfaces between timber layers capable of transferring stresses. Considering the very small shear strength of insulation respect to timber a simplification is considered: this panel is regarded as two CLT panels each of 2 layers working "in parallel" and the insulation is not considered to be loaded. With this consideration shear stresses are:

$$\tau_{xy} = \tau_{xy1} = \tau_{xy5} = \frac{v}{t_1 + t_5} \tag{4.1}$$

$$\tau_{yx} = \tau_{yx2} = \tau_{yx4} = \frac{v}{t_2 + t_4} \tag{4.2}$$

For this particular case where all layers have equal thickness the two previous stresses are equal:

$$\tau_{v,\text{net}} = \frac{v}{2 \cdot t_i} \tag{4.3}$$

7

Regarding torsional shear stresses the calculation would be:

$$\tau_T = 3 \cdot \frac{\tau_{xy} \cdot t_1}{b_l} = 3 \cdot \frac{v}{2 \cdot t_i} \cdot \frac{t_1}{b_l} = \frac{3}{2} \cdot \frac{v}{b_l} \tag{4.4}$$

Regarding net shear strength there still isn't common agreement on values, some mean strength values are present in literature, such as $f_{v,\text{net}} = 12,8\,\text{MPa}$ in [9], $f_{v,\text{net}} = 9\,\text{MPa}$ in [5], $f_{v,\text{net}} = 7,5\,\text{MPa}$ in [6]. A paper testing the same setup is the one of Andreolli et al. [1] which presented a mean value $f_{v,\text{net}} = 12,7\,\text{MPa}$.

Using the last value as a reference for net shear strength it is possible to obtain $F_{\max} = 528\,\text{kN}$. Note that this number is far from certain, firstly because there is a big uncertainty on strength value (for example, taking $f_{v,\text{net}} - 7,5\,\text{MPa}$ the maximum force would be $F_{\max} - 311\,\text{kN}$) and then because a big simplification has been done considering this specimen as two 2 layer CLT panels with insulation in the middle but since the torsional behaviour of insulation is not know there is the possibility that detachments/torsional failures in insulation occur well before net shear failure in timber.

Also regarding torsional shear stress there are uncertainties on strength values, for examples tests on single node provide mean values of $f_{v,t} = 3,07\,\text{MPa}$ [3]; $f_{v,t} = 3,5\,\text{MPa}$ [10]; $f_{v,t} = 3,1\,\text{MPa}$ [4]. Strength value in real scale panels though appears to be much higher, such as $f_{v,t} = 5,2\,\text{MPa}$ in the diagonal compression test of Andreolli et al. [1]. If torsional shear failure occurs, considering the last value, the maximum force would be $F_{\max} = 206\,\text{kN}$

8

Bibliography

[1] Andreolli, M., Rigamonti, M., and Tomasi, R. Diagonal Compresion Test on Cross Laminated Timber Panels. In *Proceedings of WCTE-World Conference on Timber Engineering* (2014).

[2] Andreolli, M., Tomasi, R., and Polastri, A. Experimental investigation on in-plane behaviour of cross-laminated timber elements. In *Proceedings of CIB-W18* (2012).

[3] Blass, H., and Görlacher, R. Zum trag- und verformungsverhalten von lignotrend elementen bei beanspruchung in plattenebene. Tech. rep., Universitt Karlsruhe, 2001.

[4] Bogensperger, T., Moosbrugger, T., and Silly, G. Verification of CLT-plates under loads in plane. In *Proceedings of WCTE-World Conference on Timber Engineering* (2010).

[5] Brandner, R., Bogensperger, T., and Schickhofer, G. In plane shear strength of cross laminated timber (clt): test configuration, quantification and influencing parameters. In *Proceedings of 46th CIB-W18 Meeting, Vancouver* (2013).

[6] Brandner, R., Dietsch, P., Dröscher, J., Schulte-Wrede, M., Kreuzinger, H., and Sieder, M. Cross laminated timber (clt) diaphragms under shear: Test configuration, properties and design. *Construction and Building Materials 147* (2017), 312–327.

[7] Brandner, R., Tomasi, R., Moosbrugger, T., Serrano, E., and Dietsch, P. *Properties, Testing and Design of Cross Laminated Timber, a state-of-the-art report by COST Action FP1402 / WG 2.* 2018.

[8] Dietsch, P., Schickhofer, G., Brunauer, A., Tomasi, R., Hübner, U., Krenn, H., Mestek, P., Moosbrugger, T., and Tobias Wiegand, y. . Eurocode 5:2022 Einführung in die neuen Abschnitte Brettsperrholz und Verstärkungen".

[9] Jöbstl, R., Bogensperger, T., and Schickhofer, G. In-plane shear strength of cross laminated timber. In *Proceedings of 41th CIB-W18 Meeting, St. Andrews* (2008).

[10] Jöbstl, R. A., Bogensperger, T., Schickhofer, G., and Jeitler, G. Mechanical behaviour of two orthogonally glued boards. In *Proceedings of 8th World Conference on Timber Engineering (WCTE2004), Portland* (2004).

Appendix B: Bending test

Material data:

$E_t := 13000\ \boldsymbol{N \cdot mm^{-2}}$ Young's modulus for timber (T22)

$G_t := 810\ \boldsymbol{N \cdot mm^{-2}}$ Shear modulus for timber (T22)

$E_{iso} := 0\ \boldsymbol{N \cdot mm^{-2}}$ Young's modulus for the insulation material

$G_{iso\_Instron} := 8.838\ \boldsymbol{N \cdot mm^{-2}}$ Shear modulus for the insulation material (Based on vertical deformations)

$G_{iso\_LaVision} := 52.57\ \boldsymbol{N \cdot mm^{-2}}$ Shear modulus for the insulation material (Based on optical analysis)

$E_1 := E_t = 13000\ \boldsymbol{N \cdot mm^{-2}}$ Young's modulus for layer 1 (timber)

$E_2 := E_{iso} = 0\ \boldsymbol{N \cdot mm^{-2}}$ Young's modulus for layer 2 (insulation)

$E_3 := E_t = 13000\ \boldsymbol{N \cdot mm^{-2}}$ Young's modulus for layer 3 (timber)

$G_1 := G_t = 810\ \boldsymbol{N \cdot mm^{-2}}$ Shear modulus for layer 1

$G_3 := G_t = 810\ \boldsymbol{N \cdot mm^{-2}}$ Shear modulus for layer 3 (timber)

$G_{2\_Instron} := G_{iso\_Instron}$ Shear modulus for layer 2 (Based on vertical deformations)

$G_{2\_LaVision} := G_{iso\_LaVision}$ Shear modulus for layer 2 (Based on optical analysis)

$\kappa := \frac{6}{5}$ Timoshenko shear coefficient

Static data and cross section parameters:

$L := 2 \cdot 875\ mm = 1750\ mm$ Length of composite beam

$w := 80\ mm$ Width of composite beam

$t_1 := 20\ mm$ Thickness of top layer

$t_2 := 35\ mm$ Thickness of central layer

$t_3 := 20\ mm$ Thickness of bottom layer

$A_1 := w \cdot t_1 = 1600\ mm^2$ Area of top layer

$A_2 := w \cdot t_2 = 2800\ mm^2$ Area of central layer

$A_3 := w \cdot t_3 = 1600\ mm^2$ Area of bottom layer

$z_1 := \frac{t_1 + t_2 + t_3}{2} - \frac{t_1}{2} = 27.5\ mm$ Radius of gyration for top layer

$z_3 := \frac{t_1 + t_2 + t_3}{2} - \frac{t_3}{2} = 27.5\ mm$ Radius of gyration for bottom layer

$a := z_1 + z_3 = 55\ mm$ Internal distance between centers of gravity

Stiffness in the case of full composite action (Shear Analogy):

$$EI_A := E_1 \cdot \frac{w \cdot t_1^{\,3}}{12} + E_3 \cdot \frac{w \cdot t_3^{\,3}}{12}$$ Bending stiffness, virtual beam A

$$EI_B := E_t \cdot A_1 \cdot z_1^{\,2} + E_t \cdot A_3 \cdot z_3^{\,2}$$ Bending stiffness, virtual beam B

$$EI_{eff} := EI_A + EI_B = 32.847 \ \boldsymbol{kN \cdot m^2}$$ Total effective bending stiffness

$$GA_{B\_Instron} := \frac{a^2}{\frac{t_1}{2 \cdot G_1 \cdot w} + \frac{t_2}{G_{2\_Instron} \cdot w} + \frac{t_3}{2 \cdot G_3 \cdot w}}$$ Shear stiffness, virtual beam B (Based on Instron deformations)

$$GA_{B\_LaVision} := \frac{a^2}{\frac{t_1}{2 \cdot G_1 \cdot w} + \frac{t_2}{G_{2\_LaVision} \cdot w} + \frac{t_3}{2 \cdot G_3 \cdot w}}$$ Shear stiffness, virtual member B (Based on optical analysis)

$$GA_{eff\_Instron} := GA_{B\_Instron} = 60.73 \ \boldsymbol{kN}$$ Total effective shear stiffness (Based on Instron deformations)

$$GA_{eff\_LaVision} := GA_{B\_LaVision} = 350.486 \ \boldsymbol{kN}$$ Total effective shear stiffness (Based on optical analysis)

Stiffness in the case of no composite action:

$$EI_0 := E_1 \cdot \frac{w \cdot t_1^{\,3}}{12} + E_3 \cdot \frac{w \cdot t_3^{\,3}}{12} = 1.387 \ \boldsymbol{kN \cdot m^2}$$ Local bending stiffness, layer 1+3

$$GA_0 := G_1 \cdot w \cdot t_1 + G_3 \cdot w \cdot t_3 = 2592 \ \boldsymbol{kN}$$ Local shear stiffness, layer 1+3

Theoretical stiffness of equivalent springs:

$$K_0 := \frac{1}{\frac{L^3}{48 \cdot EI_0} + \frac{L \cdot \kappa}{4\ GA_0}} = 12.4\ N \cdot mm^{-1}$$

No composite action

Without composite action, the stiffness of the beam should be 12.4N/mm.

$$K_{eff\_1} := \frac{1}{\frac{L^3}{48 \cdot EI_{eff}} + \frac{L \cdot \kappa}{4\ GA_{eff\_Instron}}} = 83.0\ \frac{N}{mm}$$

Stiffness of equivalent spring (Based on Instron deformations)

Given a shear modulus of 8.838N/mm², the stiffness of the beam should be 83.0N/mm.

$$K_{eff\_2} := \frac{1}{\frac{L^3}{48 \cdot EI_{eff}} + \frac{L \cdot \kappa}{4\ GA_{eff\_LaVision}}} = 204.2\ \frac{N}{mm}$$

Stiffness of equivalent spring (Based on optical analysis)

Given a shear modulus of 52.57N/mm², the stiffness of the beam should be 204.2/mm.

Appendix C: Conceptual roof slab

Static data:

$L := 7\ m$ Span length of conceptual roof slab

$w := 1\ m$ Width of conceptual roof slab

Material data:

$E_0 := 13000\ N \cdot mm^{-2}$ Modulus of elasticity for timber (T22)

$G_0 := 810\ N \cdot mm^{-2}$ Longitudinal shear modulus for timber (T22)

$G_{90} := 69\ N \cdot mm^{-2}$ Rolling shear modulus for timber (T22)

$G_{fiber\_boards} := 50\ N \cdot mm^{-2}$ Assumed shear modulus for fiber boards

$E_1 := E_0 = 13000\ N \cdot mm^{-2}$ Modulus of elasticity for layer 1

$E_2 := 0\ N \cdot mm^{-2}$ Modulus of elasticity for layer 2

$E_3 := 150\ N \cdot mm^{-2}$ Assumed modulus of elasticity for layer 3

$E_4 := 0\ N \cdot mm^{-2}$ Modulus of elasticity for layer 4

$E_5 := E_0 = 13000\ N \cdot mm^{-2}$ Modulus of elasticity for layer 5

$G_1 := G_0 = 810\ N \cdot mm^{-2}$ Shear modulus for layer 1

$G_2 := G_{90} = 69\ N \cdot mm^{-2}$ Shear modulus for layer 2

$G_3 := G_{fiber\_boards} = 50\ N \cdot mm^{-2}$ Shear modulus for layer 3

$G_4 := G_{90} = 69\ N \cdot mm^{-2}$ Shear modulus for layer 4

$G_5 := G_0 = 810\ N \cdot mm^{-2}$ Shear modulus for layer 5

Cross-section geometry:

$h_1 := 40\ mm$	Thickness of layer 1
$h_2 := 25\ mm$	Thickness of layer 2
$h_3 := 250\ mm$	Thickness of layer 3
$h_4 := 25\ mm$	Thickness of layer 4
$h_5 := 40\ mm$	Thickness of layer 5
$h_{tot} := h_1 + h_2 + h_3 + h_4 + h_5 = 380\ mm$	Total thickness
$A_1 := w \cdot h_1 = 40000\ mm^2$	Local cross-section area of layer 1
$A_2 := w \cdot h_2 = 25000\ mm^2$	Local cross-section area of layer 2
$A_3 := w \cdot h_3 = 250000\ mm^2$	Local cross-section area of layer 3
$A_4 := w \cdot h_4 = 25000\ mm^2$	Local cross-section area of layer 4
$A_5 := w \cdot h_5 = 40000\ mm^2$	Local cross-section area of layer 5
$z_1 := \frac{h_{tot}}{2} - \frac{h_1}{2} = 170\ mm$	Distance from neutral axis to center of layer 1
$z_2 := \frac{h_{tot}}{2} - h_1 - \frac{h_2}{2} = 137.5\ mm$	Distance from neutral axis to center of layer 2
$z_3 := 0\ mm$	Layer 3 lies in the global neutral axis
$z_4 := \frac{h_{tot}}{2} - h_5 - \frac{h_4}{2} = 137.5\ mm$	Distance from neutral axis to center of layer 4
$z_5 := \frac{h_{tot}}{2} - \frac{h_5}{2} = 170\ mm$	Distance from neutral axis to center of layer 5
$a := z_1 + z_5 = 340\ mm$	Distance between centers of layer 1 and 5

Cross-section stiffness parameters (Shear Analogy Method):

$$I_1 := \frac{w \cdot h_1^{\,3}}{12} = \left(5.333 \cdot 10^{6}\right)\ mm^4$$

$$I_2 := \frac{w \cdot h_2^{\,3}}{12} = \left(1.302 \cdot 10^{6}\right)\ mm^4$$

$$I_3 := \frac{w \cdot h_3^{\,3}}{12} = \left(1.302 \cdot 10^{9}\right)\ mm^4$$

$$I_4 := \frac{w \cdot h_4^{\,3}}{12} = \left(1.302 \cdot 10^{6}\right)\ mm^4$$

$$I_5 := \frac{w \cdot h_5^{\,3}}{12} = \left(5.333 \cdot 10^{6}\right)\ mm^4$$

$$EI_A := E_1 \cdot I_1 + E_2 \cdot I_2 + E_3 \cdot I_3 + E_4 \cdot I_4 + E_5 \cdot I_5 = \left(3.34 \cdot 10^{11}\right)\ N \cdot mm^2$$

$$EI_B := E_1 \cdot A_1 \cdot z_1^{\,2} + E_2 \cdot A_2 \cdot z_2^{\,2} + E_3 \cdot A_3 \cdot z_3^{\,2} + E_4 \cdot A_4 \cdot z_4^{\,2} + E_5 \cdot A_5 \cdot z_5^{\,2} = \left(3.01 \cdot 10^{13}\right)\ N \cdot mm^2$$

$$GA_B := \frac{a^2}{\frac{h_1}{2 \cdot G_1 \cdot w} + \frac{h_2}{G_2 \cdot w} + \frac{h_3}{G_3 \cdot w} + \frac{h_4}{G_4 \cdot w} + \frac{h_5}{2 \cdot G_5 \cdot w}} = \left(2.002 \cdot 10^{4}\right)\ kN$$

$$EI_{eff} := EI_A + EI_B = \left(3.04 \cdot 10^{4}\right)\ kN \cdot m^2$$

$$GA_{eff} := GA_B = \left(2.002 \cdot 10^{4}\right)\ kN$$

$$\kappa := \frac{6}{5} = 1.2 \qquad \text{(Timoshenko shear coefficient)}$$

Applied loads:

$\gamma_{timber} := 470\ \boldsymbol{kg \cdot m^{-3}} \cdot g = 4.609\ \boldsymbol{kN \cdot m^{-3}}$ Density of timber

$\gamma_{fiber\_boards} := 250\ \boldsymbol{kg \cdot m^{-3}} \cdot g = 2.452\ \boldsymbol{kN \cdot m^{-3}}$ Density of fiber boards

$q_{dead\_self} := 1\ \boldsymbol{m} \cdot \left(\gamma_{timber} \cdot \left(h_1 + h_2 + h_4 + h_5\right) + \gamma_{fiber\_boards} \cdot h_3\right)$ Total self weight of slab

$q_{dead\_applied} := w \cdot 0.5\ \boldsymbol{kN \cdot m^{-2}}$ Additional dead load

$q_{dead} := q_{dead\_self} + q_{dead\_applied} = 1.712\ \boldsymbol{kN \cdot m^{-1}}$ Total dead load

$q_{snow} := 3.0\ \boldsymbol{kN \cdot m^{-1}}$ Snow load

Characteristic deformation (long term effects not included):

$$\delta := \frac{5}{384} \cdot \frac{\left(q_{dead} + q_{snow}\right) \cdot L^4}{EI_{eff}} + \frac{1}{8} \cdot \frac{\left(q_{dead} + q_{snow}\right) \cdot L^2 \cdot \kappa}{GA_{eff}} = 6.6\ \boldsymbol{mm} \quad \approx \quad \frac{L}{1050} = 6.7\ \boldsymbol{mm}$$

Comparing results to ANSYS-model:

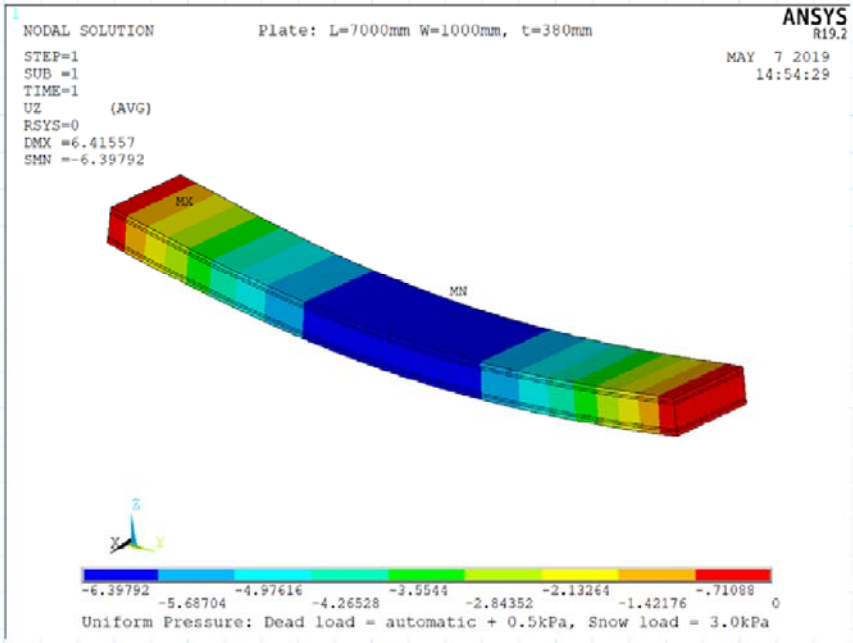

Calculating material parameters for finite element analysis:

$I_A := \frac{w \cdot h_{tot}^{\,3}}{12} = (4.573 \cdot 10^9)\ mm^4$ — Area moment of inertia for member A

$I_B := I_A = (4.573 \cdot 10^9)\ mm^4$ — Area moment of inertia for member B

$A_A := w \cdot h_{tot} = (3.8 \cdot 10^5)\ mm^2$ — Cross-section area for member A

$A_B := A_A = (3.8 \cdot 10^5)\ mm^2$ — Cross-section area for member B

$E_A := \frac{EI_A}{I_A} = 73.0\ N \cdot mm^{-2}$ — Modulus of elasticity for member A

$E_A := \frac{EI_B}{I_B} = 6573.0\ N \cdot mm^{-2}$ — Modulus of elasticity for member B

$G_B := \frac{GA_B}{A_B} = 52.7\ N \cdot mm^{-2}$ — Shear modulus for member B

Force distribution among members (ULS - 1,2 x dead + 1.5 x snow):

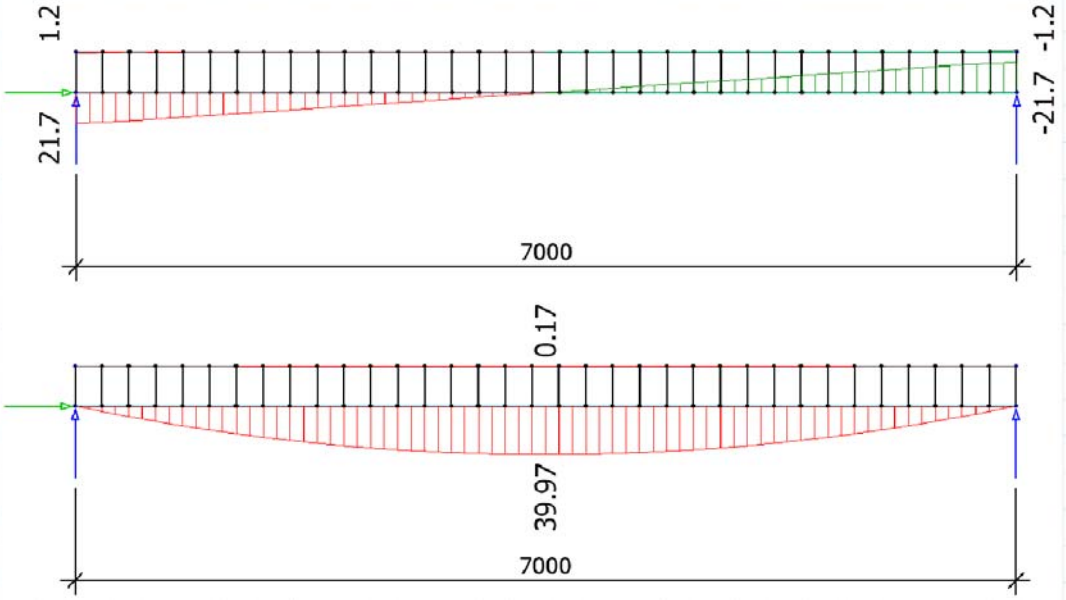

$V_A := 1.2\ kN$ $V_B := 21.7\ kN$ $M_A := 0.17\ kN \cdot m$ $M_B := 39.97\ kN \cdot m$

Calculating maximum shear stress in the central layer (layer 3):

$$\tau_{A.3} := -\frac{V_A \cdot E_3}{EI_A} \cdot \left(0 - \frac{h_3^{\,2}}{8}\right) = 0.004 \ \boldsymbol{N \cdot mm^{-2}}$$ Parabolic shear - eq. (27)

$$\tau_{B.3\_0} := \frac{V_B}{EI_B} \cdot \left(E_1 \cdot z_1 \cdot h_1 + E_2 \cdot z_2 \cdot h_2\right) = 0.064 \ \boldsymbol{N \cdot mm^{-2}}$$ Accumulated shear - eq. (28)

$$\tau_{max} := \tau_{A.3} + \tau_{B.3\_0} = 0.068 \ \boldsymbol{N \cdot mm^{-2}}$$ Total shear stress

Comparing results to FEM-design model:

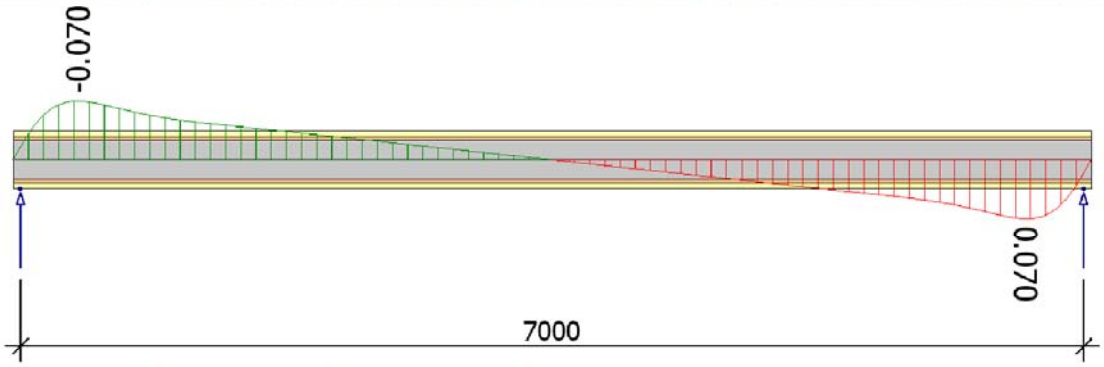

Calculating longitudinal stress in the outer layers (layer 1):

$$M_{A.1} := M_A \cdot \frac{E_1 \cdot I_1}{EI_A} = 0.035 \ \boldsymbol{kN \cdot m}$$ Bending moment - eq. (23)

$$N_{B.1} := M_B \cdot \frac{E_1 \cdot A_1 \cdot z_1}{EI_B} = 117.6 \ \boldsymbol{kN}$$ Normal force - eq. (24)

$$\sigma_{A.1} := \frac{M_{A.1}}{I_1} \cdot \frac{h_1}{2} = 0.132 \ \boldsymbol{N \cdot mm^{-2}}$$ Bending stress - eq. (25)

$$\sigma_{B.1} := \frac{N_{B.1}}{A_1} = 2.939 \ \boldsymbol{N \cdot mm^{-2}}$$ Normal stress - eq. (26)

$$\sigma_{max} := \sigma_{A.1} + \sigma_{B.1} = 3.071 \ \boldsymbol{N \cdot mm^{-2}}$$ Total longitudinal stress

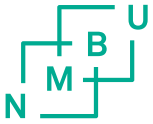

Norges miljø- og biovitenskapelige universitet
Noregs miljø- og biovitskapelege universitet
Norwegian University of Life Sciences

Postboks 5003
NO-1432 Ås
Norway